The Dissertation Committee for Christopher Scott Simmons
certifies that this is the approved version of the following dissertation:

Development of a computational framework for quantitative vibronic coupling and its application to the NO_3 radical

Committee:

John F. Stanton, Supervisor

Peter J. Rossky

Robert E. Wyatt

Eric V. Anslyn

Daniel P. Miranker

Development of a computational framework for quantitative vibronic coupling and its application to the NO_3 radical

by

Christopher Scott Simmons, B.S.

DISSERTATION

Presented to the Faculty of the Graduate School of

The University of Texas at Austin

in Partial Fulfillment

of the Requirements

for the Degree of

DOCTOR OF PHILOSOPHY

THE UNIVERSITY OF TEXAS AT AUSTIN

May 2012

Dedicated to my family.

Acknowledgments

If I were to acknowledge all of the people who helped, urged, fought, begged and pleaded with me to get to this destination, this acknowledgement would double the size of the included work. First and foremost, I'd like to thank Dr. John F. Stanton for his infinite patience (with me at least) and understanding as we worked through this problem together. Without question, he tolerated my rather hectic commitments outside of this work and was always my biggest supporter.

Secondly, I'd like to thank all of the people in ICES who continued to put their trust in me and who constantly increased my responsibility while allowing me the time and freedom to finish this work. First and foremost I'd like to thank Dr. Peter Rossky who stood up for me when no one else would. Within ICES, I'd like to thank Dr. Oden and Dr. Bass for my original opportunity within ICES and I'd like to thank Dr. Moser for allowing me to continue to challenge myself day to day while this work was being finished.

I'd also like to thank Drs. Takatoshi Ichino and Karl Schulz. Both of them contributed to this work and helped me overcome obstacles. Without their help, this would likely still be a work in progress.

Finally, I'd like to thank all of the research staff, postdocs and faculty within the PECOS center. Everyone has always treated me with the utmost

respect and never looked down on me for being a “graduate student”. I have the greatest respect and admiration for each and everyone of you and I look forward to continuing our research.

Development of a computational framework for quantitative vibronic coupling and its application to the NO_3 radical

Publication No. _____

Christopher Scott Simmons, Ph.D.
The University of Texas at Austin, 2012

Supervisor: John F. Stanton

The Born–Oppenheimer approximation is a mainstay in molecular physics and chemistry and can be considered a two step process. The first step is to solve the electronic problem with nuclei fixed in space while the second step is to then determine the nuclear dynamics on a given electronic potential energy surface. This first-step calculation of the wavefunction and electronic energies for fixed nuclei has been at the center of modern quantum chemistry for decades. While the majority of chemical processes can be investigated by considering these single electronic surface dynamics, there exist problems in which the dynamics are not constrained to a single electronic surface.

One such problem that justifies going beyond the typical adiabatic approximation is the determination of energy levels in systems with strongly coupled electronic states. While some work has been done using diabatic or

quasidiabatic Hamiltonians to describe such systems, the work has historically been of qualitative accuracy. Model Hamiltonians have been constructed using experimental data to help calibrate the model parameters aided by the use of lower level adiabatic calculations to help inform the model. It is only within the last few years that theorists have been able to attempt parameterization of such models using only *ab initio* methods. The goal of this work is to develop a computational framework for the parameterization of quantitatively accurate quasidiabatic Hamiltonians based purely on *ab initio* information and apply it to a notoriously difficult problem that has plagued the theoretical community for decades — high accuracy treatment of the energy levels of the NO_3 radical.

In this dissertation, high-level *ab initio* calculations that employ the equation-of-motion coupled-cluster method in the single, doubles and triples (EOMIP-CCSDT) have been used in conjunction with a quasidiabatic *ab initio* approximation to construct a vibronic Hamiltonian for the strongly coupled X^2A_2' and B^2E' states of the NO_3 radical. A quartic vibronic coupling model potential of the form advocated by Köppel et al. has been used to determine the energy levels of this system to quantitative accuracy when compared to experimental data.

In order to obtain sufficiently accurate potential energy surfaces necessary to parameterize a quantitatively accurate model hamiltonian, thousands of large calculations had to be run that do not fit in memory on even the largest HPC systems. The resulting large, out-of-core solves do not map to traditional systems in a way to enable any reasonable parallelization. As a result, a new

MPI-based utility has been developed to support out-of-core methods on distributed memory systems. This and other advances in scientific computing form the basis of the developed computational framework.

Table of Contents

List of Tables

List of Figures

Chapter 1

Introduction

1.1 Motivation

The Born–Oppenheimer approximation [8, 9] is a mainstay in molecular physics and chemistry and can be considered a two step process. The first step is to solve the electronic problem with nuclei fixed in space while the second step is to then determine the nuclear dynamics on a given electronic potential energy surface. This first-step calculation of the wavefunction and electronic energies for fixed nuclei has been at the center of modern quantum chemistry for decades. The software to support such "adiabatic" calculations has been developed to such a degree, that alternatives are rarely considered. Fortunately, the majority of chemical processes can be treated this way. This type of treatment of considering the dynamics on a single electronic surface (usually the ground state) has been quite successful in describing molecular vibrations, relaxation of excited vibrational levels in polyatomic molecules, calculation of reaction cross-sections in atom-molecule collisions as well as the recent developments of extrapolative methods that allows thermochemical properties to be calculated with very high accuracies.

While the majority of chemical processes can be investigated by consid-

ering these single electronic surface dynamics, there exist problems in which the dynamics are not constrained to a single electronic surface. One such problem that justifies going beyond the typical adiabatic approximation is the determination of energy levels in systems with strongly coupled electronic states. While some work has been done using diabatic or quasidiabatic Hamiltonians to describe such systems, the work has historically been of qualitative accuracy.

Model (quasidiabatic) Hamiltonians have been constructed for decades using experimental data to help calibrate the model parameters aided by the use of lower level adiabatic calculations to help inform the model. It is only within the last few years that theorists have been able to attempt parameterization of such models using only *ab initio* methods. The goal of this work is to develop a computational framework for the parameterization of quantitatively accurate quasidiabatic Hamiltonians based purely on *ab initio* information and apply it to a notoriously difficult problem that has plagued the theoretical community for decades – high accuracy treatment of the energy levels of the NO_3 radical.

It is possible that the nitrate radical (NO_3) may have been the first polyatomic radical to be detected spectroscopically; the position of several absorption bands were recorded in 1880 [12, 96], but attributed finally to NO_3 and systematically investigated by Jones and Wulf in 1937 [40]. It is now known that these spectroscopic features are due to the $\tilde{\mathbf{B}}^2\mathrm{E}' \leftarrow \tilde{\mathbf{X}}^2\mathrm{A}_2'$ electronic transition. This band system is widely used analytically to detect the presence and

concentration of NO_3, which plays an important role in the chemistry of the stratosphere and troposphere [98]. Produced chiefly by the reaction of NO_2 and ozone, NO_3 is readily photolyzed by sunlight, but thought to be the dominant oxidant in the atmosphere at night [61]. Motivated by the atmospheric relevance of NO_3, a flurry of activity roughly a quarter century ago produced a number of important spectroscopic studies. This activity continues today and the current state of experimental information on NO_3 will be discussed in §2.2.1

In this dissertation, high-level *ab initio* calculations that employ the equation-of-motion coupled-cluster method in the single, doubles and triples (EOMIP-CCSDT) have been used in conjunction with a quasidiabatic *ab initio* approximation to construct a vibronic Hamiltonian for the strongly coupled X^2A_2' and B^2E' states of the NO_3 radical. A quartic vibronic coupling model potential of the form advocated by Köppel et al. has been used to determine the energy levels of this system to quantitative accuracy when compared to experimental data.

In order to obtain sufficiently accurate potential energy surfaces necessary to parameterize a quantitatively accurate model hamiltonian, thousands of large calculations had to be run that do not fit in memory on even the largest HPC systems. The resulting large, out-of-core solves do not map to traditional systems in a way to enable any reasonable parallelization. As a result, a new MPI-based utility has been developed to support out-of-core methods on distributed memory systems.

1.2 Accomplishments of the Dissertation

In this work, the most quantitative quasidiabatic model Hamiltonian ever to be constructed was applied to one of the hardest problems in chemical physics. The resulting energy levels from the fully optimized quartic Hamiltonian compare very well to experimental data and suggest the location of additional levels that should be explored spectroscopically. If the procedure outlined in this work is applied to molecular systems of similar size and difficultly, quantitative results are likely to be obtained.

In order to accomplish the many large adiabatic calculations required for this work, a new out-of-core solver implementation has been developed which will allow these type of calculations to map very well to current and next generation HPC systems. This out-of-core solver has potential applications to areas outside of quantum chemistry as well.

1.3 Structure of the Dissertation

The structure of this work is as follows. In chapter 2, a brief introduction to the KDC model will be given. This will be followed by previous work on both the (quasi)diabatic Hamiltonian applied to NO_3 as well as a discussion of recent attempts at the construction of quantitative diabatic Hamiltonians. Finally, a brief survey of the currently available experimental results and an establishment of the literature-based vibronic energy levels for NO_3 will be provided.

In chapter 3, a review of the computational details will be presented. This includes a brief discussion of the methods used in this work as well as a discussion of the adiabatic calculations performed with CFOUR needed to parameterize the quartic hamiltonian. Finally, this chapter will present new software that was developed in order to assist in remapping the workload generated by CFOUR for large basis set calculations at the CCSDT level.

Chapter 4 presents all of the vibronic model anzatzes that are used in this work. It includes discussion of the resulting energy levels, comparisons of the relative performance of each different parameterization as well as extensions to the quartic model aided by intuition and experimental data to obtain a quantitatively accurate parametrization.

The final chapter will discuss the theoretical results and future research directions as well as possible other uses for the supporting software that was generated as part of this work.

Chapter 2

The KDC Quasidiabatic Hamiltonian and Previous Work

2.1 The KDC Quasidiabatic Hamiltonian

The Born–Oppenheimer approximation [8, 9] and the resulting "adiabatic" quantum chemistry calculations have dominated the theoretical landscape for the last 40+ years. This approximation allows the electronic problem to be first calculated assuming that the nuclei are fixed in space. The second step is then to determine the nuclear dynamics on this electronic potential energy surface. This first step, referred to as an "adiabatic" calculation, has been at the center of software development to support quantum chemistry for the same 40+ years. Because this adiabatic approach has dominated research for so long, alternatives are rarely considered.

While the majority of chemical process are amenable to such a treatment, the problem of interest in this work is not. The goal of this work is to determine to a quantitative accuracy the level positions for NO_3 below 2000 cm^{-1} from the origin. As will be discussed in the following sections, the typical adiabatic methods do not map well to this problem. This is due to the fact that there are large Jahn-Teller (JT) and pseudo Jahn-Teller (PJT or some-

times referred to as second-order Jahn-Teller) effects which govern the energy levels of NO_3. Thus, one potential energy surface is not sufficient to describe the physics of NO_3 due to the coupling of the X^2A_2' and degenerate B^2E' states via multiple vibrational modes. This is referred to as a nonadiabatic interaction or nonadiabatic effect and thus must be treated differently.

While the adiabatic electronic wavefunctions, which are derived by application of the Born–Oppenheimer approximation, vary dramatically with respect to nuclear coordinates near avoided crossings and conical intersections, diabatic electronic wavefunctions do not. They are smooth functions with respect to the nuclear displacements. Due to nonadiabatic effects, not all electronic states can be considered separable. However, in order to represent these effects accurately, it is not necessary to abandon the Born–Oppenheimer approximation completely. Only those electronic states which interact need to have further parametrizations and the remaining problem can be treated adiabatically. Such a representation is referred to as quasidiabatic.

The representations of these quasidiabatic models have been explored in great detail by Köppel et al. [47] to formulate what is referred to as the KDC-model Hamiltonian. Additional work has been done to apply the KDC-model Hamiltonians to a range of nonadiabatic problems [4, 27, 37] through various methods of parameterization resulting in qualitative descriptions of the nonadiabatic effects.

Unfortunately, *ab initio* electronic structure calculations do not provide these quasidiabatic potential energy surfaces. However, there are techniques

for transforming adiabatic potential energy surfaces (and their resulting adiabatic force constants) to those that govern the quasidiabatic potential energy surfaces. The quasidiabatic model form for this work will be described in the remainder of this section and the resulting parameterization and performance of this model will be the subject of the remainder of this work.

The starting point for any treatment of nonadiabatic effects is the Born-Huang ansatz [8]. In Equation 2.1, the wavefunction of the vibronic state k where $\psi_i(r;R)$ are elements of an orthonormal set of electronic wavefunctions is $\Psi_k(r,R)$. These depend on electronic coordinates r and vary with nuclear coordinates R.

$$\Psi_k(r,R) = \sum_i \psi_i(r;R)\Omega_i^{(k)}(R) \tag{2.1}$$

In Equation 2.1, $\Omega_i^{(k)}(R)$ is the part of the vibrational wavefunction that is associated with $\psi_i(r;R)$. Both of these wavefunctions are given in terms of a basis set expansion. The electronic basis set expansion is well known and the vibrational wavefunctions expansion is seen in 2.2, where χ_m are harmonic oscillator functions in terms of R, the nuclear coordinates.

$$\Omega_i^{(k)}(R) = \sum_m c_m^{(k;i)} \quad \chi_m(R) \tag{2.2}$$

If the molecular Hamiltonian as seen in Equation 2.3 is then projected onto a finite Born-Huang basis as discussed in [32] and the resulting matrix

is diagonalized, variational approximations to the vibronic energies and wavefunctions are obtained, where $\hat{\mathbf{T}}_N$ is the nuclear kinetic energy operator and $\hat{\mathbf{H}}_e$ is the electronic Hamiltonian.

$$\hat{\mathbf{H}} = \hat{\mathbf{T}}_N + \hat{\mathbf{H}}_e \tag{2.3}$$

Eigenvectors of the resulting matrix are the coefficients in Equation 2.2 and the matrix elements of $\hat{\mathbf{H}}$ are detailed in [32]. There are two forms that the resulting electronic wavefunction, $\Psi_i(r;R)$, can take; the adiabatic representation and the quasidiabatic representation. The adiabatic representation is discussed in detail in [32] and the quasidiabatic representation is described in the remainder of this section.

For the majority of quantum chemical applications, the assumption that the electronic wavefunction varies slowly with respect to nuclear coordinates is justified. For these applications, the energy levels determined by solving the Schrödinger equation for the ground electronic state at a high-level of theory is more than adequate for determining typical quantities of interest. However, there remains a small, understudied selection of problems in which these adiabatic surfaces cross or exhibit avoided crossings such that the necessary assumptions to obtain these simple potential energy surfaces breakdown. Thus, one is forced to deal with the coupling of excited electronic states with one or more vibrational modes.

In order to study these phenomena, one must employ diabatic or qua-

sidiabatic methods. The quasidiabatic model popularized by Köppel et al. [47] is one such model. The KDC model can be discussed by investigating the Born-Huang expansion as follows; at each nuclear coordinate, a block diagonalization of the electronic Hamiltonian occurs in the static Born-Huang basis and as such isolates the interacting electronic states. If one were to take the Born-Huang Hamiltonian representation in the adiabatic sense, the following diagrammatic representation seen in Figure 2.1 would be obtained.

Pictorially, a case of strong coupling is demonstrated in Figure 2.1 where the darker shading is the off-diagonal blocks of the nuclear kinetic energy matrix. This indicates that two electronic states are mixed by appreciable derivative coupling in the adiabatic basis.

This second parameterization of the two interacting states builds in the "following the nuclear displacements" behavior that should be expected of these electronic wavefunctions but which is completely lacking in the static electronic basis. However, the rapid variation of wavefunctions which results from strong interaction and/or quasidegeneracy can be avoided if the set of isolated states comprises all those that are effectively decoupled from the remainder of the spectrum.

This choice of basis represents an exact unitary transformation of the adiabatic electronic basis, but the nuclear kinetic energy operator is only approximately diagonal in this basis. This can be seen in Figure 2.2.

In order to build in this required "follow the nuclear displacements"

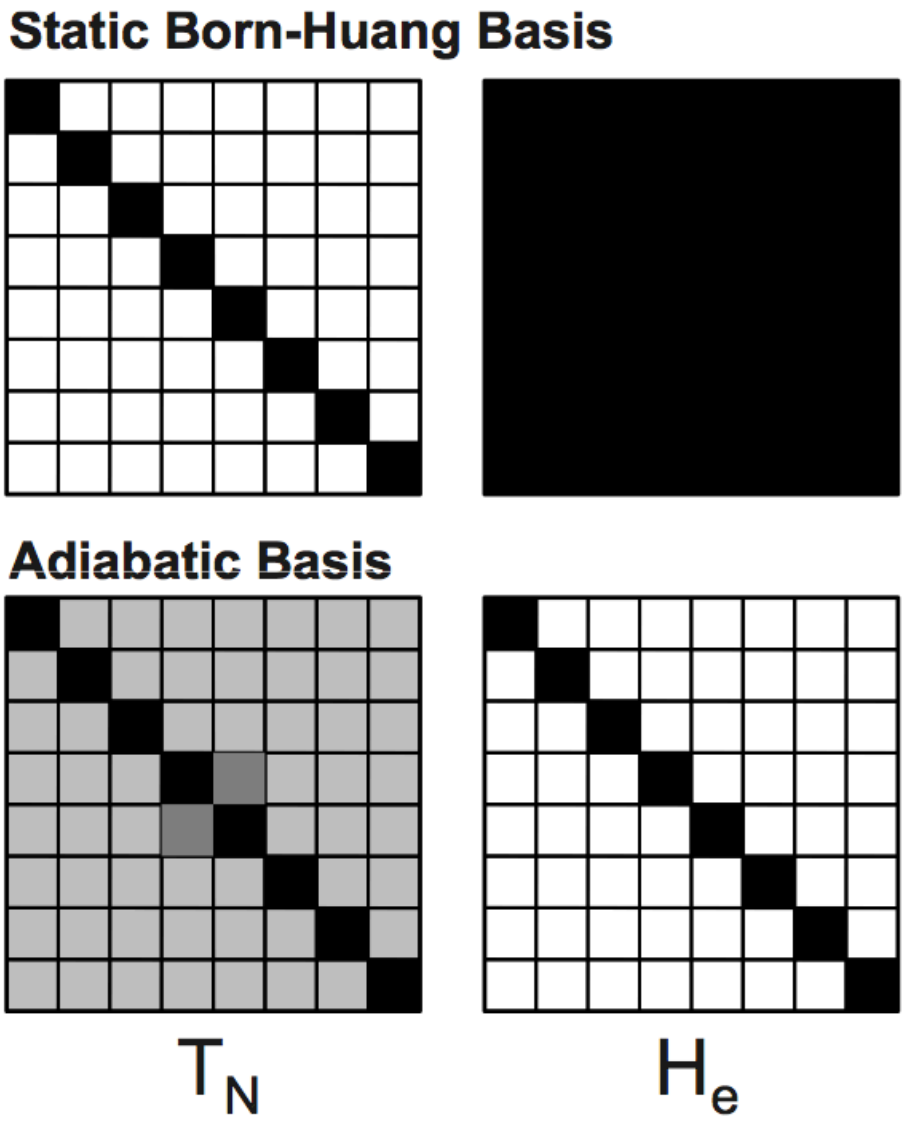

Figure 2.1: Adiabatic representation after the block diagonalization of the static Born-Huang basis

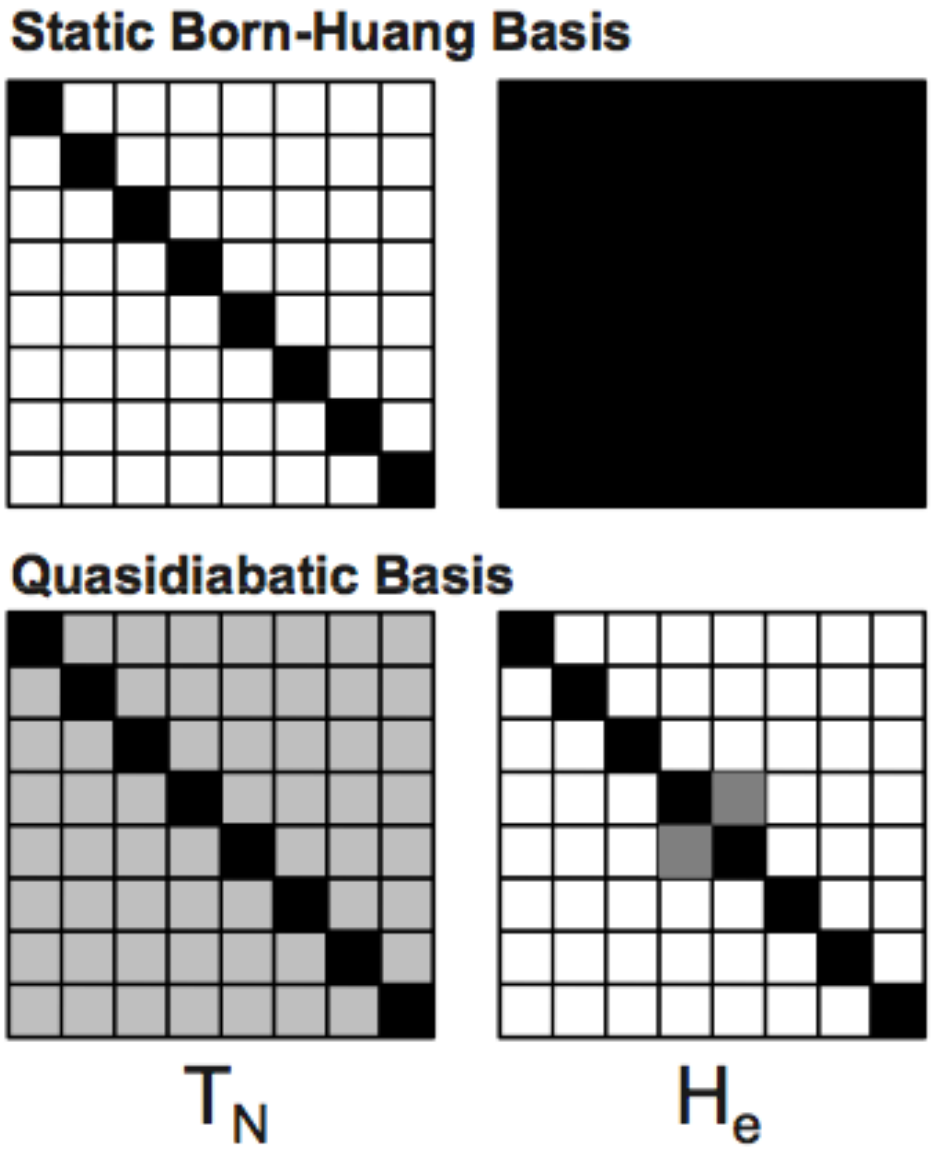

Figure 2.2: Diabatic representation after the block diagonalization of the static Born-Huang basis

behavior, the KDC model Hamiltonian is parameterized via a Taylor series expansion in the reduced normal coordinates of some reference state. This general form can be seen in Equation 2.4.

$$\mathbf{V} = \begin{pmatrix} \sum_k \kappa_{k;1} q_k + \frac{1}{2}\kappa_{kl;1} q_k q_l + \cdots & \sum_k \lambda_{k;12} q_k + \cdots & \cdots \\ \sum_k \lambda_{k,12} q_k + \cdots & \Delta_2 + \sum_k \kappa_{k;2} q_k + \frac{1}{2}\kappa_{kl;2} q_k q_l + \cdots & \cdots \\ \vdots & \vdots & \ddots \end{pmatrix}. \tag{2.4}$$

For the work presented here, the KDC-model Hamiltonian will be a 3 x 3 matrix with each expansion parameterized along 5 normal coordinates of the anion. These coordinates are discussed in more details in §3.3.1.

$$\mathbf{V} = \begin{pmatrix} \sum_k \kappa_{k;\tilde{\mathbf{X}}} q_k + \frac{1}{2}\sum_{ij} \kappa_{jk;\tilde{\mathbf{X}}} q_j q_k & \sum_k \lambda_{k;\tilde{\mathbf{X}}\tilde{\mathbf{A}}} q_k & \sum_k \lambda_{k;\tilde{\mathbf{X}}\tilde{\mathbf{B}}} q_k \\ \sum_k \lambda_{k;\tilde{\mathbf{X}}\tilde{\mathbf{A}}} q_k & \Delta_A + \sum_k \kappa_{k;\tilde{\mathbf{A}}} q_k + \frac{1}{2}\sum_{ij} \kappa_{jk;\tilde{\mathbf{A}}} q_j q_k & \sum_k \lambda_{k;\tilde{\mathbf{A}}\tilde{\mathbf{B}}} q_k \\ \sum_k \lambda_{k;\tilde{\mathbf{X}}\tilde{\mathbf{B}}} q_k & \sum_k \lambda_{k;\tilde{\mathbf{A}}\tilde{\mathbf{B}}} q_k & \Delta_B + \sum_k \kappa_{k;\tilde{\mathbf{B}}} q_k + \frac{1}{2}\sum_{ij} \kappa_{jk;\tilde{\mathbf{B}}} q_j q_k \end{pmatrix} \tag{2.5}$$

The form listed in Equation 2.5 has been truncated to only include quadratic terms, however, parameterizations that include up to quartic terms will be discussed. The remainder of this chapter discusses experimental work on NO_3 as well as previous theoretical work on NO_3 as well as previous quantitative vibronic coupling parameterizations. After that discussion, the remainder of this work deals with how the above KDC parameterization was done. It includes discussions on the adiabatic calculations needed in order to parameterize the models as well as a discussion of performance of each model chosen when compared to experimental results.

2.2 Survey of Previous Work

In the following three subsections, previous work, both experimentally and theoretically, for the NO_3 radical will be discussed. Methods in modern quantum chemistry as well as a fresh, new take on experimental results will help explain the energy levels (and thus spectroscopy) of this seemingly difficult molecule.

2.2.1 Experimental work on the NO_3 radical

There have been numerous spectroscopic studies of the NO_3 radical over the last 80+ years. A series of absorption bands between 15000 cm^{-1} and 23000 cm^{-1} was attributed to the NO_3 radical as early as 1937 by Jones and Wulf [40]. Detailed studies of the excitation from the ground X^2A_2' state to the excited B^2E' state was attempted as early as 1963 by Ramsay [68]. Multiple other early studies agreed that NO_3 is strongly predissociated in higher excited vibrational levels of the B^2E' state and because of the atypical position of the band origin, it has been used to study the behavior of NO_3 in gas-phase systems [19, 39, 59].

For the work presented here, the focus of the study will be on the level positions of the Nitrate radical that appear below 2000 cm^{-1} from the origin. As discussed in several of the works cited above, the transition from X^2A_2' to B^2E' is 662 nm $\pm$1 nm. Thus, the experimental value for this excitation will be 15106 cm^{-1}. Several works have measured the levels of interest, but the seminal work of Ishiwata et al. [35] contains the first assignments of many of

Table 2.1: Positions of absorptions below 2000 (in $cm^{-}1$) for the Nitrate radical

Medium	Experimental
Gas	365
Ne Matrix	1173
Ne Matrix	1413
Gas	1492
Gas	1562
Gas	1927

the levels that will be discussed herein and the recent work of Jacox et al. [36] contains levels not seen previously.

Table 2.2.1 contains the value and the medium in which it was measured for the levels that will be used as the experimental references for the remainder of this work. The Gas values originate from Ishiwata et al. [35] while the Neon matrix values come from Jacox et al. [36].

2.2.2 Theoretical work on the NO_3 radical

About 10 years before Ishiwata et al. [35] published their seminal experimental work on the NO_3 radical, theorist began studying it. For the better part of two decades, the main focus of theoretical research on NO_3 was determining whether or not the ground X^2A_2' state was D_{3h} or C_{2v} symmetry [7, 20, 41, 43, 56, 60, 79, 87, 88]. While it was eventually settled that the NO_3 radical is of D_{3h} symmetry, the one fact that everyone agreed on at this time was that the potential energy surface of the X^2A_2' ground state is extremely

flat.

Adding additional complications for quantum chemistry to treat this flat X^2A_2' surface is the fact that the NO_3 molecule itself is vulnerable to very strong symmetry breaking caused by instabilities introduced by zeroth-order wavefunctions [16, 85]. However, even if multireference methods are used to attempt to address these zeroth-order introduced instabilities, the flatness of the surface remains [86]. This is suggestive that the symmetry breaking is not of the artificial type introduced by the computation but has a physical origin. In the work of Mayer et al. [58], pseudo jahn-teller (PJT) effects between the ground X^2A_2' and excited B^2E' states were used to qualitatively justify the photodetachment spectra of NO_3. While the adiabatic potential energy surfaces generated by quantum chemical methods is complex, relatively simple quasidiabatic models are able to capture the relevant physics and qualitatively reproduce experimental data.

The previous paragraph provides the motivation for applying higher-level quasidiabatic parameterizations of the KDC type to NO_3. While even the highest level of quantum chemistry methods have not been able to provide adequate information to understand experimental work on the NO_3 radical, simple diabatic methods have. However, only relatively simple diabatic parameterizations have been applied to NO_3. If these worlds could be combined such that the highest-level adiabatic calculations could be used to parameterize an equally sophisticated diabatic Hamiltonian, can quantitative level positions be obtained? The answer to this question is found in the remainder

of this work.

2.2.3 Quantitative Vibronic Coupling Models

Up until recently, there has been no attempts at parameterizing a vibronic coupling model that was truly quantitative and thus eventually predictive. Most of the work has focused on using Linear Vibronic Coupling models to gain qualitative insight into the nonadiabatic effects that appear in spectroscopic studies [58]. In fact, often these same LVC models are parameterized by the spectroscopic data itself.

In the literature, there exists very few examples of sophisticated vibronic models that have been parameterize by equally sophisticated adiabatic calculations. The recent work of Klein et al. [44] and Ichino et al. [33] are the best examples of combining equally sophisticated adiabatic and diabatic calculations to understand complex nonadiabatic phenomena.

In the work of Klein et al. [44], different modeling choices were explored for the parameterization of a KDC-type Hamiltonian as applied to the formyloxyl radical, HCO_2. In this work, two electronic states were coupled by two vibrational modes. The CCSD(T) method, that is coupled cluster with singles and doubles with an additional noniterative, perturbative correction, was applied to generate the necessary potential energy surfaces necessary to parameterize the quasidiabatic Hamiltonian. The Hamiltonian was constructed such that all quadratic terms were used and additional cubic and quartic terms for diagonal blocks of the potential were presented. While the agreement with

experiment was indeed excellent, the coupling in the formyloxyl radical is not nearly as strong as the more troublesome treatment of NO_3. While this work does help to validate the types of parameterizations discussed in this work, the NO_3 levels will be a much stronger (and difficult) validation test.

In the work of Ichino et al. [33], the cyclopentadienyl radical was subjected to the same type of KDC parametrization, however, the adiabatic potential energy surfaces were only at the EOMIP-CCSD level. Here, linear and bilinear jahn-teller coupling terms were used to help understand the complex photoelectronic spectrum of $C_5H_5^-$. While the agreement with spectrum was very good and the essential physics were recovered by the parameterized quasidiabatic Hamiltonian, the results can be best described as very insightful but qualitative.

Chapter 3

Computational Details

3.1 CFOUR

As a starting point for the adiabatic calculations used in this work, the CFOUR [30] program package was used. CFOUR (Coupled-Cluster techniques for Computational Chemistry) is an application for performing high-level quantum chemical calculations which is under active development by research groups at UT Austin and Universität Mainz, Germany. This suite of programs can be used for performing high-level quantum chemical calculations on atoms and molecules. The program suite has a large collection of high-level ab initio methods for the calculation of atomic and molecular properties. Virtually all approaches based on Møller-Plesset (MP) perturbation theory and the coupled-cluster approximation (CC) are available. For most of these, analytic first and second-derivative approaches are available within the package.

From this large array of capabilities, only a few are needed in order to provide the calculations necessary to parameterize our model Hamiltonians. While CFOUR is particularly well suited for high-level coupled cluster calculates, the computational framework developed in this work is program

agnostic. Any appropriate high-level calculations (from any number of programs) for the adiabatic potential energy surfaces are sufficient to parameterize our model Hamiltonians.

In the following section, the quantum chemical methods used for this work are first discussed. This is followed by a discussion of the actual calculations run and the logic that went into deciding how best to obtain the needed information. Over the course of running these calculations, a large computational hurdle had to be overcome which resulting in the development of a new utility that enables remapping of workloads of typical quantum calculations to suite those of current generation HPC systems. Finally, the computational details are discussed on how vibronic energy levels are obtained from the model hamiltonians.

3.2 Quantum Chemical Methods

3.2.1 Hartree-Fock

The starting point for electronic structure theory is the Hartree-Fock (HF) approximation. In HF, the wavefunction is approximated by a single reference determinant of spin orbitals. The resulting wavefunction can be represented as a product of spin orbitals as in Equation 3.1.

$$|\Psi_{HF}(X_1, X_2, X_3...X_n)\rangle = |\chi_1(X_1)\chi_2(X_2)\chi_3(X_3)\chi_4(X_4)...\chi_n(X_n)\rangle \qquad (3.1)$$

Because the resulting Hartree product fails to satisfy antisymmetry constraints, self consistent field (SCF) approximations replace this with the

usual n-electron slater determinant $|\Phi_0\rangle$.

$$|\Phi_0\rangle \quad = \quad |\chi_1\chi_2\chi_3\cdots\chi_n\rangle \equiv \sqrt{\frac{1}{n!}} \begin{vmatrix} \chi_1(X_1) & \chi_2(X_1) & \cdots & \chi_n(X_1) \\ \chi_1(X_2) & \chi_2(X_2) & \cdots & \chi_n(X_2) \\ \chi_1(X_3) & \chi_2(X_3) & \cdots & \chi_n(X_3) \\ \vdots & \vdots & \ddots & \vdots \\ \chi_1(X_n) & \chi_2(X_n) & \cdots & \chi_n(X_n) \end{vmatrix} \tag{3.2}$$

$|\Phi_0\rangle$ is an antisymmetric wavefunction that can be used to solve the Hartree-Fock equations. A wavefunction of this form gives gives the lowest energy for

$$E_0 = \langle\Phi_0|\hat{H}|\Phi_0\rangle \tag{3.3}$$

where $\hat{H}$ is the full electronic Hamiltonian. It can be shown that the Hartree-Fock problem can be written using the one-electron Fock operator cast as an eigenvalue problem.

$$f\,\chi_i = \epsilon_i\chi_i \tag{3.4}$$

where the ϵ_n are assumed to be the energies of the corresponding orthonormal orbitals ϕ_n obtained by solving Equation 3.3 and are the Hartree-Fock molecular orbitals; f being the so-called one-electron Fock operator.

$$\chi_i = \sum_{\mu}^{k} C_{\mu i}\phi_\mu \tag{3.5}$$

If one then introduces a basis set, such as the one shown in 3.5 where ϕ_μ are atomic orbital basis functions in the Hartree-Fock equations, the Roothaan-Hall equations can be obtained as in 3.6

$$\sum_{\nu} F_{\mu\nu} C_{\nu i} = \epsilon_i \sum_{\nu} S_{\mu\nu} C_{\nu i} \tag{3.6a}$$

$$F_{\mu\nu} = \int \phi_{\mu}^{*} \phi_{\nu} dX_1 \tag{3.6b}$$

$$S_{\mu\nu} = \int \phi_{\mu}^{*} f(X_1) \phi_{\nu} dX_1 \tag{3.6c}$$

Typically, the Roothaan equations are written in the matrix form in 3.7.

$$\mathbf{FC} = \epsilon \mathbf{SC} \tag{3.7}$$

where **S** is the overlap matrix. Solving this equation requires an iterative process because the **F** matrix depends on its own eigenvectors. This is referred to as the self consistent field method or just SCF. The downside of Hartree-Fock theory is that it fails to account for correlated motion of the electrons and thus cannot accurately capture the interactions between them. In SCF, the procedure calls for selecting an electron moving in a space where all the other electrons are frozen and is just experiencing the average potential. This is then repeated for all of the electrons and repeatedly solved iteratively until convergence is obtained.

Several approaches have been developed over the years to calculate this correlation energy. In this work, coupled cluster theory will be used. An intro to CC theory is given in the following subsection.

3.2.2 Coupled-cluster

As mentioned previously, there have been many methods developed that account for the lack of correlation that appears in HF theory. One such method, and the method used throughout this work is coupled cluster theory [18, 25, 66]. It was posed as an alternative to configuration interaction that preserves size consistency while truncating excitation operators. To accomplish this, coupled cluster theory uses an exponential expansion of the cluster or excitation operator $\hat{T}$. Similar to the configuration interaction operator, $\hat{T}$ is formed by a sum of creation and annihilation operators weighted by the coupled cluster amplitudes (t_i^a, t_{ij}^{ab}, t_{ijk}^{abc}, ...) as follows

$$\hat{T_1} \equiv \sum_{ia} t_i^a a_a^\dagger a_i \tag{3.8}$$

$$\hat{T_2} \equiv \frac{1}{4} \sum_{ijab} t_{ij}^{ab} a_a^\dagger a_b^\dagger a_j a_i \tag{3.9}$$

$$\hat{T_3} \equiv \frac{1}{36} \sum_{ijkabc} t_{ijk}^{abc} a_a^\dagger a_b^\dagger a_c^\dagger a_k a_j a_i \tag{3.10}$$

or a general n-orbital cluster operator may be defined as

$$\hat{T_n} \equiv \frac{1}{(n!)^2} \sum_{ijk...abc...} t_{ijk...}^{abc...} a_a^\dagger a_b^\dagger a_c^\dagger .....a_k a_j a_i \tag{3.11}$$

Using this cluster operator, the coupled cluster wavefunction is written as

$$|\Psi_{CC}\rangle = e^{\hat{T}}|\psi_0\rangle \tag{3.12}$$

where

$$\hat{T} = \hat{T}_1 + \hat{T}_2 + \hat{T}_3 + ... + \hat{T}_n \tag{3.13}$$

and $|\psi_0\rangle$ is a Slater determinant that is, in the implementations used here, the Hartree-Fock wavefunction.

In order to generate the resulting coupled cluster wavefunctions, the coupled cluster amplitudes are needed. By taking the Schrödinger equation,

$$\hat{H}|\Psi\rangle = E|\Psi\rangle \tag{3.14}$$

and introducing the coupled cluster wavefunction, the following equation is obtained.

$$\hat{H}e^{\hat{T}}|\psi_0\rangle = E_{CC}e^{\hat{T}}|\psi_0\rangle \tag{3.15}$$

If the left hand side is then multiplied by the reference determinant, the coupled cluster energy is obtained.

$$\langle\psi_0|\hat{H}e^{\hat{T}}|\psi_0\rangle = \langle\psi_0|E_{CC}e^{\hat{T}}|\psi_0\rangle \equiv E_{CC} \tag{3.16}$$

While equation 3.16 is useful to understand the concepts of CC theory, it is unfortunately not well-suited for implementation into software. By rewriting 3.16 in terms of second quantization operators, Equation 3.17 is obtained.

$$\hat{H} = \sum_{pq} h_{pq}a_p^\dagger a_q + \frac{1}{4}\sum_{pqrs}\langle pq||rs\rangle a_p^\dagger a_q^\dagger a_s a_r \tag{3.17}$$

where h_{pq} is the one-electron component of the Hamiltonian and $\langle pq||rs\rangle$ the two-electron antisymmetrized counterpart.

If instead, the coupled cluster equations from Equation 3.15 are multiplied by $e^{-\hat{T}}$ Equation 3.18 obtained

$$\langle\psi_0|e^{-\hat{T}}\hat{H}e^{\hat{T}}|\psi_0\rangle = E_{CC}. \tag{3.18}$$

The equation derived above for the coupled cluster energy along with Equation 3.19

$$\langle\psi_{ijk\ldots}^{abc\ldots}|e^{-\hat{T}}\hat{H}e^{\hat{T}}|\psi_0\rangle = 0. \tag{3.19}$$

form the basis for the development of all coupled cluster methods used in this work. Unlike previously, the energy and cluster amplitudes are decoupled and thus are amenable to software implementation.

3.2.3 Basis Sets

All quantum-chemical methods discussed previously require the use of a one-electron basis composed of a finite number of atomic orbitals, centered at the atomic nucleus within the molecule. Nowadays, linear combinations of Gaussian orbitals are chosen because it is easier to calculate two-electron and other integrals with Gaussian basis functions than with, for example, Slater orbitals. The basis sets employed in this work are briefly described below.

In atomic natural orbital (ANO) basis sets the contraction coefficients are defined by the natural orbitals obtained from atomic calculations using

Table 3.1: Number of basis functions for NO_3^- and NO_3 cm^-1

Number of ANO Basis Functions		
	NO_3^-	NO_3
ANO0	56	57
ANO1	120	121

large primitive basis sets. In this work, a smaller and a larger contraction of the ANO basis set of Taylor and Almlöf [3] are used. For the smaller basis set, the orbitals for all atoms is truncated to 3s2p1d. This basis, which will be referred to as ANO0, is relatively small and is comparable to the size of the well known cc-PVDZ. However, it appears that for anharmonic force fields, ANO0 does better than cc-PVDZ. comparable to that of cc-PVTZ.[84] The larger of the basis sets that will be used for this work consists of 4s3p2d1f orbitals for Nitrogen and Oxygen and 4s2p1d orbitals for Hydrogen. This basis set will be referred to as ANO1. All electronic structure calculations using either ANO0 or ANO1 basis sets did not include core electrons in the correlation treatment. This is often referred to as the frozen-core approximation. The number of basis functions for both the nitrate radical and anion can be seen in Table 3.1

3.3 Adiabatic Calculations Needed for Parameterization

In order to parameterize the vibronic Hamiltonian, a large number of fixed-nuclei adiabatic calculations must be performed. Based on previous work [32, 44, 83, 84], and iterative comparisons of vibronic energy levels determined from purely *ab initio* calculations to those obtained from experiments, the minimum level of theory and basis set size to obtain quantitative accuracy was determined to be EOMIP-CCSDT with an ANO1 basis. The process used for making this determination is described below.

Many "cheap" *ab initio* parameterizations were attempted and resulted in an unacceptable quantitative description of the known energy levels. These parameterizations were done at the EOMIP-CCSD level with both the ANO0 and ANO1 basis sets and were discarded as incapable of describing the NO_3 system in a quantitative fashion. Additionally, when comparing results of parameterization at the CCSD level with a hierarchy of Atomic Natural Orbital basis sets, the following observations were made. The difference between parameters and thus levels at CCSD/ANO0 and CCSD/ANO1 was significant. The difference between CCSD/ANO1 and CCSD/ANO2 was minimal. Thus, the basis set and level of theory combination that was concluded to be the bare minimum for quantitative work on NO_3 was EOMIP-CCSDT/ANO1. While it would be fruitful to consider parameterizations beyond the EOMIP-CCSDT level, current computational resources and code bases prohibit such a calculation. As discussed later (§3.4, even the "minimal" calculations prove to be

quite challenging and posed several obstacles that had to be overcome.

Once the level of theory and the minimum acceptable size of the basis set was determined, there still remained many other computationally-related decisions to be made which are discussed below.

3.3.1 Frequency Calculations and Coordinate System

In order to parameterize our model Hamiltonians, a new coordinate system must be defined. Because the open-shell system NO_3 is quite challenging for even the most advanced multi-reference methods, the Nitrate Anion will be used as the reference state. For all calculations in this work, the well-behaved NO_3^- will be used for the geometry, the source of harmonic vibrational frequencies, ω_i, as well as provide the new coordinate system that will be used to generate the adiabatic potential energy surfaces.

Below is the optimized geometry for the Nitrate radical obtained at CCSDT using an ANO1 basis set.

Table 3.2: Approximate mode description and symmetries of normal coordinates used in the KDC Hamiltonian

Normal coordinates and symmetry species		
q_1	a_1'	symmetric NO stretch
q_3	e'	degenerate NO stretch
q_4	e'	degenerate ONO bend

```
nitrate anion geometry optimization CCSDT/ANO1

O

N 1 R

O 2 R 1 A

O 2 R 1 A 3 T


R    =     1.2582

A    =      120.0

T    =      180.0
```

Then, CCSDT/ANO1 was used employing analytical derivatives to obtain the vibrational frequences of the anion as well as the reduced normal coordinate system.

Table 3.3: Harmonic Vibration Frequencies for the Nitrate Anion ($cm^{-}1$)

	Values at CCSDT/ANO1
ω_1	1060.6
ω_2	858.1
ω_3	1432.4
ω_4	716.4

The resulting reduced normal coordinates in cartesian coordinates (bohr) is as follows:

$q_1 =$

```
 0.0000000000    0.0421222217   -0.0243192760
 0.0000000000    0.0000000000    0.0000000000
 0.0000000000    0.0000000000    0.0486385520
 0.0000000000   -0.0421222217   -0.0243192760
```

$q_2 =$

```
 0.0257007880    0.0000000000    0.0000000000
-0.0880696430    0.0000000000    0.0000000000
 0.0257007880    0.0000000000    0.0000000000
 0.0257007880    0.0000000000    0.0000000000
```

$q_{3a} =$

```
 0.0000000000   -0.0101823876    0.0132127262
```

0.0000000000	0.0000000000	-0.0654215064
0.0000000000	0.0000000000	0.0308491388
0.0000000000	0.0101823876	0.0132127262

$q_{3b} =$

0.0000000000	0.0249703346	-0.0101823876
0.0000000000	-0.0654215064	0.0000000000
0.0000000000	0.0073339220	0.0000000000
0.0000000000	0.0249703346	0.0101823876

$q_{4a} =$

0.0000000000	0.0491882194	0.0363006266
0.0000000000	0.0000000000	-0.0270773122
0.0000000000	0.0000000000	-0.0488958685
0.0000000000	-0.0491882194	0.0363006266

$q_{4b} =$

0.0000000000	-0.0204970368	0.0491882194
0.0000000000	-0.0270773122	0.0000000000
0.0000000000	0.0646994583	0.0000000000
0.0000000000	-0.0204970368	-0.0491882194

3.3.2 Vertical Excitation Energy

Because the vertical excitation energies at the geometry of the reference state used to calculate our force fields is the energy gap of interest, the Nitrate Anion (NO_3^-) geometry at the CCSDT/ANO1 level was used for all energy calculations.

This corresponds to the following geometry:

```
nitrate anion geometry optimization CCSDT/ANO1
O
N 1 R
O 2 R 1 A
O 2 R 1 A 3 T

R    =     1.2582
A    =      120.0
T    =      180.0
```

In this work, two different ways to obtain the vertical gap were explored. First, in order to be consistent with the level of theory used for the remaining calculations in this work (including the adiabatic potential energy surfaces), the vertical cap at CCSDT/ANO1 was considered. A second option for parameterization is to look at a hierarchical series of basis sets and extrap-

Table 3.4: Vertical energy gaps – EOMIP-CCSDT/ANO1

EOMIP-CCSDT/ANO1 energies and resulting gaps at the reference geometry			
	Anion	X^2A_2'	$B^2E'A$
$E_{EOMIP-CCSDT}$ (a.u.)	-280.021154	-279.886169	-279.815974
Vertical gap (e.v.)	-3.67	0	1.910
Vertical gap (cm^-1)	-29626	0	15406

olate the energies of both states (and thus the gap) to their complete basis set (CBS) limit. Both options are explored below.

The vertical gap was first calculated by calculating the single point energy of the ground state (X^2A_2') of nitrate as well as the energy of the A component of the 2nd excited state B^2E' . Both of these calculations were done using the optimized geometry of the anion using EOMIP-CCSDT with the ANO1 basis set. The results are summarized in Table 3.4.

In order to parameterize the vertical energy gap via extrapolation to the CBS limit, the single point energies for the ground electronic state and the second excited state for the Nitrate radical were obtained at the reference anion geometry for the series of basis sets cc-PCVXZ (where X=D,T,Q,5). These calculations were done at the CCSD(T) level with full electron correlation (no dropped core) with a UHF reference.

Table 3.5: CCSDT(T) adiabatic energies at reference geometry

CCSD(T) @ CCSDT/ANO1 (in a.u.)				
	cc-pCVDZ	cc-pCVTZ	cc-pCVQZ	cc-pCV5Z
Anion total energy	-279.840248	-280.201818	-280.313827	-280.351635
X^2A_2' ground state	-279.727710	-280.063661	-280.168727	-280.196174
B^2E' 2nd excited state	-279.660656	-279.998287	-280.098401	-280.130399

To specify the correct state, the occupations were explicitly set.

- Anion occupation - 8-2-5-1 / 8-2-5-1
- X^2A_2' radical ground state - 8-2-5-1 / 8-2-4-1
- $^2A_1$ component of the B^2E' state - 8-2-5-1 / 7-2-5-1

Next we will extrapolate to the CBS limit via two different extrapolations. First the SCF energies will be extrapolated using the formula advocated by Feller:

$$E_{HF}^X = E_{HF}^\infty + a\exp(-bX)$$

where E_{HF}^X are the HF-SCF energies obtained with the cc-pCVXZ basis sets where X=(D,T,Q,5). The parameters a, b, and E_{HF}^∞ can then be uniquely

Table 3.6: Extrapolated HC-SFC energies at reference geometry

HF-SCF extrapolated adiabatic energies (a.u.)			
	Anion	X^2A_2' ground state	B^2E' 2nd excited state
cc-pCVDZ	-278.930282	-278.811289	-278.715841
cc-pCVTZ	-279.026487	-278.900225	-278.803511
cc-pCVQZ	-279.050194	**-278.882165**	-278.824289
cc-pCV5Z	-279.057372	-278.926731	-278.829187
E_{HF}^{234}	-279.057947		-278.830743
E_{HF}^{345}	-279.060489		-278.830699

determined from any 3 of the energies in the basis set series. While the extrapolation using either X=D,T,Q or X=T,Q,5 would provide enough information to inform the parameters, using the above formula with X=D gives horrible results. The cc-pCVDZ calculation is just there to serve as a sanity check. In table 3.6, E_{HF}^{∞} extrapolated with X=T,Q,5 will be referred to as E_{HF}^{345}

At a first cursory glance at table 3.6, it might appear everything looks correct. However, closer inspection of the cc-pCVQZ SCF energy for the ground electronic state (X^2A_2') for the radical shows that it is actually higher in energy when compared to the same state calculated with the smaller cc-pCVTZ basis set. For each of these states, there exists two solutions: one that is symmetry breaking and one that is not. It would appear that in some

Table 3.7: QRHF-CC seeded SCF energy

SCF extrapolation at the reference geometry			
	Anion	X^2A_2'	$B^2E'A$
cc-pCVDZ	-278.930282	-278.772309	-278.715842
cc-pCVTZ	-279.024959	-278.860467	-278.803511
cc-pCVQZ	-279.050195	-278.882165	-278.824289
cc-pCV5Z	-279.057372	-278.887400	-278.829187
E_{HF}^{345}	-279.060225	-278.889064	-278.830699

cases, the SCF energy is converging to the wrong state, the symmetry breaking one. To resolve this, a QRHF-CC method with the closed shell anion was used as the initial guess. This ensures the resulting CCSD(T) calculation has the desired SCF solution. The results for the CCSD(T) energy energy using a QRHC-CC reference based on the close shell anion and set to the desired SCF solution can be seen in Table 3.7.

By comparing the SCF results from the CCSD(T) methods where occupations were explicitly set to the QRHF based methods where SCF occupation for the excited states are estimated by starting from the converged SCF for the reference (anion) state, it can be seen that all of the X^2A_2' calculations (except for cc-pCVQZ) are converging to the symmetry breaking solution. Additionally, it would appear that the Anion calculation at CCSD(T) / cc-pcVTZ is

Table 3.8: QRHF-CC seeded CCSD(T) energy

CCSDT(T) energy at the reference geometry			
	Anion	X^2A_2'	$B^2E'A$
cc-pCVDZ	-279.840248	-279.731357	-279.660656
cc-pCVTZ	-280.201818	-280.068183	-279.998287
cc-pCVQZ	-280.313827	-280.168727	-280.098401
cc-pCV5Z	-280.351635	-280.200874	-280.130399

also converging to the wrong solution.

Next, the $\Delta E_{CCSD(T)}$ energy will be extrapolated to the CBS limit. This is done by taking the difference between the $E_{CCSD(T)}$ energy and the E_{HF} at the same basis set size and then extrapolating this ΔE using the following formula:

$$\Delta E^{X}_{CCSD(T)} = \Delta E^{\infty}_{CCSD(T)} + \frac{a}{X^3}$$

The resulting extrapolated correlation energy can be seen in Table 3.9

Finally, by summing the CBS extrapolated SCF energies and the extrapolated correlation energies, the vertical energy gap for the CBS limit for CCSD(T) and the series of basis sets cc-PCVXZ (X = D,T,Q,5) is obtained. These results are summarized in 3.10

Table 3.9: QRHF-CC seeded correlation energies

Q(CCSD(T)-SCF ($\Delta E_{CCSD(T)}$) at reference geometry			
	Anion	X^2A_2'	$B^2E'A$
cc-pCVDZ	-0.90997	-0.959048	-0.944815
cc-pCVTZ	-1.176860	-1.207716	-1.194776
cc-pCVQZ	-1.263632	-1.286562	-1.274112
cc-pCV5Z	-1.294262	-1.313474	-1.301211
$\Delta E^{45}_{CCSD(T)}$	-1.326399	-1.341710	-1.329643

Table 3.10: Extrapolated vertical energy gaps

Extrapolated CCSD(T) energies at the reference geometry			
	Anion	X^2A_2'	$B^2E'A$
$E^{345}_{CCSD(T)}$	-280.386624	-280.230773	-280.160342
vertical gap (e.v.)	-4.240	0	1.917
vertical gap (cm^-1)	-33880	0	15458

3.3.3 Adiabatic Potential Energy Surfaces

Now that the reduced normal coordinate system, reference state symmetry and vibrational modes have been determined, all that is left computational to start parameterizing the model Hamiltonians are the adiabatic potential energy surfaces for the X^2A_2' state and the A and B components of the B^2E' states.

Three separate three dimensional surfaces must be run and then fit to a 4th order Taylor series to obtain the adiabatic force constants. Each single point is a large calculation in and of itself. At the CCSDT/ANO1 level, a single point for NO_3 takes on the order of 24 hours to complete but more important each point is too large to run within memory of a conventional system. Thus, out-of-core methods must be used. In order to reduce the number of points that must be calculated, a grid refinement study was done.

A number of different grids were run that ranged from 3 x 3 x 3 (27 points) all the way to 25 x 25 x 25 (15625). These calculations were done at the CCSD/ANO0 level, are relatively fast and even the 15625 point calculation finished in minutes when run on a large HPC system due to the conveniently parallel nature of the problem and that each point could easily fit in memory. All of the resulting grids were fit to a 4th order Taylor series.

By comparing the results from the 25 x 25 x 25 and treating it as the true solution, it was able to be determined that the fewest number of points that could be run and still recover adiabatic force constants within a cm^{-1}

was the 9 x 9 x 9 grid.

A series of grids were then run at the CCSDT/ANO1 level over the reduced normal coordinates q_1, q_{3a}, and q_{4a} from -0.2 to 0.2 in increments of 0.05 for a total of 729 points. While this seems trivial to say that these calculations were done, the computational resources required to do such calculations was immense. The main problem stems from the fact that over 2000 jobs have to be run which require large out-of-core solves. Most HPC systems do not have enough node local storage to house the out of job files. Thus, the out-of-core solves must be done over global (network-based) storage. This is sufficient to run a few jobs simultaneously but once one tries to exploit the conveniently parallel nature of these grid runs, many problems occur. On more than one occasion, running as few as 8 points simultaneously were able to bring down some of the largest HPC systems in the world.

In order to combat this, a new method for approaching out-of-core solves in which instead of using global storage, the memory of remote nodes are used to form a pseudo RAM disk that is able to be access by the node running the CFOUR job via MPI and infiniband was developed. The development of this is detailed in §3.4.

3.4 Mapping Out-of-Core Methods to HPC Clusters

Out-of-core methods are encountered in a range of scientific computing disciplines [34, 48, 49, 94] and arise when a single thread does not have sufficient memory locally to support all the data structures required to complete an

analysis. In these cases, application programmers often leverage available disk storage (either local or global depending on the application flexibility and system configuration) to offload excessive data temporarily onto disk. When the application needs to access specific temporary data, it then rereads the data back from disk and continues the analysis and this temporary I/O process is repeated as required. While this approach is effective to circumvent memory constraints for local threads, it does place additional programming requirements on application developers in order to use block storage efficiently. For example, a tuned out-of-core method will require I/O operations to occur on fixed block sizes which may not map directly to the underlying application data structures. In these cases, an aggregation approach is often required within the application. Furthermore, when using a global file system for out-of-core storage, the constant I/O imposed by these methods at large scale can overwhelm even the most capable of parallel file systems causing slower application performance and impacting I/O performance for other system users. Indeed, this file system contention was encountered when CFOUR (§3.1) was used to perform the large adiabatic potential energy surfaces discussed in §3.3.3 on the Ranger system at the Texas Advanced Computing Center (TACC). This experience resulted ultimately in the development of an MPI based out-of-core utility presented herein.

As was discussed previously, high-level *ab initio* calculations that utilize an equation-of-motion coupled-cluster method for singles, doubles and triples (EOMIP-CCSDT) was used to parameterize the model Hamiltonians. Dur-

ing the course of an EOMIP-CCSDT calculation, the storage of the derivative molecular orbital amplitude information requires the largest resources. The storage requirements depend on the number of occupied orbitals, the number of virtual orbitals and the order of the molecular point group. For displaced points from the origin of the NO_3 anion using an ANO1 basis set, the storage of the derivative molecular orbital amplitudes can use up to 57 GB. The compute nodes of the HPC resources used in this work have a max of 48 GB of RAM. While there exist parallel algorithms for the perturbative triples correction calculations used by CCSD(T) calculations, no such algorithm has been developed for CCSDT or EOMIP-CCSDT levels of theory. Thus, out of core methods are required to accomplish the computational task at hand.

As mentioned previously, the initial calculations were performed on the Ranger system and when running small numbers of points simultaneously, the wall clock time for an entire calculation was on the order of two days. However, when running a larger number of points, I/O loads for the global file system increased dramatically, turn around time increased and the system became unresponsive for all users. After further investigation, it was determined that a mere 16 points was consuming the entire global bandwidth for the system. After working with the TACC consulting team, it was requested that only 4 points be run at a time. Assuming an optimistic 24 hour turn around time (including queue time), what remained was well over a year of real time in order to obtain the results. In order to overcome this challenge, an effort was undertaken that allows the aping of this non-traditional workload to modern

HPC systems. By rerouting the out of core workload to the memory of remote nodes (what amounts to a distributed RAM disk) over the highspeed interconnects, the global file system (and thus the 4 simultaneous jobs restriction) can be bypassed entirely. What follows is a discussion of the design of the MPI *Ocore* implementation, the dramatic decrease in real time turn around and future directions and applications will be discussed.

The design and motivation for a RAM based out-of-core utility for use on distributed memory clusters was based on experiences running the CFOUR quantum chemistry application on multiple HPC resources at TACC. From an implementation point of view, the high level goals for this effort were defined as follows:

- provide a flexible API for offloading fixed-length records to remote storage pools which mimics the typical use case of out-of-core methods in quantum chemistry;
- leverage existing HPC point-to-point data transfer mechanisms (MPI) for distributed memory processing;
- remove excessive I/O burden to Lustre file systems at TACC from out-of-core methods and enable the support of multiple user jobs running simultaneously which perform repeated out-of-core solves;
- improve application performance by replacing disk-based I/O with data transfers across high-speed interconnects, e.g. InfiniBand;

- enable quantum chemistry analysis which has traditionally run on small clusters of workstations (configured with large amounts of local scratch disk to accommodate out-of-core solves) to efficiently leverage larger HPC clusters for parametric studies.

Based on these design goals, a prototype version of a RAM-based record offload utility was written in Fortran90 directly within CFOUR. The prototype version was able to successfully intercept disk-based out-of-core operations and offload to a RAM storage pool off-node using MPI to generate simulation results which were identical to the original version. To support a broader community and programming APIs for both C/C++ and Fortran, the prototype was reimplemented and further enhanced within the GRVY toolkit library which has been under active development by the Center for Predictive Engineering and Computational Science (PECOS) center at the Institute for Computational Engineering and Sciences (ICES) over the last several years. This library serves as a centralizing point for housing a variety of support functions often required for application development of HPC scientific applications (including input parsing, logging, floating-point traps, and I/O utilities) for C/C++ and Fortran development [53]. The majority of the library is written in C++ using the popular GNU Autotools build system [95] and provides a directly linkable Fortran interface using *iso_c_bindings* which provides an interoperability layer between C and Fortran included as part of the new Fortran 2003 standard [69]. The library is released under the GNU Lesser GPL license [23].

The overall design of the GRVY out-of-core implementation (*Ocore*) is presented in Figure 3.1 which shows that as opposed to solely using disk-based I/O to support out-of-core methods, the library provides a record-based API to use one or more processes to serve as remote memory pools. *Ocore* provides routines in C/C++ and F95 to offload out-of-core read/write operations to a pool of distributed shared-memory nodes using MPI for data transfer. An additional level of indirection can be enabled to offload less-frequently accessed data to one or more disk-based files.

Note from the figure that the *Ocore* implementation uses point-to-point MPI semantics as the underlying method for performing remote data transfers to/from the main application threads. The total number of Ocore memory pools that are defined remains a runtime choice (guided by application storage requirements) and the library currently adopts a simple round-robin allocation approach to determine which Ocore thread will host newly defined records (for cases when more than 1 Ocore thread is enabled). Once initialized, Ocore threads are solely dedicated to performing read/write operations and the library adopts a polling method in order to respond to Ocore queries from the application. Figure 3.1 also highlights a tiered approach for offloading Ocore records. The first offload mechanism is to RAM based memory pools which effectively serve as a high-performance distributed memory cache. The second offload mechanism possible is to store less frequently accessed records directly to disk when the available RAM-based storage pools become full. This *overflow* storage design was included within the library as a result of the non-

uniform record access pattern that we observed when working with CFOUR (see §3.4 for additional discussion).

Overall, the current design allows a single application thread to offload temporary storage to one or more storage pools via MPI and then offload less-frequently accessed data to disk-based storage if desired. This approach not only minimizes (or removes) the temporary I/O operations from being committed to disk, but can also provide faster read/write access to the out-of-core data on systems with high speed interconnects (e.g. InfiniBand based systems).

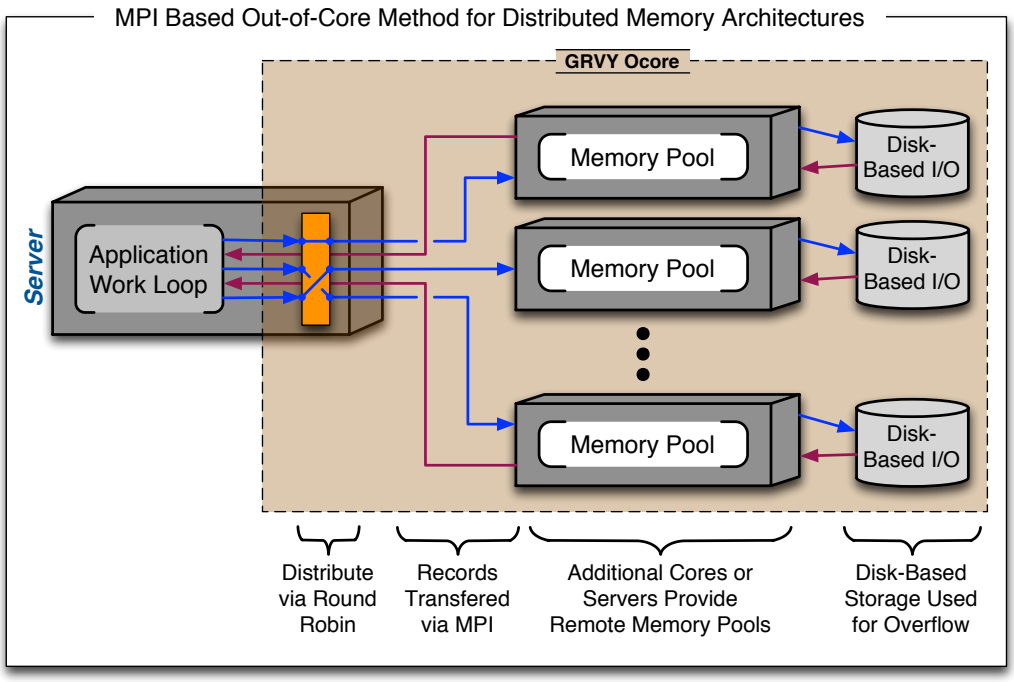

Figure 3.1: Overview of GRVY Ocore design

Example API: To demonstrate Ocore usage, the minimum set of calls necessary to perform out-of-core offloads using the library via the provided C API (and companion APIs exist via a C++ class and F90 module) is presented below. In all cases, the distributed RAM-based memory pools are instantiated via an initialization step which allocates memory buffers based on input controls provided in a keyword driven input file (allowing the application user to set maximum memory constraints and a number of Ocore runtime options).

```
int  grvy_ocore_init (const char *input_file)
```

On completion, Ocore data structures are cleaned up via a simple finalize call which will also generate read/write offload statistics and runtime performance for the application if desired.

```
void grvy_ocore_finalize()
```

Actual data transfer to one or more remote memory pools is accomplished with provided read/write routines based on the underlying transfer datatype. An example illustrating the C API for double precision words is shown as follows:

```
int grvy_ocore_write_double (size_t record_id,
                             double *data)
int grvy_ocore_read_double  (size_t record_id,
                             double *data)
```

Note that to support arbitrary sparse record offloads, the API takes user-provided record Ids and maps them to contiguous internal indices using containers in the Standard Template Library. Similar APIs exist for other intrinsics including *int*, *long int*, and *float* along with their corresponding corollaries in Fortran.

An additional use case identified during the process of including the GRVY *Ocore* implementation within CFOUR was the necessity to dump the instantaneous state of all previously written records. This temporary staging of the current out-of-core state to disk is required as part of the CFOUR workflow which uses the output state from one portion of the analysis as input for a subsequent component. Since the particular file format for saving the state of an out-of-core method is likely to be application specific, the approach taken herein is to provide additional utilities within the library to allow application developers to retrieve sequential Ocore records using a stack pop mechanism to retrieve all active records. An example of this API for C is shown below. In this case, the *size_t* return value from the function is the user-provided Ocore index for the record being returned.

While CFOUR itself is quite a complicated and large code base (1.4 Million lines of code), the actual changes to it to support this new C++ based implementation is astonishingly small. All of the I/O for the out-of-core solves needed to shape a workload for target HPC systems occurs in one routine for reading and one routing for writing. In §A.1, there are the two patchfiles that were generated in order to enable out-of-core support for CFOUR. Other than

error checking, the only real change was to use Ocore's read (or write) function instead of CFOUR's read (or write) function.

By examining the patchfile described in §A.1, it can be seen that CFOUR's read function

```
READ()
```

was replaced with a call to GRVY's *Ocore* function for reading from MPI-based records.

```
grvy_ocore_read_int8()
```

For a more detailed discussion on Ocore and CFOUR integration and implementation, refer to §A.2

In the following discussion, results are presented using the MPI Ocore implementation presented in §3.4 via benchmarking performed on the *Longhorn* cluster [92] at the Texas Advanced Computing Center (TACC). Longhorn has 256 total compute nodes and each node is comprised of dual-socket Intel Nehalem processors running at 2.5GHz for a total of 8 cores per node. Longhorn's high-speed interconnect is supported via a quad data-rate (QDR) InfiniBand (IB) network and all MPI and Lustre I/O traffic runs over this dedicated network. Longhorn was designed to support large-scale data and visualization

analysis (in addition to traditional HPC) and includes 48GB of RAM per node, making it particularly well suited for the MPI-based Ocore method described herein.

To quantify the performance of the GRVY Ocore implementation, a standalone benchmarking test was constructed which mimics the characteristics of an external application reading and writing fixed records in random order as part of an out-of-core solve procedure. To support this effort, a sequence of 1 million random integers was generated using the standard C library implementation of `random()` on the interval $[0, 1000000]$. Note that repeat integer values are included in this sequence to mimic an out-of-core solver overwriting a previous record as part of the solution process. Of the 1 million integers in the sequence, 63.2% are unique values with the remainder being repeated integer values.

To perform the micro-benchmark, the random integer sequence was used as input to define record indices which were sequentially written to one or more Ocore threads on alternate compute nodes. Thus the micro-benchmark requires a minimum of 2 MPI tasks: the first thread uses the GRVY Ocore API to perform a sequence of writes for a fixed blocksize (writing 8-byte doubles in these benchmarks), while the second (and any additional threads) serve as remote Ocore storage pools. For the micro-benchmarking tests, three individual record blocksizes were considered (4K, 8K, and 16K). The CFOUR application is configured to used record blocksizes of 8K, but the GRVY Ocore API supports arbitrary blocksizes and three sizes were considered here to ascertain

performance variations with underlying MPI message sizes. Recall from §3.4 that the Ocore implementation currently utilizes a simple round-robin allocator to map new Ocore records to multiple remote memory pools and adopts a master/slave polling method between the application thread and each remote memory pool task in order to respond to Ocore queries from the application. Consequently, there is some expected overhead associated with the remote record bookkeeping and the micro-benchmark tests include multiple MPI task counts to quantify this overhead. Note that all benchmarking results presented herein were performed on Longhorn in normal production operation. The micro-benchmarks and corresponding GRVY library source (v0.32.0) were compiled using the Intel compiler (v11.1) with MVAPICH2 (v1.4) as the underlying MPI implementation.

In order to provide a baseline for quantifying the MPI Ocore micro-benchmark performance, the raw MPI point-to-point bandwidth of the QDR IB network on Longhorn between two individual hosts was measured using the OSU micro-benchmark suite [55]. Results were averaged over two successive runs and the results are presented in Figure 3.2 with transfer rates of 3000 MB/sec being observed for message sizes in excess of 32KB. These results are typical for a QDR IB network and they help to illustrate an important performance consideration, namely that an application needs to transfer reasonably large messages to take full advantage of the bandwidth afforded by the high-speed MPI network. Fortunately, similar requirements exist to maximize I/O performance and out-of-core solver implementations are often

configured to use larger blocksizes which maps well onto the current MPI Ocore implementation.

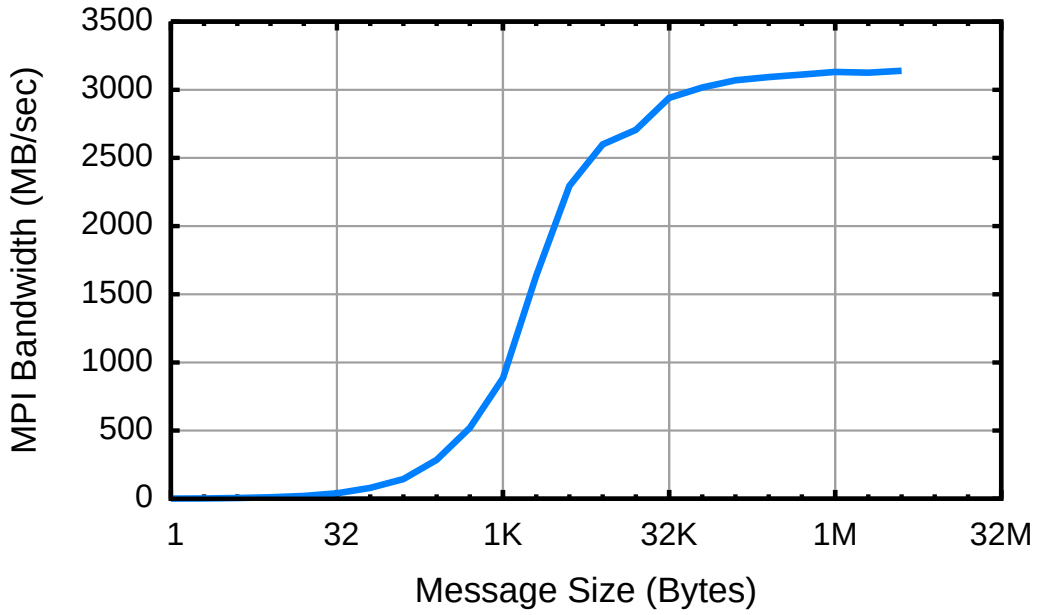

Figure 3.2: Maximum uni-directional point-to-point MPI performance from TACC's Longhorn system running QDR InfiniBand.

The first set of micro-benchmarking results using random record indices are shown in Figure 3.3. These results present the average write performance (as measured via performance timers on the master thread) obtained over two successive runs. For these tests, the benchmark was configured to offload a fixed aggregate amount of data (8GB in total) from the master application thread; consequently the total number of records written varied depending on the chosen record sizes of 4K, 8K, or 16K. For quantitative comparison, the left-most column block of Figure 3.3 shows the raw MPI measurements for

the three blocksizes considered. The left-most column of results are raw MPI measurements from Figure 3.2 for the three block sizes considered and provide a baseline for the maximum MPI bandwidth expected between nodes. Using this baseline, efficiencies of the GRVY Ocore implementation ranged between 83% to 99% for these micro-benchmark measurements. The remaining blocks present the MPI based Ocore performance when offloading to 1, 2, 4 and 8 compute nodes (with 1 Ocore MPI task assigned per node). From this figure, it is evident that larger blocksizes garner slightly improved performance as expected by the raw MPI behavior. In addition, the measured results show no additional overhead incurred in the GRVY Ocore implementation when offloading to multiple nodes; in fact, a slight performance benefit is seen as the node count increases which is most directly attributable to caching benefits engendered as smaller remote memory pools are required with additional nodes. Using the raw MPI measurements as a baseline for efficiency, the Ocore offload speeds in Figure 3.3 ranged from 83% to 99% of the raw MPI bandwidth.

To further quantify the potential benefits of utilizing multiple Ocore threads as remote memory pools on multi-core nodes, a second set of micro-benchmarking tests were performed. In this case, only two compute nodes from Longhorn were used: the first node was again dedicated to utilizing the Ocore API to offload a sequence of random writes (32GB in total for this test), while the second node serves as a remote memory pool. Four different Ocore configurations were considered for the offload node as follows:

- 1 Ocore task - 32GB allocated for memory pool

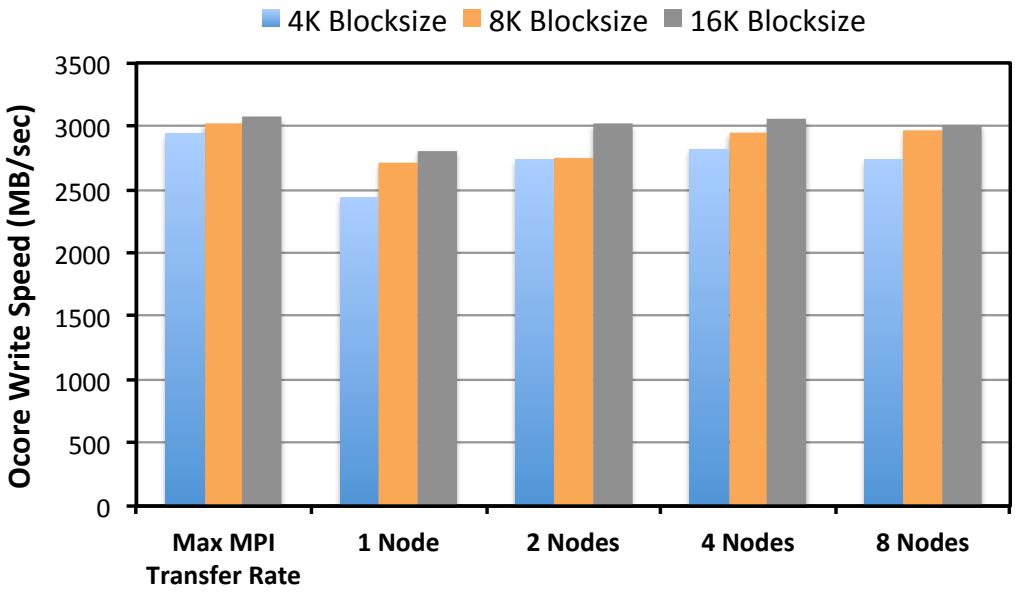

Figure 3.3: Measured write performance of Ocore micro-benchmark offloading a random sequence of records for 4K, 8K, and 16K Ocore blocksizes.

- 2 Ocore tasks - 16GB allocated per memory pool
- 4 Ocore tasks - 8 GB allocated per memory pool
- 8 Ocore tasks - 4 GB allocated per memory pool

The results (averaged over two successive runs) for these tests are shown in Figure 3.4. These results show that the offload performance increases with the number of Ocore tasks assigned per node. In particular, the 8 Ocore tasks per node configuration outperformed 1 Ocore task per node by 21%. Consequently, the recommended task layout configuration when using the GRVY Ocore implementation is to allocate one Ocore task per core on multi-core node configurations. With respect to offload transfer rates, the results in Figure 3.4 ranged between 77% and 93% of the raw MPI performance for the chosen blocksize of 8K.

As mentioned previously, while the original testing was done on Ranger, once the MPI *Ocore* effort was started, the calculations were moved to Longhorn. While the overall system is much smaller, there were four main reasons for the move:

- Faster high-speed interconnect (QDR vs. SDR)
- More memory per compute node (48 GB versus 32 GB)
- Local storage on each compute node (30 GB versus none),
- Shorter queue times.

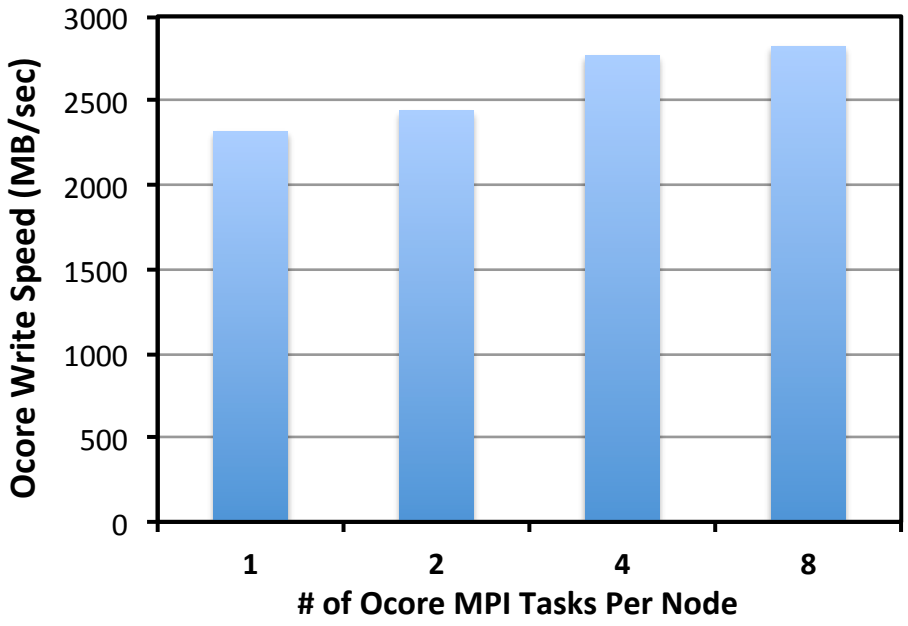

Figure 3.4: Measured write performance of Ocore micro-benchmark offloading 32GB of data (using an 8K blocksize) to a companion 8-core compute node.

While the interconnect of Longhorn is faster than that of Ranger, the $SCRATCH file system is smaller and it is still possible to saturate the bandwidth of the global file system with a relatively small number of CFOUR out of core to disk jobs. In order to determine the effect concurrent out of core to disk jobs would have on the run time of a single fixed-nuclei calculation (a single point in our 9 x 9 x 9 grid), a number of calculations were performed. Only the most resource intensive part of the calculation was run for this test. This bottleneck involves the transformation of perturbed two-electron integrals from an AO basis to a MO basis and the solution of these perturbed amplitude equations. This allows the calculation of second derivatives and excitation energies and is the only portion of these calculations that necessitates out-of-core methods. While running 1 job and 4 jobs at the same time resulted in the same total run time (around 6.5 hours), the average run time for each of 16 points running concurrently was 6% higher or 7 hours. More importantly was that as in the case of Ranger, the global file system became much slower and adversely impacted the work of all users.

The next step was to use the MPI *Ocore* implementation along with the information obtained from the micro-benchmarks detailed above to guide our allocation of resources. All 2200 single point calculations were run using two compute nodes. Four cores of one compute node and 10 GB of memory were used for the main calculation (OpenMP parallelization was obtained using the threaded Intel Math Kernel Libraries) while 32 GB of this same compute node's memory and 32 GB from the second compute node were used to con-

struct our MPI-based RAM disk. Because our largest storage requirement for this series of calculations was 57 GB as previously discussed, this allowed the entire calculation to effectively be run in-core; half of the storage local to the job and the other half accessible in the RAM of the second node accessible via the QDR interconnect. Run time for these jobs were again about 6.5 hours. However, unlike the previous set of calculations, this number did not depend on the number of concurrent CFOUR jobs running on the system. As many as 50 single points were run at the same time with no impact on the global file system. The maximum number of jobs was capped by local policies set via queue restrictions and not any load incurred by the cluster. While each single point remained on average the same speed, the number of points that could be run per day increased dramatically. This coupled with the shorter queue times allowed the total average turn around time for each point to be 12 hours. More importantly, 50 points could be running at the same time. This took our total calculation real time from well over a year to under 30 days.

Another important consideration is the total amount of data *not* written to disk. While the maximum file size needed for the calculation is 57 GB, this is not the total amount of data written to disk but the maximum that must be stored at any one time. For each of these single points that must be run, the derivative molecular orbital amplitude information written during each point is on average 380 GB. Over the course of the entire series of calculations (729 points per state for 3 states), nearly *1 petabyte* is written. Because of the MPI *Ocore* implementation this data was written to local and remote RAM instead

of the global file system.

Due to the nature of EOMIP-CCSDT and its implementation in CFOUR, not all records within the storage of the derivative molecular orbital amplitudes are accessed the same number of times. In the calculations discussed in the previous paragraphs where two nodes were used for the calculation (and 64 GB of RAM over those two nodes used for the RAM disk), all records are treated equally, however, not all records are accessed equally. In fact, there is a large difference between the least accessed record ($<$ 10 reads) and the most accessed record ($>$ 100s of reads).

From Figure 3.5, a fairly non-uniform access pattern can be seen with the majority of the records re-read 100 times or less. Indeed, data from only 25% of the total records defined accounts for 58% of the total data transferred during the analysis. This motivated the creation of a second level of indirection for the GRVY Ocore implementation which allows less frequently accessed records to be offloaded to disk when a high-watermark is reached from available RAM-based storage. The tracking of which records are kept in RAM and which records have been offloaded to disk is done automatically by *Ocore* and is transparent to the application developer. In doing this it is possible to offer storage tiers that are transparent to the application and the data locality is automatically tuned based on usage heuristics.

Because Longhorn compute nodes contain 48 GB of RAM and 30 GB of local scratch disk, this automated data triage allows each single fixed-nuclei calculation to use only one compute node (instead of the two detailed above)

and still be able to bypass the global file system. For this particular CFOUR configuration, approximately 700,000 individual 8K records were read during the out-of-core process requiring in excess of 280 GB of data to be recalled. While the run time can be expected to increase because some of the records will be access via a local disk as opposed to the high speed interconnect, as long as the actual run time is less than twice the 2-node implementation, it is still a net win in terms of resources consumed. In actuality, the resulting one node job was only about 7% slower than the corresponding two node job. By using the overflow options to local disk, the workload was customized for the hardware available and provided a significant savings in required resources.

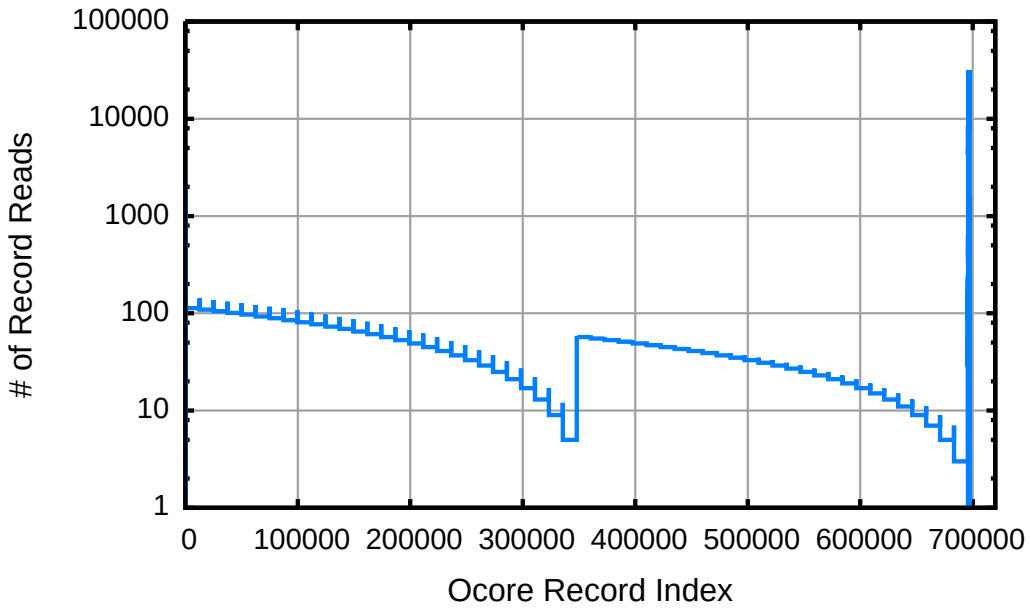

Figure 3.5: Example out-of-core access pattern from CFOUR using GRVY Ocore monitoring

Chapter 4

Models, Parameters and Energy Levels for NO_3

4.1 Anzatzes for a Model Hamiltonian Hierarchy

Over the course of the next several sections, different model anzatzes will be defined which will result in a modeling hierarchy. Models defined and parameterized range from the relatively simple LVC model all the way to a full quartic hamiltonian including linear and bilinear λ terms, full Jahn-Teller effects and will be the most sophisticated quasidiabatic hamiltonian applied to NO_3 (and arguably any molecule) to date.

The remaining sections in this chapter will detail modifications to the full quartic *ab initio* quasidiabatic hamiltonian that rely on group theory arguments as well as experimental data and modeling experience to augment the model such that a predictive model hamiltonian is arguably achieved.

4.2 Linear Vibronic Coupling

The Linear Vibronic Coupling (LVC) model is the simplest of the vibronic coupling models that one can consider. By taking the model proposed by Köppel et al as discussed in §2.1 and truncating after linear terms, there

remains only 10 unique parameters that must be obtained. All of these parameters can be obtained directly from adiabatic calculations.

The gap between the X^2A_2' and B^2E' states (denoted as Δ) was calculated using EOMIP-CCSDT with an ANO1 basis. The geometry of both the ground and excited states used was that of the anion (NO_3^-) optimized at the CCSDT level of theory. This is often referred to as the "vertical gap". The vibrational frequencies ($\omega_1, \omega_3, \omega_4$) are those of the anion as well and were also done at EOMIP-CCSDT / ANO1 using standard finite difference techniques.

The linear coupling constants (e.g. $\lambda_{3;\tilde{\mathbf{X}}\tilde{\mathbf{B}}_\mathbf{b}}$) were calculated analytically using CFOUR.While the reference geometry was the same geometry as those in the previous calculations (Anion; CCSDT/ANO1), this calculation can only be run using EOMIP-CCSD. Unfortunately, EOMIP-CCSDT analytical λ terms have not been implemented as of yet. While this is something that would be of some utility, it is a tremendous undertaking.

The diabatic force constants for LVC were determined as follows. A 4th order Taylor series fit to a series of adiabatic potential energy surfaces was used to determine adiabatic force constants. These surfaces were generated using CFOUR as well. If our coordinate system for these grid calculations is set such that our 3 displacement dimensions are along the reduced normal coordinates q_1, q_{3a}, and q_{4a} discussed in §3.3.1, the resulting adiabatic force constants can be used to determine their diabatic counterparts.

In order to preserve symmetry of the resulting model Hamiltonian, the

relationships listed in equations 4.1 – 4.5 must be obeyed.

$$F_{1;\tilde{\mathbf{B}}_\mathbf{b}} = F_{1;\tilde{\mathbf{B}}_\mathbf{a}} = 440.5 \tag{4.1}$$

$$F_{3;\tilde{\mathbf{B}}_\mathbf{b}} = -F_{3;\tilde{\mathbf{B}}_\mathbf{a}} = -440.7; F_{5;\tilde{\mathbf{B}}_\mathbf{a}\tilde{\mathbf{B}}_\mathbf{b}} = F_{3;\tilde{\mathbf{B}}_\mathbf{a}} = 440.7 \tag{4.2}$$

$$F_{4;\tilde{\mathbf{B}}_\mathbf{b}} = -F_{4;\tilde{\mathbf{B}}_\mathbf{a}} = -762.2; F_{6;\tilde{\mathbf{B}}_\mathbf{a}\tilde{\mathbf{B}}_\mathbf{b}} = F_{3;\tilde{\mathbf{B}}_\mathbf{a}} = 762.2 \tag{4.3}$$

$$\lambda_{5;\tilde{\mathbf{X}}\tilde{\mathbf{B}}_\mathbf{a}} = \lambda_{3;\tilde{\mathbf{X}}\tilde{\mathbf{B}}_\mathbf{b}} = 2974.5 \tag{4.4}$$

$$\lambda_{6;\tilde{\mathbf{X}}\tilde{\mathbf{B}}_\mathbf{a}} = \lambda_{4;\tilde{\mathbf{X}}\tilde{\mathbf{B}}_\mathbf{b}} = -1141.1 \tag{4.5}$$

If the LVC Hamiltonian constants shown in table 4.2 are used along with the equations defined in 4.1 – 4.5, the full LVC hamiltonian is obtained. This hamiltonian is then solved iteratively using 2500 lanczos recursions with a basis set of 20 on each of the 5 vibrational modes (ω_1 and the doubly degenerate ω_3 and ω_4) in this coupled hamiltonian the following e' levels are obtain as listed in Table 4.2.

While the LVC model is simple to parameterize, it appears to be lacking most of the physics need to start to describe the complex vibronic interactions that plague NO_3. As will be seen in the following sections, bilinear λ terms,

Table 4.1: LVC Hamiltonian Constants (in $cm^{-}1$)

Hamiltonian constants	
Parameter	EOMIP-CCSDT/ANO1
Δ	15406
ω_1	1060.6
ω_3	1432.4
ω_4	716.4
$F_{1;\tilde{\mathbf{X}}}$	-868.2
$F_{1;\tilde{\mathbf{B}}_\mathbf{a}}$	440.5
$F_{3;\tilde{\mathbf{B}}_\mathbf{a}}$	440.7
$F_{4;\tilde{\mathbf{B}}_\mathbf{a}}$	762.2
$\lambda_{3;\tilde{\mathbf{X}}\tilde{\mathbf{B}}_\mathbf{b}}$	2974.5
$\lambda_{4;\tilde{\mathbf{X}}\tilde{\mathbf{B}}_\mathbf{b}}$	-1141.1

Table 4.2: Levels versus Experimental Values (in $cm^{-}1$) for the LVC

LVC	Experimental
460	365
953	?
989	?
1474	1173
1486	1413
1537	1492
1959	1562
1986	
1990	
2000	
2041	1917
2047	
2068	

quadratic Jahn-teller terms, and even cubic λ terms and cubic and quartic Jahn-Teller distortions play an important roll in not only quantitatively level determined but also even in qualitative behavior.

4.3 Quadratic Vibronic Coupling

For the Quadratic Vibronic Coupling (QVC) modeling, two different QVC models were actually constructed. The first model considered below is a QVC model with all Jahn-Teller distortions removed. During the construction of the LVC model above, the values for the force constants for the B component of the B^2E' state were explicitly set to those of the A component. However, if these two constants were independently obtained from their re-

spective fits, they would still be equivalent. This is not the case for quadratic force constants. This arises from Jahn-Teller interactions. In order to ascertain the impact that this diabatic effect has on the energy levels, the first model constructed artificially removes these contributions by averaging the diabatic force constants for the A and B components thus removing it altogether. This model will be referred to as QVC.1. The second QVC model constructed will be the full quadratic diabatic model of the KDC form described earlier in §2.1. This model will be referred to as QVC.2 or full QVC.

4.3.1 QVC with No Jahn-Teller Coupling – QVC.1

The first of our two Quadratic Vibronic Coupling (QVC) models presented in this work involves the simple extension of the LVC model presented above by adding additional terms that appear along the diagonal of our model Hamiltonian. Thus, no Jahn-Teller splitting of the two components of the B^2E' state is considered. What remains are 21 unique parameters which much be obtained.

As in the LVC, as well as the remaining of our pure *ab initio* model hamiltonians, the vertical gap (Δ) and the vibration frequences ($\omega_1, \omega_3, \omega_4$) were obtained with adiabatic calculations done with CFOUR as detailed in §4.2. Furthermore, the same adiabatic potential energy surfaces were used to determine the adiabatic force constants. Unlike the LVC case, not all of the fitted adiabatic force constants obtained are equivalent to their diabatic force constant counterparts. Due to the off-diagonal linear λ terms, one must obtain

the so-called "diabatic correction". The diabatic correction when applied to the adiabatic force constants gives you the corresponding diabatic force constant. This can be seen in Equation 4.6 where $F_{mm;\tilde{\mathbf{S}}}$ is the quadratic diabatic force constant for mode mm of state S, $f_{mm;\tilde{\mathbf{S}}}$ is the quadratic adiabatic force constant for mode mm of state S and $\delta_{mm;\tilde{\mathbf{S}}}$ is the difference between them.

$$F_{mm;\tilde{\mathbf{S}}} = f_{mm;\tilde{\mathbf{S}}} - \delta_{mm;\tilde{\mathbf{S}}} \tag{4.6}$$

In the LVC model, it was specifically enforced that the diabatic force constants for each mode were equivalent for the degenerate B^2E' states. If this were not the case, and the force constants had been obtained by separate fits to their respective adiabatic force fields, the values would still be equal. There are no effects present at the LVC level which would cause their values to differ. This is not the case for the parameterization of this QVC model. For instance, the adiabatic value obtained for $f_{33;\tilde{\mathbf{B}}_\mathbf{a}}$ is 819.1 cm^{-1} while the value for $f_{33;\tilde{\mathbf{B}}_\mathbf{b}}$ is 2027.0 cm^{-1}. Additionally, while the diabatic $F_{33;\tilde{\mathbf{B}}_\mathbf{a}}$ is equal to the adiabatic $f_{33;\tilde{\mathbf{B}}_\mathbf{a}}$ obtained from the fits, this is not the case for the B component of the B^2E' state. The additional diabatic correction discussed above must be obtained.

As was discussed previously, the diabatic corrections for the quadratic coupling constants can be obtained in a straightforward manner. The result can be seen in Equation 4.7. Once the diabatic force constants for both the A and B components of the B^2E' state are derived, they are still not equivalent

unlike their linear counterparts. This is the result of Jahn-Teller distortions. In order to preserve symmetry an additional term must be added if the full QVC were being constructed. However, for this particular model, no JT distortions are considered. In order to artificially force this, a new value will be assigned to both diabatic constants which will be the average of their adiabatic values. These new parameters will be referred to as $F'_{mn;\tilde{\mathbf{B}}_\mathbf{a}}$ and $F'_{mn;\tilde{\mathbf{B}}_\mathbf{b}}$ respectively.

$$F_{mn;\tilde{\mathbf{S}}} = f_{mn;\tilde{\mathbf{S}}} - \frac{2\lambda_m\lambda_n}{\Delta} \tag{4.7}$$

What follows are the relationships that must be obeyed in order to preserve symmetry. Also listed below are the averaging of the JT effected parameters in order to remove this effect. The adiabatic values obtained from the fits as well as the diabatic corrections are listed in §B.1

$$F_{1;\tilde{\mathbf{B}}_\mathbf{b}} = F_{1;\tilde{\mathbf{B}}_\mathbf{a}} = 440.5 \tag{4.8}$$

$$\lambda_{5;\tilde{\mathbf{X}}\tilde{\mathbf{B}}_\mathbf{a}} = \lambda_{3;\tilde{\mathbf{X}}\tilde{\mathbf{B}}_\mathbf{b}} = \ 2974.5 \tag{4.9a}$$

$$\lambda_{6;\tilde{\mathbf{X}}\tilde{\mathbf{B}}_\mathbf{a}} = \lambda_{4;\tilde{\mathbf{X}}\tilde{\mathbf{B}}_\mathbf{b}} = -1141.1 \tag{4.9b}$$

$$F_{11;\tilde{\mathbf{B}}_\mathbf{b}} = F_{11;\tilde{\mathbf{B}}_\mathbf{a}} = 1070.8 \tag{4.10}$$

$$F_{55;\tilde{\mathbf{X}}} = F_{33;\tilde{\mathbf{X}}} = 1573.0 \tag{4.11a}$$

$$F_{66;\tilde{\mathbf{X}}} = F_{44;\tilde{\mathbf{X}}} = 575.6 \tag{4.11b}$$

$$F_{56;\tilde{\mathbf{X}}} = F_{34;\tilde{\mathbf{X}}} = -34.6 \tag{4.11c}$$

$$F_{33;\tilde{\mathbf{B}}_\mathbf{a}} = 819.1; F_{33;\tilde{\mathbf{B}}_\mathbf{b}} = 878.4 \tag{4.12a}$$

$$F'_{33;\tilde{\mathbf{B}}_\mathbf{a}} = \frac{F_{33;\tilde{\mathbf{B}}_\mathbf{a}} + F_{33;\tilde{\mathbf{B}}_\mathbf{b}}}{2} = 848.75 \tag{4.12b}$$

$$F'_{55;\tilde{\mathbf{B}}_\mathbf{b}} = F'_{33;\tilde{\mathbf{B}}_\mathbf{b}} = F'_{55;\tilde{\mathbf{B}}_\mathbf{a}} = F'_{33;\tilde{\mathbf{B}}_\mathbf{a}} = 848.75 \tag{4.12c}$$

$$F_{44;\tilde{\mathbf{B}}_\mathbf{a}} = 677.5; F_{44;\tilde{\mathbf{B}}_\mathbf{b}} = 557.2 \tag{4.13a}$$

$$F'_{44;\tilde{\mathbf{B}}_\mathbf{a}} = \frac{F_{44;\tilde{\mathbf{B}}_\mathbf{a}} + F_{44;\tilde{\mathbf{B}}_\mathbf{b}}}{2} = 617.35 \tag{4.13b}$$

$$F'_{66;\tilde{\mathbf{B}}_\mathbf{b}} = F'_{44;\tilde{\mathbf{B}}_\mathbf{b}} = F'_{66;\tilde{\mathbf{B}}_\mathbf{a}} = F'_{44;\tilde{\mathbf{B}}_\mathbf{a}} = 617.35 \tag{4.13c}$$

$$F_{34;\tilde{\mathbf{B}}_\mathbf{a}} = 83.0; F_{34;\tilde{\mathbf{B}}_\mathbf{b}} = 156.2 \tag{4.14a}$$

$$F'_{34;\tilde{\mathbf{B}}_\mathbf{a}} = \frac{F_{34;\tilde{\mathbf{B}}_\mathbf{a}} + F_{34;\tilde{\mathbf{B}}_\mathbf{b}}}{2} = 119.6 \tag{4.14b}$$

$$F'_{56;\tilde{\mathbf{B}}_\mathbf{b}} = F'_{34;\tilde{\mathbf{B}}_\mathbf{b}} = F'_{56;\tilde{\mathbf{B}}_\mathbf{a}} = F'_{34;\tilde{\mathbf{B}}_\mathbf{a}} = 119.6 \tag{4.14c}$$

$$F_{13;\tilde{\mathbf{B}}_\mathbf{b}} = -F_{13;\tilde{\mathbf{B}}_\mathbf{a}}; F_{15;\tilde{\mathbf{B}}_\mathbf{a}\tilde{\mathbf{B}}_\mathbf{b}} = F_{13;\tilde{\mathbf{B}}_\mathbf{a}} \tag{4.15}$$

$$F_{14;\tilde{\mathbf{B}}_\mathbf{b}} = -F_{14;\tilde{\mathbf{B}}_\mathbf{a}}; F_{16;\tilde{\mathbf{B}}_\mathbf{a}\tilde{\mathbf{B}}_\mathbf{b}} = F_{14;\tilde{\mathbf{B}}_\mathbf{a}} \tag{4.16}$$

4.3.2 QVC with Jahn-Teller Coupling – QVC.2

In the LVC model, the linear contributions for both components of the B^2E' electronic state were equivalent. Additionally, the diabatic values are the same as those obtained from fitting of the adiabatic force field. This is not the case for the quadratic terms. As discussed in §4.3.1, due to the linear λ terms, symmetry and Jahn-Teller distortions, only the quadratic force constants for the A component of the B^2E' state are equivalent for adiabatic and diabatic. However, from the analytically obtained linear λ terms, the resulting diabatic corrections that were discussed previously, and the following relationships in Equations 4.17 –4.30 all of the necessary force constants can be obtained. The resulting QVC.2 model has 23 unique parameters which then can be used to obtain all of the force constants needed to preserve symmetry.

The linear terms that appear in the QVC.2 model hamiltonian are the same ones that were detailed previously in sections §4.2 and §4.3.1. The adiabatic force constants that were used as a starting point to determine the diabatic values are listed in §B.2 as well as their corresponding analytically determined diabatic correction.

$$F_{11;\tilde{\mathbf{B}}_\mathbf{b}} = F_{11;\tilde{\mathbf{B}}_\mathbf{a}} = 1070.8 \tag{4.17}$$

Table 4.3: QVC Hamiltonian Constants (in $cm^{-}1$) Neglecting Jahn-Teller

Hamiltonian constants for QVC.1	
Parameter	EOMIP-CCSDT/ANO1
Δ	15406
ω_1	1060.6
ω_3	1432.4
ω_4	716.4
$F_{1;\tilde{\mathbf{X}}}$	-868.2
$F_{1;\tilde{\mathbf{B}}_\mathbf{a}}$	440.5
$F_{3;\tilde{\mathbf{B}}_\mathbf{a}}$	440.7
$F_{4;\tilde{\mathbf{B}}_\mathbf{a}}$	762.2
$\lambda_{3;\tilde{\mathbf{X}}\tilde{\mathbf{B}}_\mathbf{b}}$	2974.5
$\lambda_{4;\tilde{\mathbf{X}}\tilde{\mathbf{B}}_\mathbf{b}}$	-1141.1
$F_{11;\tilde{\mathbf{X}}}$	960.3
$F_{11;\tilde{\mathbf{B}}_\mathbf{a}}$	1070.8
$F_{33;\tilde{\mathbf{X}}}$	1573.0
$F_{44;\tilde{\mathbf{X}}}$	575.6
$F_{34;\tilde{\mathbf{X}}}$	-34.6
$F'_{33;\tilde{\mathbf{B}}_\mathbf{a}}$	848.75
$F'_{44;\tilde{\mathbf{B}}_\mathbf{a}}$	617.35
$F_{34;\tilde{\mathbf{B}}_\mathbf{a}}$	83.0
$F_{34;\tilde{\mathbf{B}}_\mathbf{b}}$	156.2
$F_{13;\tilde{\mathbf{B}}_\mathbf{a}}$	-61.3
$F_{14;\tilde{\mathbf{B}}_\mathbf{a}}$	66.4

$$F_{55;\tilde{\mathbf{X}}} = F_{33;\tilde{\mathbf{X}}} = 1573.0 \tag{4.18a}$$

$$F_{66;\tilde{\mathbf{X}}} = F_{44;\tilde{\mathbf{X}}} = 575.6 \tag{4.18b}$$

$$F_{56;\tilde{\mathbf{X}}} = F_{45;\tilde{\mathbf{X}}} = -34.6 \tag{4.19}$$

$$F_{55;\tilde{\mathbf{B}}_\mathbf{b}} = F_{33;\tilde{\mathbf{B}}_\mathbf{a}} = 819.1 \tag{4.20}$$

$$F_{55;\tilde{\mathbf{B}}_\mathbf{a}} = F_{33;\tilde{\mathbf{B}}_\mathbf{b}} = 878.4 \tag{4.21}$$

$$F_{35;\tilde{\mathbf{B}}_\mathbf{a}\tilde{\mathbf{B}}_\mathbf{b}} = \frac{F_{33;\tilde{\mathbf{B}}_\mathbf{a}} - F_{33;\tilde{\mathbf{B}}_\mathbf{b}}}{2} = \frac{819.1 - 878.4}{2} = -29.65 \tag{4.22}$$

$$F_{66;\tilde{\mathbf{B}}_\mathbf{b}} = F_{44;\tilde{\mathbf{B}}_\mathbf{a}} = 677.5 \tag{4.23}$$

$$F_{66;\tilde{\mathbf{B}}_\mathbf{a}} = F_{44;\tilde{\mathbf{B}}_\mathbf{b}} = 557.2 \tag{4.24}$$

$$F_{46;\tilde{\mathbf{B}}_\mathbf{a}\tilde{\mathbf{B}}_\mathbf{b}} = \frac{F_{44;\tilde{\mathbf{B}}_\mathbf{a}} - F_{44;\tilde{\mathbf{B}}_\mathbf{b}}}{2} = \frac{677.5 - 557.2}{2} = 60.15 \tag{4.25}$$

$$F_{56;\tilde{\mathbf{B}}_\mathbf{b}} = F_{34;\tilde{\mathbf{B}}_\mathbf{a}} = 83.0 \tag{4.26}$$

$$F_{56;\tilde{\mathbf{B}}_\mathbf{a}} = F_{34;\tilde{\mathbf{B}}_\mathbf{b}} = 156.2 \tag{4.27}$$

$$F_{54;\tilde{\mathbf{B}}_\mathbf{a}\tilde{\mathbf{B}}_\mathbf{b}} = \frac{F_{34;\tilde{\mathbf{B}}_\mathbf{b}} - F_{34;\tilde{\mathbf{B}}_\mathbf{a}}}{2} = \frac{156.2 - 83.0}{2} = 36.6 \tag{4.28a}$$

$$F_{36;\tilde{\mathbf{B}}_\mathbf{a}\tilde{\mathbf{B}}_\mathbf{b}} = \frac{F_{34;\tilde{\mathbf{B}}_\mathbf{b}} - F_{34;\tilde{\mathbf{B}}_\mathbf{a}}}{2} = \frac{156.2 - 83.0}{2} = 36.6 \tag{4.28b}$$

$$F_{13;\tilde{\mathbf{B}}_\mathbf{b}} = -F_{13;\tilde{\mathbf{B}}_\mathbf{a}} = 61.3 \tag{4.29a}$$

$$F_{15;\tilde{\mathbf{B}}_\mathbf{a}\tilde{\mathbf{B}}_\mathbf{b}} = F_{13;\tilde{\mathbf{B}}_\mathbf{a}} = -61.3 \tag{4.29b}$$

$$F_{14;\tilde{\mathbf{B}}_\mathbf{b}} = -F_{14;\tilde{\mathbf{B}}_\mathbf{a}} = -66.4 \tag{4.30a}$$

$$F_{16;\tilde{\mathbf{B}}_\mathbf{a}\tilde{\mathbf{B}}_\mathbf{b}} = F_{14;\tilde{\mathbf{B}}_\mathbf{a}} = 66.4 \tag{4.30b}$$

Just like with the LVC hamiltonian, the hamiltonians constructed for QVC.1 and QVC.2 (or full JT QVC) were solved via Lanczos recursions and 20 harmonic basis functions per mode. The results for these models as well as LVC, experimental values and the difference between QVC.1 and QVC.2 (and thus the effect of quadratic JT) is shown in Table 4.3.2.

As expected, the QVC.1 gives horrible results. This parameterization was not expected to reflect a reasonable parametrization for the problem under study, but was meant to be used to ascertain how strong these JT distortions

Table 4.4: QVC Hamiltonian Constants (in $cm^{-}1$) with Jahn-Teller Distortions

Hamiltonian constants for QVC.2	
Parameter	EOMIP-CCSDT/ANO1
Δ	15406
ω_1	1060.6
ω_3	1432.4
ω_4	716.4
$F_{1;\tilde{\mathbf{X}}}$	-868.2
$F_{1;\tilde{\mathbf{B}}_\mathbf{a}}$	440.5
$F_{3;\tilde{\mathbf{B}}_\mathbf{a}}$	440.7
$F_{4;\tilde{\mathbf{B}}_\mathbf{a}}$	762.2
$\lambda_{3;\tilde{\mathbf{X}}\tilde{\mathbf{B}}_\mathbf{b}}$	2974.5
$\lambda_{4;\tilde{\mathbf{X}}\tilde{\mathbf{B}}_\mathbf{b}}$	-1141.1
$F_{11;\tilde{\mathbf{X}}}$	960.3
$F_{11;\tilde{\mathbf{B}}_\mathbf{a}}$	1070.8
$F_{33;\tilde{\mathbf{X}}}$	1573.0
$F_{44;\tilde{\mathbf{X}}}$	575.6
$F_{34;\tilde{\mathbf{X}}}$	-34.6
$F_{33;\tilde{\mathbf{B}}_\mathbf{a}}$	819.1
$F_{33;\tilde{\mathbf{B}}_\mathbf{b}}$	878.4
$F_{44;\tilde{\mathbf{B}}_\mathbf{a}}$	677.5
$F_{44;\tilde{\mathbf{B}}_\mathbf{b}}$	557.2
$F_{34;\tilde{\mathbf{B}}_\mathbf{a}}$	83.0
$F_{34;\tilde{\mathbf{B}}_\mathbf{b}}$	156.2
$F_{13;\tilde{\mathbf{B}}_\mathbf{a}}$	-61.3
$F_{14;\tilde{\mathbf{B}}_\mathbf{a}}$	66.4

Table 4.5: Levels versus Experimental Values (in cm^-1) for LVC QVC.1 and QVC.2

LVC	QVC.1	QVC.2	$\delta_{qvc1;qvc2}$	Experimental
460	197	374	177	365
953	554	777	223	?
989	773	1188	415	?
1474	922	1380	458	1173
1486	1102	1390	288	1413
1537	1185	1615	430	1492
1959	1196	1636	440	1562
1986	1216	1774	558	
1990	1291	1790	499	
2000	1318	1830	512	
2041	1408	1983	575	1917
2047	1546	2005	459	
2068	1569	2053	484	

are in this molecule and is one of the sources of frustration for computational chemists and spectroscopists.

4.4 Quartic Vibronic Coupling

As mentioned previously, the end goal of this work was to parameterize a quantitatively accurate pure *ab initio* model Hamiltonian. As seen when comparing the resulting levels from QVC.1 and QVC.2, Jahn-Teller distortions greatly impact the vibronic level position. This is in agreement with theoretical work that has been done on the nitrate radical in the literature. However, none of the previous work on NO_3 has gone beyond the quadratic vibronic coupling model. Due to the large distortions imparted by quadratic Jahn-Teller and, as will be seen, the rather large bilinear λ terms, it stands to reason that cubic and quartic contributions should impact the level positions significantly.

In order to construct the full Quartic Vibronic Coupling (4VC) model, a method for obtaining bilinear λ terms as well as the numerous diabatic correction terms must be determined. As discussed in §3.2.2 and §4.2, CFOUR has the capability to obtain linear λ terms analytically, although this is limited to the EOMIP-CCSD level. In order to obtain bilinear λ terms, multiple linear λ terms calculations can be run at different geometries. These geometries are generated such that the molecular structure is following the motion of the reduced normal coordinate system of the Nitrate anion. Using these results along with standard finite difference methods, the bilinear λ terms can be obtained. Five such groups of calculations were run in order to determine the

minimum number of bilinear λ terms to parameterize the 4VC Hamiltonian. The remaining bilinear λ terms can be obtained via symmetry arguments. The relationships need to obtain all of the bilinear λ terms are listed in Equations 4.31 – 4.35 and the values obtained from CFOUR via finite difference are in Table 4.6.

$$\lambda_{15;\tilde{\mathbf{X}}\tilde{\mathbf{B}}_\mathbf{a}} = \lambda_{13;\tilde{\mathbf{X}}\tilde{\mathbf{B}}_\mathbf{b}} = 136.0 \tag{4.31}$$

$$\lambda_{16;\tilde{\mathbf{X}}\tilde{\mathbf{B}}_\mathbf{a}} = \lambda_{14;\tilde{\mathbf{X}}\tilde{\mathbf{B}}_\mathbf{b}} = -127.0 \tag{4.32}$$

$$\lambda_{55;\tilde{\mathbf{X}}\tilde{\mathbf{B}}_\mathbf{b}} = -\lambda_{33;\tilde{\mathbf{X}}\tilde{\mathbf{B}}_\mathbf{b}} = -126.0 \tag{4.33a}$$

$$\lambda_{35;\tilde{\mathbf{X}}\tilde{\mathbf{B}}_\mathbf{a}} = -\lambda_{33;\tilde{\mathbf{X}}\tilde{\mathbf{B}}_\mathbf{b}} = -126.0 \tag{4.33b}$$

$$\lambda_{66;\tilde{\mathbf{X}}\tilde{\mathbf{B}}_\mathbf{b}} = -\lambda_{44;\tilde{\mathbf{X}}\tilde{\mathbf{B}}_\mathbf{b}} = 141.0 \tag{4.34a}$$

$$\lambda_{46;\tilde{\mathbf{X}}\tilde{\mathbf{B}}_\mathbf{a}} = -\lambda_{44;\tilde{\mathbf{X}}\tilde{\mathbf{B}}_\mathbf{b}} = 141.0 \tag{4.34b}$$

$$\lambda_{56;\tilde{\mathbf{X}}\tilde{\mathbf{B}}_\mathbf{b}} = -\lambda_{34;\tilde{\mathbf{X}}\tilde{\mathbf{B}}_\mathbf{b}} = -40.0 \tag{4.35a}$$

$$\lambda_{36;\tilde{\mathbf{X}}\tilde{\mathbf{B}}_\mathbf{a}} = -\lambda_{34;\tilde{\mathbf{X}}\tilde{\mathbf{B}}_\mathbf{b}} = -40.0 \tag{4.35b}$$

$$\lambda_{54;\tilde{\mathbf{X}}\tilde{\mathbf{B}}_\mathbf{a}} = -\lambda_{34;\tilde{\mathbf{X}}\tilde{\mathbf{B}}_\mathbf{b}} = -40.0 \tag{4.35c}$$

Table 4.6: 4VC Bilinear λ terms in $cm^{-}1$)

Hamiltonian constants for 4VC	
Parameter	EOMIP-CCSDT/ANO1
$\lambda_{13;\tilde{\mathbf{X}}\tilde{\mathbf{B}}_\mathbf{b}}$	136.0
$\lambda_{14;\tilde{\mathbf{X}}\tilde{\mathbf{B}}_\mathbf{b}}$	-127.0
$\lambda_{33;\tilde{\mathbf{X}}\tilde{\mathbf{B}}_\mathbf{b}}$	126.0
$\lambda_{44;\tilde{\mathbf{X}}\tilde{\mathbf{B}}_\mathbf{b}}$	-141.0
$\lambda_{34;\tilde{\mathbf{X}}\tilde{\mathbf{B}}_\mathbf{b}}$	136.0

Now that the bilinear λ terms have been obtained, all that remains is a method by which to generate the diabatic corrections so that the easily obtained adiabatic force constant can be mapped to their diabatic counterparts. While this could be done analytically (as was done for the quadratic parameters), the shear number of corrections that must be obtained begs for an implementation whereby they can be obtained numerically. Once a numeric implemented is determined, it can then be automated via software. In addition, once one has a software implementation to obtain diabatic corrections numerically, it can be applied to any system of interest. An analytical implementation would need to be redone for every new molecular system.

In order to define numerically the mapping from adiabatic to diabatic

coupling constant, one must understand why the difference arises in the first place. Adiabatic surfaces capture diagonal terms in the potential energy term of our hamiltonian. Any non-diagonal term that appears in our Hamiltonian (be it λ terms or Jahn-Teller distortions) results in a difference between the diabatic and adiabatic force constant. Using this reasoning, the following method for determined the diabatic corrections numerically can be deduced.

As we have seen in the previous sections, once we have the adiabatic surfaces along the three reduced normal coordinates, q_1, q_3a, q_4a, most of the linear and quadratic diabatic constants can be obtained directly from the adiabatic force constants obtained by fitting a 4th order Taylor series. Depending on symmetry, the diabatic force constant is either equivalent to its adiabatic counterpart or a simple analytical correction (that depends on λ and the gap) can be applied. Also, as detailed previously, CFOUR has analytical linear λ terms and the necessary bilinear λ terms can be generated via finite difference.

As was seen in §4.3.1, the linear λ terms cause Jahn-Teller distortions such that some coupling constants for the A and B components of the B^2E' state are not necessarily equivalent. This again is symmetry dependent. The bilinear λ terms cause cubic terms to be subjected to Jahn-Teller distortions (and λ terms that appear in the cubic terms effect the quartic terms).

If the diabatic QVC Hamiltonian described in §4.3.2 is used to solve for the energy of one state along the reduced normal coordinate system, the exact adiabatic energies must be recovered. If this resulting potential energy surface is then fit to a Taylor series, the adiabatic force constants should be

obtained. However, if the QVC model Hamiltonian is augmented with the bilinear λ terms, a surface is generated and is then fit to a Taylor series, the cubic terms that are affected by the bilinear λ terms return non-zero values for some cubic constants. These differences from zero for the affected cubic force constants are the cubic diabatic corrections.

In order to obtain the quartic diabatic corrections, the augmented QVC Hamiltonian is then additionally parameterized with the diabatic cubic force constants obtained and then again is solved for a single surface along our reduced normal coordinate system. These resulting surfaces are again fit to a Taylor series and the obtained values for the quartic force constants are the quartic diabatic corrections. These values are listed in Table B.3 and B.4 in §B.3

$$F_{155;\tilde{\mathbf{x}}} = F_{111;\tilde{\mathbf{x}}} = 290.0 \tag{4.36}$$

$$F_{166;\tilde{\mathbf{x}}} = F_{144;\tilde{\mathbf{x}}} = 52.0 \tag{4.37}$$

$$F_{156;\tilde{\mathbf{x}}} = F_{134;\tilde{\mathbf{x}}} = 69.8 \tag{4.38}$$

$$F_{355;\tilde{\mathbf{x}}} = -F_{333;\tilde{\mathbf{x}}} = 191.7 \tag{4.39}$$

$$F_{466;\tilde{\mathbf{X}}} = -F_{444;\tilde{\mathbf{X}}} = -48.5 \tag{4.40}$$

$$F_{554;\tilde{\mathbf{X}}} = -F_{334;\tilde{\mathbf{X}}} = 33.9 \tag{4.41a}$$

$$F_{356;\tilde{\mathbf{X}}} = -F_{334;\tilde{\mathbf{X}}} = 33.9 \tag{4.41b}$$

$$F_{366;\tilde{\mathbf{X}}} = -F_{344;\tilde{\mathbf{X}}} = 34.2 \tag{4.42a}$$

$$F_{546;\tilde{\mathbf{X}}} = -F_{344;\tilde{\mathbf{X}}} = 34.2 \tag{4.42b}$$

$$F_{113;\tilde{\mathbf{B}}_\mathbf{b}} = -F_{113;\tilde{\mathbf{B}}_\mathbf{a}} = 12.0 \tag{4.43a}$$

$$F_{115;\tilde{\mathbf{B}}_\mathbf{a}\tilde{\mathbf{B}}_\mathbf{b}} = F_{113;\tilde{\mathbf{B}}_\mathbf{a}} = -12.0 \tag{4.43b}$$

$$F_{155;\tilde{\mathbf{B}}_\mathbf{b}} = F_{133;\tilde{\mathbf{B}}_\mathbf{a}} = 231.4 \tag{4.44a}$$

$$F_{155;\tilde{\mathbf{B}}_\mathbf{a}} = F_{133;\tilde{\mathbf{B}}_\mathbf{b}} = 243.2 \tag{4.44b}$$

$$F_{135;\tilde{\mathbf{B}}_\mathbf{a}\tilde{\mathbf{B}}_\mathbf{b}} = \frac{F_{133;\tilde{\mathbf{B}}_\mathbf{b}} - F_{155;\tilde{\mathbf{B}}_\mathbf{b}}}{2} = 6.5 \tag{4.44c}$$

$$F_{355;\tilde{\mathbf{B}}_\mathbf{a}} = -(\frac{F_{333;\tilde{\mathbf{B}}_\mathbf{a}}}{3} + \frac{2F_{333;\tilde{\mathbf{B}}_\mathbf{b}}}{3}) = 218.6 \tag{4.45a}$$

$$F_{355;\tilde{\mathbf{B}}_\mathbf{b}} = -(\frac{2F_{333;\tilde{\mathbf{B}}_\mathbf{a}}}{3} + \frac{F_{333;\tilde{\mathbf{B}}_\mathbf{b}}}{3}) = 316.7 \tag{4.45b}$$

$$F_{555;\tilde{\mathbf{B}}_\mathbf{a}\tilde{\mathbf{B}}_\mathbf{b}} = \frac{F_{333;\tilde{\mathbf{B}}_\mathbf{a}} - F_{333;\tilde{\mathbf{B}}_\mathbf{b}}}{2} = -147.15 \tag{4.45c}$$

$$F_{335;\tilde{\mathbf{B}}_\mathbf{a}\tilde{\mathbf{B}}_\mathbf{b}} = \frac{F_{355\tilde{\mathbf{B}}_\mathbf{a}\tilde{\mathbf{B}}_\mathbf{b}}}{3} = -49.05 \tag{4.45d}$$

$$F_{114;\tilde{\mathbf{B}}_\mathbf{b}} = -F_{114;\tilde{\mathbf{B}}_\mathbf{a}} = -7.5 \tag{4.46a}$$

$$F_{116;\tilde{\mathbf{B}}_\mathbf{a}\tilde{\mathbf{B}}_\mathbf{b}} = F_{114;\tilde{\mathbf{B}}_\mathbf{a}} = 7.5 \tag{4.46b}$$

$$\tag{4.46c}$$

$$F_{166;\tilde{\mathbf{B}}_\mathbf{b}} = F_{144;\tilde{\mathbf{B}}_\mathbf{a}} = 63.6 \tag{4.47a}$$

$$F_{166;\tilde{\mathbf{B}}_\mathbf{a}} = F_{144;\tilde{\mathbf{B}}_\mathbf{b}} = 43.8 \tag{4.47b}$$

$$F_{146;\tilde{\mathbf{B}}_\mathbf{a}\tilde{\mathbf{B}}_\mathbf{b}} = \frac{F_{144;\tilde{\mathbf{B}}_\mathbf{b}} - F_{166;\tilde{\mathbf{B}}_\mathbf{b}}}{2} = -9.9 \tag{4.47c}$$

$$F_{466;\tilde{\mathbf{B}}_\mathbf{a}} = -(\frac{F_{444;\tilde{\mathbf{B}}_\mathbf{a}}}{3} + \frac{2F_{444;\tilde{\mathbf{B}}_\mathbf{b}}}{3}) = -33.8 \tag{4.48a}$$

$$F_{466;\tilde{\mathbf{B}}_\mathbf{b}} = -(\frac{2F_{444;\tilde{\mathbf{B}}_\mathbf{a}}}{3} + \frac{F_{444;\tilde{\mathbf{B}}_\mathbf{b}}}{3}) = 39.6 \tag{4.48b}$$

$$F_{666;\tilde{\mathbf{B}}_\mathbf{a}\tilde{\mathbf{B}}_\mathbf{b}} = \frac{F_{444;\tilde{\mathbf{B}}_\mathbf{a}} - F_{444;\tilde{\mathbf{B}}_\mathbf{b}}}{2} = 8.7 \tag{4.48c}$$

$$F_{446;\tilde{\mathbf{B}}_\mathbf{a}\tilde{\mathbf{B}}_\mathbf{b}} = \frac{F_{444;\tilde{\mathbf{B}}_\mathbf{a}\tilde{\mathbf{B}}_\mathbf{b}}}{3} = -49.05 \tag{4.48d}$$

$$F_{156;\tilde{\mathbf{B}}_\mathbf{b}} = F_{134;\tilde{\mathbf{B}}_\mathbf{a}} = 81.2 \tag{4.49a}$$

$$F_{156;\tilde{\mathbf{B}}_\mathbf{a}} = F_{134;\tilde{\mathbf{B}}_\mathbf{b}} = 82.8 \tag{4.49b}$$

$$F_{136;\tilde{\mathbf{B}}_\mathbf{a}\tilde{\mathbf{B}}_\mathbf{b}} = \frac{F_{134;\tilde{\mathbf{B}}_\mathbf{b}} - F_{156;\tilde{\mathbf{B}}_\mathbf{b}}}{2} = 0.8 \tag{4.49c}$$

$$F_{145;\tilde{\mathbf{B}}_\mathbf{a}\tilde{\mathbf{B}}_\mathbf{b}} = \frac{F_{134;\tilde{\mathbf{B}}_\mathbf{b}} - F_{156;\tilde{\mathbf{B}}_\mathbf{b}}}{2} = 0.8 \tag{4.49d}$$

$$F_{455;\tilde{\mathbf{B}}_\mathbf{a}} = -(\frac{F_{334;\tilde{\mathbf{B}}_\mathbf{a}} + F_{334;\tilde{\mathbf{B}}_\mathbf{b}}}{2}) = 65.5 \tag{4.50a}$$

$$F_{455;\tilde{\mathbf{B}}_\mathbf{b}} = -(\frac{F_{334;\tilde{\mathbf{B}}_\mathbf{a}} + F_{334;\tilde{\mathbf{B}}_\mathbf{b}}}{2}) = 65.5 \tag{4.50b}$$

$$F_{356;\tilde{\mathbf{B}}_\mathbf{a}} = F_{455;\tilde{\mathbf{B}}_\mathbf{b}} + \frac{F_{334;\tilde{\mathbf{B}}_\mathbf{a}} - F_{334;\tilde{\mathbf{B}}_\mathbf{b}}}{4} = 64.86 \tag{4.50c}$$

$$F_{356;\tilde{\mathbf{B}}_\mathbf{b}} = F_{455;\tilde{\mathbf{B}}_\mathbf{b}} - \frac{F_{334;\tilde{\mathbf{B}}_\mathbf{a}} - F_{334;\tilde{\mathbf{B}}_\mathbf{b}}}{4} = -1.3 \tag{4.50d}$$

$$F_{345;\tilde{\mathbf{B}}_\mathbf{a}\tilde{\mathbf{B}}_\mathbf{b}} = \frac{F_{556;\tilde{\mathbf{B}}_\mathbf{a}\tilde{\mathbf{B}}_\mathbf{b}}}{2} = -0.65 \tag{4.50e}$$

$$F_{366;\tilde{\mathbf{B}}_\mathbf{a}} = -(\frac{F_{443;\tilde{\mathbf{B}}_\mathbf{a}} + F_{443;\tilde{\mathbf{B}}_\mathbf{b}}}{2}) = -8.6 \tag{4.51a}$$

$$F_{366;\tilde{\mathbf{B}}_\mathbf{b}} = -(\frac{F_{443;\tilde{\mathbf{B}}_\mathbf{a}} + F_{443;\tilde{\mathbf{B}}_\mathbf{b}}}{2}) = -8.6 \tag{4.51b}$$

$$F_{465;\tilde{\mathbf{B}}_\mathbf{a}} = F_{366;\tilde{\mathbf{B}}_\mathbf{b}} + \frac{F_{443;\tilde{\mathbf{B}}_\mathbf{a}} - F_{443;\tilde{\mathbf{B}}_\mathbf{b}}}{4} = -12.9 \tag{4.51c}$$

$$F_{465;\tilde{\mathbf{B}}_\mathbf{b}} = F_{366;\tilde{\mathbf{B}}_\mathbf{b}} - \frac{F_{443;\tilde{\mathbf{B}}_\mathbf{a}} - F_{443;\tilde{\mathbf{B}}_\mathbf{b}}}{4} = -4.3 \tag{4.51d}$$

$$F_{665;\tilde{\mathbf{B}}_\mathbf{a}\tilde{\mathbf{B}}_\mathbf{b}} = \frac{F_{443;\tilde{\mathbf{B}}_\mathbf{a}} - F_{443;\tilde{\mathbf{B}}_\mathbf{b}}}{2} = -8.6 \tag{4.51e}$$

$$F_{436;\tilde{\mathbf{B}}_\mathbf{a}\tilde{\mathbf{B}}_\mathbf{b}} = \frac{F_{665;\tilde{\mathbf{B}}_\mathbf{a}\tilde{\mathbf{B}}_\mathbf{b}}}{2} = -4.3 \tag{4.51f}$$

Table 4.7: 4VC Diabatic cubic force constants(in $cm^{-}1$) for X^2A_2'

Hamiltonian constants for 4VC	
Parameter	EOMIP-CCSDT/ANO1
$F_{111;\tilde{\mathbf{X}}}$	197.3
$F_{133;\tilde{\mathbf{X}}}$	290.0
$F_{144;\tilde{\mathbf{X}}}$	52.0
$F_{134;\tilde{\mathbf{X}}}$	69.8
$F_{333;\tilde{\mathbf{X}}}$	-191.7
$F_{444;\tilde{\mathbf{X}}}$	48.5
$F_{334;\tilde{\mathbf{X}}}$	-33.9
$F_{344;\tilde{\mathbf{X}}}$	-34.2
$F_{111;\tilde{\mathbf{B}}_\mathbf{a}}$	204.7
$F_{111;\tilde{\mathbf{B}}_\mathbf{b}}$	204.7
$F_{113;\tilde{\mathbf{B}}_\mathbf{a}}$	-12.0
$F_{133;\tilde{\mathbf{B}}_\mathbf{a}}$	231.4
$F_{133;\tilde{\mathbf{B}}_\mathbf{b}}$	243.2
$F_{333;\tilde{\mathbf{B}}_\mathbf{a}}$	-414.8
$F_{333;\tilde{\mathbf{B}}_\mathbf{b}}$	-120.5
$F_{114;\tilde{\mathbf{B}}_\mathbf{a}}$	7.5
$F_{144;\tilde{\mathbf{B}}_\mathbf{a}}$	63.6
$F_{144;\tilde{\mathbf{B}}_\mathbf{b}}$	43.8
$F_{444;\tilde{\mathbf{B}}_\mathbf{a}}$	45.4
$F_{444;\tilde{\mathbf{B}}_\mathbf{b}}$	28.0
$F_{134;\tilde{\mathbf{B}}_\mathbf{a}}$	81.2
$F_{134;\tilde{\mathbf{B}}_\mathbf{b}}$	82.8
$F_{334;\tilde{\mathbf{B}}_\mathbf{a}}$	-66.8
$F_{334;\tilde{\mathbf{B}}_\mathbf{b}}$	-64.2
$F_{443;\tilde{\mathbf{B}}_\mathbf{a}}$	0.0
$F_{443;\tilde{\mathbf{B}}_\mathbf{b}}$	-64.2

Table 4.8: 4VC Cubic block λ terms (in $cm^{-}1$)

Cubic λ terms Hamiltonian constants for 4VC	
Parameter	EOMIP-CCSDT/ANO1
$\lambda_{555;\tilde{\mathbf{X}}\tilde{\mathbf{B}}_\mathbf{a}}$	-90.0
$\lambda_{335;\tilde{\mathbf{X}}\tilde{\mathbf{B}}_\mathbf{a}}$	-30.0

As discussed previously, in order to obtain the numerical diabatic constants, one must first calculate the relevant λ terms which cause diabatic effects for higher-order terms. In order to obtain the full diabatic cubic force constants, the bilinear λ terms, which give rise to Jahn-Teller distortions in the cubic terms, were calculated using CFOUR and standard finite difference techniques. The same principle applies to the cubic λ terms. In table 4.8 are the cubic λ terms that were calculated using CFOUR and equations 4.52 and 4.53 show the relationships to determine the remaining λ terms and enforce symmetry constraints.

$$\lambda_{333;\tilde{\mathbf{X}}\tilde{\mathbf{B}}_\mathbf{b}} = \lambda_{333;\tilde{\mathbf{X}}\tilde{\mathbf{B}}_\mathbf{a}} = -90.0 \tag{4.52}$$

$$\lambda_{355;\tilde{\mathbf{X}}\tilde{\mathbf{B}}_\mathbf{b}} = \lambda_{335;\tilde{\mathbf{X}}\tilde{\mathbf{B}}_\mathbf{a}} = -30.0 \tag{4.53}$$

Now that the full cubic diabatic force constants have been parameterized, the same procedure used to determine the diabatic corrections at the cubic level can be applied to determine the numerical diabatic corrections for the quartic parameters. The cubic hamiltonian augmented with the cubic λ terms are solved for each single surface (the ground X^2A_2' state and both B^2E' states) along the same reduced coordinates q_1, q_{3a}, q_{4a}. The resulting three surfaces are again fit to a 4th order Taylor series. The adiabatic terms from linear through cubic must be recovered in order to be a correct diabatic parameterization. The non-zero values that appear in the quartic terms of this fit are the sought after quartic diabatic corrections. The quartic adiabatic constants and their diabatic correction counters are discussed in §B.3 and reported in Tables B.3 and B.4.

$$F_{1155;\tilde{\mathbf{X}}} = F_{1133;\tilde{\mathbf{X}}} = 43.3 \tag{4.54}$$

$$F_{1166;\tilde{\mathbf{X}}} = F_{1144;\tilde{\mathbf{X}}} = 0.3 \tag{4.55}$$

$$F_{1156;\tilde{\mathbf{X}}} = F_{1134;\tilde{\mathbf{X}}} = 21.0 \tag{4.56}$$

$$F_{1355;\tilde{\mathbf{X}}} = -F_{1333;\tilde{\mathbf{X}}} = 76.3 \tag{4.57}$$

$$F_{1466;\tilde{\mathbf{X}}} = -F_{1444;\tilde{\mathbf{X}}} = 1.0 \tag{4.58}$$

$$F_{1554;\tilde{\mathbf{X}}} = -F_{1334;\tilde{\mathbf{X}}} = 3.8 \tag{4.59a}$$

$$\tag{4.59b}$$

$$F_{1366;\tilde{\mathbf{X}}} = -F_{1344;\tilde{\mathbf{X}}} = 0.7 \tag{4.60a}$$

$$F_{1564;\tilde{\mathbf{X}}} = -F_{1344;\tilde{\mathbf{X}}} = 0.7 \tag{4.60b}$$

$$F_{5555;\tilde{\mathbf{X}}} = F_{3333;\tilde{\mathbf{X}}} = 134.2 \tag{4.61a}$$

$$F_{3355;\tilde{\mathbf{X}}} = \frac{F_{3333;\tilde{\mathbf{X}}}}{3} = 44.7\overline{3} \tag{4.61b}$$

$$F_{5556;\tilde{\mathbf{X}}} = F_{3334;\tilde{\mathbf{X}}} = 27.0 \tag{4.62a}$$

$$F_{3554;\tilde{\mathbf{X}}} = \frac{F_{3334;\tilde{\mathbf{X}}}}{3} = 9.0 F_{3356;\tilde{\mathbf{X}}} = \frac{F_{3334;\tilde{\mathbf{X}}}}{3} = 9.0 \tag{4.62b}$$

$$F_{5666;\tilde{\mathbf{X}}} = F_{3444;\tilde{\mathbf{X}}} = -7.3 \tag{4.63a}$$

$$F_{3466;\tilde{\mathbf{X}}} = \frac{F_{3444;\tilde{\mathbf{X}}}}{3} = -2.4\overline{3} \tag{4.63b}$$

$$F_{5446;\tilde{\mathbf{X}}} = \frac{F_{3444;\tilde{\mathbf{X}}}}{3} = -2.4\overline{3} \tag{4.63c}$$

$$F_{6666;\tilde{\mathbf{X}}} = F_{4444;\tilde{\mathbf{X}}} = 0.6 \tag{4.64a}$$

$$F_{4466;\tilde{\mathbf{X}}} = \frac{F_{4444;\tilde{\mathbf{X}}}}{3} = 0.2 \tag{4.64b}$$

$$\tag{4.64c}$$

$$F_{ff66;\tilde{\mathbf{X}}} = F_{3344;\tilde{\mathbf{X}}} = 24.3 \tag{4.65}$$

$$F_{5544;\tilde{\mathbf{X}}} = F_{3366;\tilde{\mathbf{X}}} = -8.9 \tag{4.66a}$$

$$F_{3546;\tilde{\mathbf{X}}} = \frac{F_{3344;\tilde{\mathbf{X}}} - F_{3366;\tilde{\mathbf{X}}}}{2} = 16.6156 \tag{4.66b}$$

$$\tag{4.66c}$$

$$F_{1113;\tilde{\mathbf{B}}_\mathbf{b}} = -F_{1113;\tilde{\mathbf{B}}_\mathbf{a}} = 1.0 \tag{4.67a}$$

$$F_{1115;\tilde{\mathbf{B}}_\mathbf{a}\tilde{\mathbf{B}}_\mathbf{b}} = F_{1113;\tilde{\mathbf{B}}_\mathbf{a}} = -1.0 \tag{4.67b}$$

$$F_{1155;\tilde{\mathbf{B}}_\mathbf{b}} = F_{1133;\tilde{\mathbf{B}}_\mathbf{a}} = 40.4 \tag{4.68a}$$

$$F_{1155;\tilde{\mathbf{B}}_\mathbf{a}} = F_{1133;\tilde{\mathbf{B}}_\mathbf{b}} = 40.4 \tag{4.68b}$$

$$F_{1135;\tilde{\mathbf{B}}_\mathbf{a}\tilde{\mathbf{B}}_\mathbf{b}} = \frac{F_{1113;\tilde{\mathbf{B}}_\mathbf{b}} - F_{1133;\tilde{\mathbf{B}}_\mathbf{a}}}{2} = 0.0 \tag{4.68c}$$

Table 4.9: Quartic Diabatic Constants (in $cm^{-}1$) for the 1 1 block (X^2A_2')

Quartic Hamiltonian constants for 4VC	
Parameter	EOMIP-CCSDT/ANO1
$F_{1111;\tilde{\mathbf{X}}}$	-32.9
$F_{1133;\tilde{\mathbf{X}}}$	43.3
$F_{1144;\tilde{\mathbf{X}}}$	0.3
$F_{1134;\tilde{\mathbf{X}}}$	21.0
$F_{1333;\tilde{\mathbf{X}}}$	-76.3
$F_{1444;\tilde{\mathbf{X}}}$	-1.0
$F_{1334;\tilde{\mathbf{X}}}$	-3.8
$F_{1344;\tilde{\mathbf{X}}}$	-0.7
$F_{3333;\tilde{\mathbf{X}}}$	134.2
$F_{3334;\tilde{\mathbf{X}}}$	27.0
$F_{3444;\tilde{\mathbf{X}}}$	-7.3
$F_{4444;\tilde{\mathbf{X}}}$	0.6
$F_{3344;\tilde{\mathbf{X}}}$	24.3
$F_{3366;\tilde{\mathbf{X}}}$	-8.9

$$F_{1355;\tilde{\mathbf{B}}_\mathbf{a}} = -(\frac{F_{1333;\tilde{\mathbf{B}}_\mathbf{a}}}{3} + \frac{2F_{1333;\tilde{\mathbf{B}}_\mathbf{b}}}{3}) = 39.2\overline{6} \tag{4.69a}$$

$$F_{1355;\tilde{\mathbf{B}}_\mathbf{b}} = -(\frac{2F_{1333;\tilde{\mathbf{B}}_\mathbf{a}}}{3} + \frac{F_{1333;\tilde{\mathbf{B}}_\mathbf{b}}}{3}) = 56.\overline{3} \tag{4.69b}$$

$$F_{1555;\tilde{\mathbf{B}}_\mathbf{a}\tilde{\mathbf{B}}_\mathbf{b}} = \frac{F_{1333;\tilde{\mathbf{B}}_\mathbf{a}} - F_{1333;\tilde{\mathbf{B}}_\mathbf{b}}}{2} = -24.7 \tag{4.69c}$$

$$F_{1335;\tilde{\mathbf{B}}_\mathbf{a}\tilde{\mathbf{B}}_\mathbf{b}} = \frac{F_{1555;\tilde{\mathbf{B}}_\mathbf{a}\tilde{\mathbf{B}}_\mathbf{b}}}{3} = -8.2\overline{3} \tag{4.69d}$$

$$F_{5555;\tilde{\mathbf{B}}_\mathbf{a}} = F_{3333;\tilde{\mathbf{B}}_\mathbf{b}} = 33.9 \tag{4.70a}$$

$$F_{5555;\tilde{\mathbf{B}}_\mathbf{b}} = F_{3333;\tilde{\mathbf{B}}_\mathbf{a}} = 134.2 \tag{4.70b}$$

$$F_{3355;\tilde{\mathbf{B}}_\mathbf{a}} = \frac{F_{3333;\tilde{\mathbf{B}}_\mathbf{a}} + F_{3333;\tilde{\mathbf{B}}_\mathbf{b}}}{6} = 28.01\overline{6} \tag{4.70c}$$

$$F_{3355;\tilde{\mathbf{B}}_\mathbf{b}} = \frac{F_{3333;\tilde{\mathbf{B}}_\mathbf{a}} + F_{3333;\tilde{\mathbf{B}}_\mathbf{b}}}{6} = 28.01\overline{6} \tag{4.70d}$$

$$F_{3335;\tilde{\mathbf{B}}_\mathbf{a}\tilde{\mathbf{B}}_\mathbf{b}} = \frac{F_{3333;\tilde{\mathbf{B}}_\mathbf{b}} - F_{3333;\tilde{\mathbf{B}}_\mathbf{a}}}{4} \tag{4.70e}$$

$$F_{3555;\tilde{\mathbf{B}}_\mathbf{a}\tilde{\mathbf{B}}_\mathbf{b}} = \frac{F_{3333;\tilde{\mathbf{B}}_\mathbf{b}} - F_{3333;\tilde{\mathbf{B}}_\mathbf{a}}}{4} \tag{4.70f}$$

$$F_{1114;\tilde{\mathbf{B}}_\mathbf{b}} = -F_{1114;\tilde{\mathbf{B}}_\mathbf{a}} = -1.0 \tag{4.71a}$$

$$F_{1116;\tilde{\mathbf{B}}_\mathbf{a}} = F_{1114;\tilde{\mathbf{B}}_\mathbf{a}} = 1.0 \tag{4.71b}$$

$$F_{1166;\tilde{\mathbf{B}}_\mathbf{b}} = F_{1144;\tilde{\mathbf{B}}_\mathbf{a}} = 5.6 \tag{4.72a}$$

$$F_{1166;\tilde{\mathbf{B}}_\mathbf{a}} = F_{1114;\tilde{\mathbf{B}}_\mathbf{b}} = 7.1 \tag{4.72b}$$

$$F_{1146;\tilde{\mathbf{B}}_\mathbf{a}\tilde{\mathbf{B}}_\mathbf{b}} = \frac{F_{1114;\tilde{\mathbf{B}}_\mathbf{b}} - F_{1166;\tilde{\mathbf{B}}_\mathbf{b}}}{2} = 0.75 \tag{4.72c}$$

$$F_{1466;\tilde{\mathbf{B}}_\mathbf{a}} = -(\frac{F_{1444;\tilde{\mathbf{B}}_\mathbf{a}}}{3} + \frac{2F_{1444;\tilde{\mathbf{B}}_\mathbf{b}}}{3}) = -5.3 \tag{4.73a}$$

$$F_{1466;\tilde{\mathbf{B}}_\mathbf{b}} = -(\frac{2F_{1444;\tilde{\mathbf{B}}_\mathbf{a}}}{3} + \frac{F_{1444;\tilde{\mathbf{B}}_\mathbf{b}}}{3}) = -4.3 \tag{4.73b}$$

$$F_{1666;\tilde{\mathbf{B}}_\mathbf{a}\tilde{\mathbf{B}}_\mathbf{b}} = \frac{F_{1444;\tilde{\mathbf{B}}_\mathbf{a}} - F_{1444;\tilde{\mathbf{B}}_\mathbf{a}}}{2} = -1.5 \tag{4.73c}$$

$$F_{1446;\tilde{\mathbf{B}}_\mathbf{a}\tilde{\mathbf{B}}_\mathbf{a}} = \frac{F_{1666;\tilde{\mathbf{B}}_\mathbf{a}\tilde{\mathbf{B}}_\mathbf{a}}}{3} = -0.5 \tag{4.73d}$$

$$F_{6666;\tilde{\mathbf{B}}_\mathbf{a}} = F_{4444;\tilde{\mathbf{B}}_\mathbf{b}} = -2.5 \tag{4.74a}$$

$$F_{6666;\tilde{\mathbf{B}}_\mathbf{b}} = F_{4444;\tilde{\mathbf{B}}_\mathbf{a}} = 1.3 \tag{4.74b}$$

$$F_{4466;\tilde{\mathbf{B}}_\mathbf{a}} = \frac{F_{4444;\tilde{\mathbf{B}}_\mathbf{a}} + F_{4444;\tilde{\mathbf{B}}_\mathbf{b}}}{6} = -0.2 \tag{4.74c}$$

$$F_{4466;\tilde{\mathbf{B}}_\mathbf{b}} = \frac{F_{4444;\tilde{\mathbf{B}}_\mathbf{a}} + F_{4444;\tilde{\mathbf{B}}_\mathbf{b}}}{6} = -0.2 \tag{4.74d}$$

$$F_{4446;\tilde{\mathbf{B}}_\mathbf{a}\tilde{\mathbf{B}}_\mathbf{b}} = \frac{F_{4444;\tilde{\mathbf{B}}_\mathbf{b}} - F_{4444;\tilde{\mathbf{B}}_\mathbf{a}}}{4} = -0.95 \tag{4.74e}$$

$$F_{4666;\tilde{\mathbf{B}}_\mathbf{a}\tilde{\mathbf{B}}_\mathbf{b}} = \frac{F_{4444;\tilde{\mathbf{B}}_\mathbf{b}} - F_{4444;\tilde{\mathbf{B}}_\mathbf{a}}}{4} = -0.95 \tag{4.74f}$$

$$F_{1156;\tilde{\mathbf{B}}_\mathbf{b}} = F_{1134:\tilde{\mathbf{B}}_\mathbf{a}} = 15.8 \tag{4.75a}$$

$$F_{1156;\tilde{\mathbf{B}}_\mathbf{a}} = F_{1134:\tilde{\mathbf{B}}_\mathbf{b}} = 10.3 \tag{4.75b}$$

$$F_{1136;\tilde{\mathbf{B}}_\mathbf{a}\tilde{\mathbf{B}}_\mathbf{b}} = \frac{F_{1134:\tilde{\mathbf{B}}_\mathbf{b}} - F_{1156;\tilde{\mathbf{B}}_\mathbf{b}}}{2} = -2.75 \tag{4.75c}$$

$$F_{1145;\tilde{\mathbf{B}}_\mathbf{a}\tilde{\mathbf{B}}_\mathbf{b}} = \frac{F_{1134:\tilde{\mathbf{B}}_\mathbf{b}} - F_{1156;\tilde{\mathbf{B}}_\mathbf{b}}}{2} = -2.75 \tag{4.75d}$$

$$F_{6555;\tilde{\mathbf{B}}_\mathbf{a}} = F_{4333;\tilde{\mathbf{B}}_\mathbf{a}} = 36.0 \tag{4.76a}$$

$$F_{6555;\tilde{\mathbf{B}}_\mathbf{b}} = F_{4333;\tilde{\mathbf{B}}_\mathbf{b}} = 54.0 \tag{4.76b}$$

$$F_{4355;\tilde{\mathbf{B}}_\mathbf{a}} = -(\frac{F_{4333;\tilde{\mathbf{B}}_\mathbf{a}}}{3} - \frac{2F_{4333;\tilde{\mathbf{B}}_\mathbf{b}}}{3}) = 24.0 \tag{4.76c}$$

$$F_{4355;\tilde{\mathbf{B}}_\mathbf{b}} = -(\frac{2F_{4333;\tilde{\mathbf{B}}_\mathbf{a}}}{3} - \frac{F_{4333;\tilde{\mathbf{B}}_\mathbf{b}}}{3}) = 6.0 \tag{4.76d}$$

$$F_{3365;\tilde{\mathbf{B}}_\mathbf{a}} = -(\frac{F_{4333;\tilde{\mathbf{B}}_\mathbf{a}}}{3} - \frac{2F_{4333;\tilde{\mathbf{B}}_\mathbf{b}}}{3}) = 24.0 \tag{4.76e}$$

$$F_{3365;\tilde{\mathbf{B}}_\mathbf{b}} = -(\frac{2F_{4333;\tilde{\mathbf{B}}_\mathbf{a}}}{3} - \frac{F_{4333;\tilde{\mathbf{B}}_\mathbf{b}}}{3}) = 6.0 \tag{4.76f}$$

$$F_{3336;\tilde{\mathbf{B}}_\mathbf{a}\tilde{\mathbf{B}}_\mathbf{b}} = \frac{F_{4333;\tilde{\mathbf{B}}_\mathbf{a}} - F_{4333;\tilde{\mathbf{B}}_\mathbf{b}}}{2} = -9.0 \tag{4.76g}$$

$$F_{4555;\tilde{\mathbf{B}}_\mathbf{a}\tilde{\mathbf{B}}_\mathbf{b}} = (\frac{F_{4333;\tilde{\mathbf{B}}_\mathbf{a}} - F_{4333;\tilde{\mathbf{B}}_\mathbf{b}}}{2}) = 9.0 \tag{4.76h}$$

$$F_{4335;\tilde{\mathbf{B}}_\mathbf{a}\tilde{\mathbf{B}}_\mathbf{b}} = \frac{F_{4333;\tilde{\mathbf{B}}_\mathbf{a}} - F_{4333;\tilde{\mathbf{B}}_\mathbf{b}}}{2} = -9.0 \tag{4.76i}$$

$$F_{3655;\tilde{\mathbf{B}}_\mathbf{a}\tilde{\mathbf{B}}_\mathbf{b}} = (\frac{F_{4333;\tilde{\mathbf{B}}_\mathbf{a}} - F_{4333;\tilde{\mathbf{B}}_\mathbf{b}}}{2}) = 9.0 \tag{4.76j}$$

$$F_{5666;\tilde{\mathbf{B}}_\mathbf{a}} = F_{3444;\tilde{\mathbf{B}}_\mathbf{a}} = 3.2 \tag{4.77a}$$

$$F_{5666;\tilde{\mathbf{B}}_\mathbf{b}} = F_{3444;\tilde{\mathbf{B}}_\mathbf{b}} = 17.7 \tag{4.77b}$$

$$F_{3466;\tilde{\mathbf{B}}_\mathbf{a}} = -(\frac{F_{3444;\tilde{\mathbf{B}}_\mathbf{a}}}{3} - \frac{2F_{3444;\tilde{\mathbf{B}}_\mathbf{b}}}{3}) = 10.7\overline{3} \tag{4.77c}$$

$$F_{3466;\tilde{\mathbf{B}}_\mathbf{b}} = (\frac{2F_{3444;\tilde{\mathbf{B}}_\mathbf{a}}}{3}) = 10.7\overline{3} \tag{4.77d}$$

$$F_{4456;\tilde{\mathbf{B}}_\mathbf{a}} = -(\frac{F_{3444;\tilde{\mathbf{B}}_\mathbf{a}}}{3} - \frac{2F_{3444;\tilde{\mathbf{B}}_\mathbf{b}}}{3}) = 10.7\overline{3} \tag{4.77e}$$

$$F_{4456;\tilde{\mathbf{B}}_\mathbf{b}} = (\frac{2F_{3444;\tilde{\mathbf{B}}_\mathbf{a}}}{3}) = -3.7\overline{6} \tag{4.77f}$$

$$F_{4445\tilde{\mathbf{B}}_\mathbf{a}\tilde{\mathbf{B}}_\mathbf{b}} = (\frac{F_{3444;\tilde{\mathbf{B}}_\mathbf{a}} - F_{3444;\tilde{\mathbf{B}}_\mathbf{b}}}{2}) = -7.25 \tag{4.77g}$$

$$\tag{4.77h}$$

$$F_{1455;\tilde{\mathbf{B}}_\mathbf{a}} = -(\frac{F_{1334;\tilde{\mathbf{B}}_\mathbf{a}} + F_{1334;\tilde{\mathbf{B}}_\mathbf{b}}}{2}) = 5.2 \tag{4.78a}$$

$$F_{1455;\tilde{\mathbf{B}}_\mathbf{b}} = -(\frac{F_{1334;\tilde{\mathbf{B}}_\mathbf{a}} + F_{1334;\tilde{\mathbf{B}}_\mathbf{b}}}{2}) = 5.2 \tag{4.78b}$$

$$F_{1356;\tilde{\mathbf{B}}_\mathbf{a}} = F_{1455;\tilde{\mathbf{B}}_\mathbf{b}} + \frac{F_{1334;\tilde{\mathbf{B}}_\mathbf{a}} - F1334;\tilde{\mathbf{B}}_\mathbf{b}}{4}) = 5.2 \tag{4.78c}$$

$$F_{1356;\tilde{\mathbf{B}}_\mathbf{a}} = F_{1455;\tilde{\mathbf{B}}_\mathbf{b}} - \frac{F_{1334;\tilde{\mathbf{B}}_\mathbf{a}} - F1334;\tilde{\mathbf{B}}_\mathbf{b}}{4}) = 5.2 \tag{4.78d}$$

$$F_{1556;\tilde{\mathbf{B}}_\mathbf{a}\tilde{\mathbf{B}}_\mathbf{b}} = (\frac{F_{1334;\tilde{\mathbf{B}}_\mathbf{a}} - F_{1334;\tilde{\mathbf{B}}_\mathbf{b}}}{2}) = 0.0 \tag{4.78e}$$

$$F_{1345;\tilde{\mathbf{B}}_\mathbf{a}\tilde{\mathbf{B}}_\mathbf{b}} = (\frac{F_{1556;\tilde{\mathbf{B}}_\mathbf{a}\tilde{\mathbf{B}}_\mathbf{b}}}{2}) = 0.0 \tag{4.78f}$$

$$F_{1366;\tilde{\mathbf{B}}_\mathbf{a}} = -(\frac{F_{1443;\tilde{\mathbf{B}}_\mathbf{a}} + F_{1443;\tilde{\mathbf{B}}_\mathbf{b}}}{2}) = 4.0 \tag{4.79a}$$

$$F_{1366;\tilde{\mathbf{B}}_\mathbf{b}} = -(\frac{F_{1443;\tilde{\mathbf{B}}_\mathbf{a}} + F_{1443;\tilde{\mathbf{B}}_\mathbf{b}}}{2}) = 4.0 \tag{4.79b}$$

$$F_{1465;\tilde{\mathbf{B}}_\mathbf{a}} = F_{1366;\tilde{\mathbf{B}}_\mathbf{b}} + (\frac{F_{1443;\tilde{\mathbf{B}}_\mathbf{a}} - F_{1443;\tilde{\mathbf{B}}_\mathbf{b}}}{4} = 5.0 \tag{4.79c}$$

$$F_{1465;\tilde{\mathbf{B}}_\mathbf{b}} = F_{1366;\tilde{\mathbf{B}}_\mathbf{b}} - \frac{F_{1443;\tilde{\mathbf{B}}_\mathbf{a}} - F_{1443;\tilde{\mathbf{B}}_\mathbf{b}}}{4} = 3.0 \tag{4.79d}$$

$$F_{1665;\tilde{\mathbf{B}}_\mathbf{a}\tilde{\mathbf{B}}_\mathbf{b}} = \frac{F_{1443;\tilde{\mathbf{B}}_\mathbf{a}} - F_{1443;\tilde{\mathbf{B}}_\mathbf{b}}}{2} = 2.0 \tag{4.79e}$$

$$F_{1665;\tilde{\mathbf{B}}_\mathbf{a}\tilde{\mathbf{B}}_\mathbf{b}} = (\frac{F_{1443;\tilde{\mathbf{B}}_\mathbf{a}} - F_{1443;\tilde{\mathbf{B}}_\mathbf{b}}}{4}) = 1.0 \tag{4.79f}$$

$$\tag{4.79g}$$

$$F_{4455;\tilde{\mathbf{B}}_\mathbf{a}} = F_{3366;\tilde{\mathbf{B}}_\mathbf{a}} = -26.0 \tag{4.80a}$$

$$F_{4455;\tilde{\mathbf{B}}_\mathbf{b}} = F_{3366;\tilde{\mathbf{B}}_\mathbf{b}} = -26.0 \tag{4.80b}$$

$$F_{5566;\tilde{\mathbf{B}}_\mathbf{a}} = F_{3344;\tilde{\mathbf{B}}_\mathbf{b}} + F_{3366;\tilde{\mathbf{B}}_\mathbf{b}} - F_{3366;\tilde{\mathbf{B}}_\mathbf{a}} = -27.4 \tag{4.80c}$$

$$F_{5566;\tilde{\mathbf{B}}_\mathbf{b}} = F_{3344;\tilde{\mathbf{B}}_\mathbf{a}} - F_{3366;\tilde{\mathbf{B}}_\mathbf{b}} + F_{3366;\tilde{\mathbf{B}}_\mathbf{a}} = 10.1 \tag{4.80d}$$

$$F_{3546;\tilde{\mathbf{B}}_\mathbf{a}} = \frac{F_{3344;\tilde{\mathbf{B}}_\mathbf{a}} + F_{3344;\tilde{\mathbf{B}}_\mathbf{b}} + F_{3366;\tilde{\mathbf{B}}_\mathbf{a}} - 3F_{3366;\tilde{\mathbf{B}}_\mathbf{b}}}{4} = 8.675 \tag{4.80e}$$

$$F_{3546;\tilde{\mathbf{B}}_\mathbf{b}} = \frac{F_{3344;\tilde{\mathbf{B}}_\mathbf{a}} + F_{3344;\tilde{\mathbf{B}}_\mathbf{b}} - 3F_{3366;\tilde{\mathbf{B}}_\mathbf{a}} + F_{3366;\tilde{\mathbf{B}}_\mathbf{b}}}{4} = 8.675 \tag{4.80f}$$

$$F_{3346;\tilde{\mathbf{B}}_\mathbf{a}\tilde{\mathbf{B}}_\mathbf{b}} = \frac{F_{3344;\tilde{\mathbf{B}}_\mathbf{b}} - F_{3344;\tilde{\mathbf{B}}_\mathbf{a}} + F_{3366;\tilde{\mathbf{B}}_\mathbf{a}} - F_{3366;\tilde{\mathbf{B}}_\mathbf{b}}}{4} = -9.375 \tag{4.80g}$$

$$F_{3544;\tilde{\mathbf{B}}_\mathbf{a}\tilde{\mathbf{B}}_\mathbf{b}} = \frac{F_{3344;\tilde{\mathbf{B}}_\mathbf{b}} - F_{3344;\tilde{\mathbf{B}}_\mathbf{a}} + F_{3366;\tilde{\mathbf{B}}_\mathbf{a}} - F_{3366;\tilde{\mathbf{B}}_\mathbf{b}}}{4} = -9.375 \tag{4.80h}$$

$$F_{3566;\tilde{\mathbf{B}}_\mathbf{a}\tilde{\mathbf{B}}_\mathbf{b}} = \frac{F_{3344;\tilde{\mathbf{B}}_\mathbf{b}} - F_{3344;\tilde{\mathbf{B}}_\mathbf{a}} + 3F_{3366;\tilde{\mathbf{B}}_\mathbf{a}} - 3F_{3366;\tilde{\mathbf{B}}_\mathbf{b}}}{4} = -9.375 \tag{4.80i}$$

$$F_{5546;\tilde{\mathbf{B}}_\mathbf{a}\tilde{\mathbf{B}}_\mathbf{b}} = \frac{F_{3344;\tilde{\mathbf{B}}_\mathbf{b}} - F_{3344;\tilde{\mathbf{B}}_\mathbf{a}} + 3F_{3366;\tilde{\mathbf{B}}_\mathbf{a}} - 3F_{3366;\tilde{\mathbf{B}}_\mathbf{b}}}{4} = -9.375 \tag{4.80j}$$

After the construction of the full 4VC Hamiltonian, any diabatic force constant that is not effected as a result of any of the λ terms or any of the JT distortions should be 0. These parameter's adiabatic counterpart need not be 0. On closer inspection of $F_{34;\tilde{\mathbf{X}}}$, which has a value of -34.6 as seen in Table 4.3.2, it can be surmised that our diabatic correction is slightly off. While the majority of the calculations in this 4VC hamiltonian were done at CCSDT/ANO1, the linear, bilinear and cubic λ terms were calculated at the EOMIP-CCSD/ANO1 level. This is due to the fact that EOMIP-CCSDT λ calculations have not been implemented into any chemistry package at this time.

It has been seen previously that EOMIP-CCSD tends to overestimate the value for these off-diagonal coupling terms. If one were able to systematically scale all of the λ terms and regenerate the resulting change to diabatic correction terms such that the value of $F_{34;\tilde{\mathbf{X}}}$ is minimized, one would have obtained the "true" diabatic corrections for the proposed model. A program was written whereby these coupling terms could be scaled and the procedure for numerically determining the diabatic corrections (and thus the diabatic terms) from the equations listed throughout this chapter was automated. After applying this technique, an optimal λ scaling value of 0.96 was determined, which when used to generate the diabatic correction for $f_{34;\tilde{\mathbf{X}}}$ results in a value for $F_{34;\tilde{\mathbf{X}}}$ of 0.08 cm^{-1}.

The newly corrected 4VC hamiltonian is then solved using the same procedure previously discussed and the resulting e' levels are listed in Table

Table 4.10: Quartic Diabatic Constants (in $cm^{-}1$) continued

Quartic constants for the 2 2, 3 3 and 2 3 blocks	
$F_{1111;\tilde{\mathbf{B}}_\mathbf{a}}$	32.7
$F_{1111;\tilde{\mathbf{B}}_\mathbf{b}}$	32.7
$F_{1113;\tilde{\mathbf{B}}_\mathbf{a}}$	-1.0
$F_{1133;\tilde{\mathbf{B}}_\mathbf{b}}$	40.4
$F_{1133;\tilde{\mathbf{B}}_\mathbf{b}}$	40.4
$F_{1333;\tilde{\mathbf{B}}_\mathbf{a}}$	-72.2
$F_{1333;\tilde{\mathbf{B}}_\mathbf{b}}$	-22.8
$F_{3333;\tilde{\mathbf{B}}_\mathbf{a}}$	134.2
$F_{3333;\tilde{\mathbf{B}}_\mathbf{b}}$	33.9
$F_{1114;\tilde{\mathbf{B}}_\mathbf{a}}$	1.0
$F_{1144;\tilde{\mathbf{B}}_\mathbf{a}}$	5.6
$F_{1144;\tilde{\mathbf{B}}_\mathbf{b}}$	7.1
$F_{1444;\tilde{\mathbf{B}}_\mathbf{a}}$	3.3
$F_{1444;\tilde{\mathbf{B}}_\mathbf{b}}$	6.3
$F_{4444;\tilde{\mathbf{B}}_\mathbf{a}}$	1.3
$F_{4444;\tilde{\mathbf{B}}_\mathbf{b}}$	-2.5
$F_{1134;\tilde{\mathbf{B}}_\mathbf{a}}$	15.8
$F_{1134;\tilde{\mathbf{B}}_\mathbf{b}}$	10.3
$F_{4333;\tilde{\mathbf{B}}_\mathbf{a}}$	36.0
$F_{4333;\tilde{\mathbf{B}}_\mathbf{b}}$	54.0
$F_{3444;\tilde{\mathbf{B}}_\mathbf{a}}$	3.2
$F_{3466;\tilde{\mathbf{B}}_\mathbf{a}}$	$10.7\overline{3}$
$F_{1334;\tilde{\mathbf{B}}_\mathbf{a}}$	-5.2
$F_{1334;\tilde{\mathbf{B}}_\mathbf{b}}$	-5.2
$F_{1443;\tilde{\mathbf{B}}_\mathbf{a}}$	-2.0
$F_{1443;\tilde{\mathbf{B}}_\mathbf{b}}$	-6.0
$F_{3344;\tilde{\mathbf{B}}_\mathbf{a}}$	10.1
$F_{3344;\tilde{\mathbf{B}}_\mathbf{b}}$	-27.4
$F_{3366;\tilde{\mathbf{B}}_\mathbf{a}}$	-26.0
$F_{3366;\tilde{\mathbf{B}}_\mathbf{b}}$	-26.0

Table 4.11: Levels versus Experimental Values(in $cm^{-}1$) for *ab initio* gap

The first 13 E' levels for unscaled and scaled λ

Unadjusted	0.95	0.975	Sensitivity	Experimental
337	397	369	64	365
726	824	777	98	?
1035	1096	1069	61	?
1077	1224	1152	147	1173
1385	1457	1424	72	1413
1443	1538	1494	95	1492
1490	1665	1579	175	1562
1566	1716	1642	150	
1689	1844	1769	155	
1793	1895	1845	102	
1841	2001	1931	160	1917
1898	2089	1989	191	
1998	2117	2080	119	

4.11. These values are listed in the column Unscaled and while these are the best results obtained thus far and seem to have sufficient physics in order to obtain the correct relative positions between experimentally observed levels, these results could be considered quasi-quantitative at best.

As was discussed above, the procedure for determining linear λ terms (and thus all higher order λ terms) tends to overestimate their values. By scaling these coupling terms, the "true" diabatic corrections were arguably obtained. This same procedure and logic can be applied to the coupling terms during the lanczos recursions that are done in order to obtain the diabatic en-

ergy levels. Initially, the above 4VC model hamiltonian was solved for diabatic energy levels using two different scaling factors; 0.95 and 0.975. These results are presented along with the unadjusted and the experimental values in Table 4.11. Also show is the difference in energy levels between an unadjusted value and a value scaled by 0.95 referred to as the "Sensitivity".

Comparing the results obtained with the 0.975 scaling factor to the experimental values shows very good agreement. Difference between our predicted energy levels and experimental values range between a few wavenumbers up to a difference of 21 wavenumbers. The fact that this mode also exhibits the greatest sensitivity to variations in coupling strength should be noted.

There remains an additional factor that can effect level positions of our predicted results that hasn't been discussed yet and that is the value used for the vertical gap. In all previous parametrizations, the vertical gap was the energy difference between the X^2A_2' ground electronic state and the B^2E' 2^{nd} excited state calculated at the geometry of the anion using EOMIP-CCSDT with an ANO1 basis. This resulting value of 15406 cm^{-1} has been used exclusively. When using this number to solve the diabatic hamiltonian, the resulting gap between ground and the excited state of interest, an excitation energy of 15497 cm^{-1} is obtained. The experimental gap for this transition is well known to be 662 nm (± 1) or 15106 cm^{-1}. This is substantially lower than the value obtained both adiabatically and diabatically. The resulting difference can be attributed to the fact that the geometry of the ground state and excite states are restricted to that of the Anion.

Table 4.12: Levels versus Experimental Values(in $cm^{-}1$) for $\Delta - 100$

The first 13 E' levels for unscaled and scaled λ

Unadjusted	0.95	0.975	Sensitivity	Experimental
333	394	365	61	365
720	818	771	98	?
1030	1093	1065	63	?
1068	1215	1142	147	1173
1379	1453	1419	74	1413
1436	1533	1488	97	1492
1479	1655	1568	176	1562
1556	1708	1634	152	
1679	1835	1759	156	
1786	1889	1839	103	
1828	1993	1922	165	1917
1887	2077	1978	190	
1987	2112	2074	125	

In order to attempt to improve upon our predicted values, the same calculations discussed above were run for the vertical gap (Δ) adjusted by 100, 200 and 300 cm^{-1}. These runs were also done with the previously used λ scaling factors of 0.95 and 0.975. These results are summarized in Table 4.12, 4.13 and 4.14.

There are several interesting things to note from these results. First, the scaled λ value of 0.975 is always better than those of the unadjusted as well as those at the scaling factor 0.95. Second, the sensitivity (difference between 0.95 and unscaled values) is consistent across all of the runs. When

Table 4.13: Levels versus Experimental Values(in $cm^{-}1$) for $\Delta - 200$

The first 13 E' levels for unscaled and scaled λ

Unadjusted	0.95	0.975	Sensitivity	Experimental
328	391	362	63	365
713	813	765	100	?
1024	1089	1061	65	?
1060	1207	1133	147	1173
1373	1449	1414	76	1413
1428	1527	1482	99	1492
1469	1645	1558	176	1562
1547	1700	1625	153	
1670	1826	1749	156	
1780	1883	1833	104	
1815	1986	1912	171	1917
1877	2066	1967	189	
1977	2107	2065	130	

Table 4.14: Levels versus Experimental Values(in $cm^{-}1$) for $\Delta - 300$

The first 13 E' levels for unscaled and scaled λ

Unadjusted	0.95	0.975	Sensitivity	Experimental
324	388	358	64	365
708	808	760	100	?
1018	1086	1057	68	?
1052	1199	1125	147	1173
1367	1445	1410	78	1413
1421	1523	1477	102	1492
1459	1643	1548	184	1562
1539	1692	1617	153	
1660	1818	1740	158	
1773	1878	1827	105	
1803	1978	1902	175	1917
1868	2054	1956	186	
1967	2103	2055	136	

considering the optimal scaling factor it should be noted that it is expected the be slightly different for each of the different gaps used. The vertical energy difference appears in the analytical diabatic corrections for the quadratic force constants. Additionally, it will also effect the cubic and quartic corrections. In order to determine the optimal scaling factor for each gap used, several runs were done for the *ab initio* gap as well as the gap - 100, 200 and 300 in which the scaling factor was varied from 0.85 to 1.10.

The results for the ab initio gap and the gap - 100 are shown in Figures 4.1 and 4.2. The results for gap - 200 and gap - 300 aren't displayed in this way because there is no discernible difference at this scale. If instead the data is zoomed in on the energy over the same scale factor range and is then fit, the resulting Figure 4.3 is obtained. As can be seen from this figure, as the gap is decreased so does the value of the scaling factor needed to reproduce the first excited vibronic level. And finally, if we zoom all the way in as in Figure 4.4, it can be seen that the optimal scaling for determining the first excited level differs by 0.003 for every 100 wavenumbers the gap is changed.

Figures 4.3 and 4.4 are the first excited vibronic level compared to the experimental value of 365 cm^{-1}. In order to confirm this trend, the same plot was done for the level observed experimentally at 1492 cm^{-1} as seen in Figure 4.5.

After looking at the resulting excitation energy obtained for the various changes to the vertical energy used in solving our model diabatic Hamiltonians, it can be extrapolated that the diabatic energy will be close to the experimental

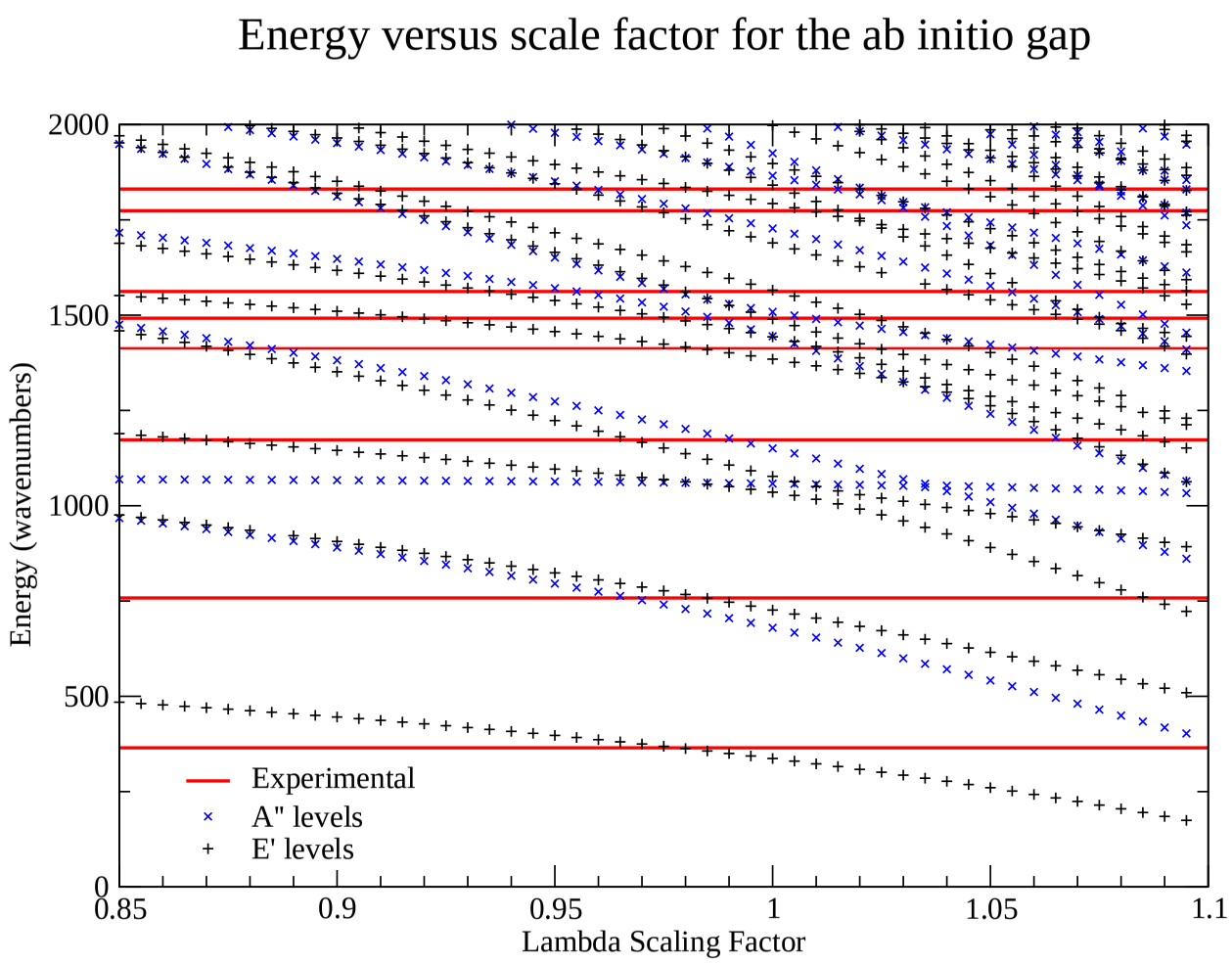

Figure 4.1: E' and A'' levels as a function of scaled λ versus Experimental data (in $cm-1$) with the *ab initio* gap

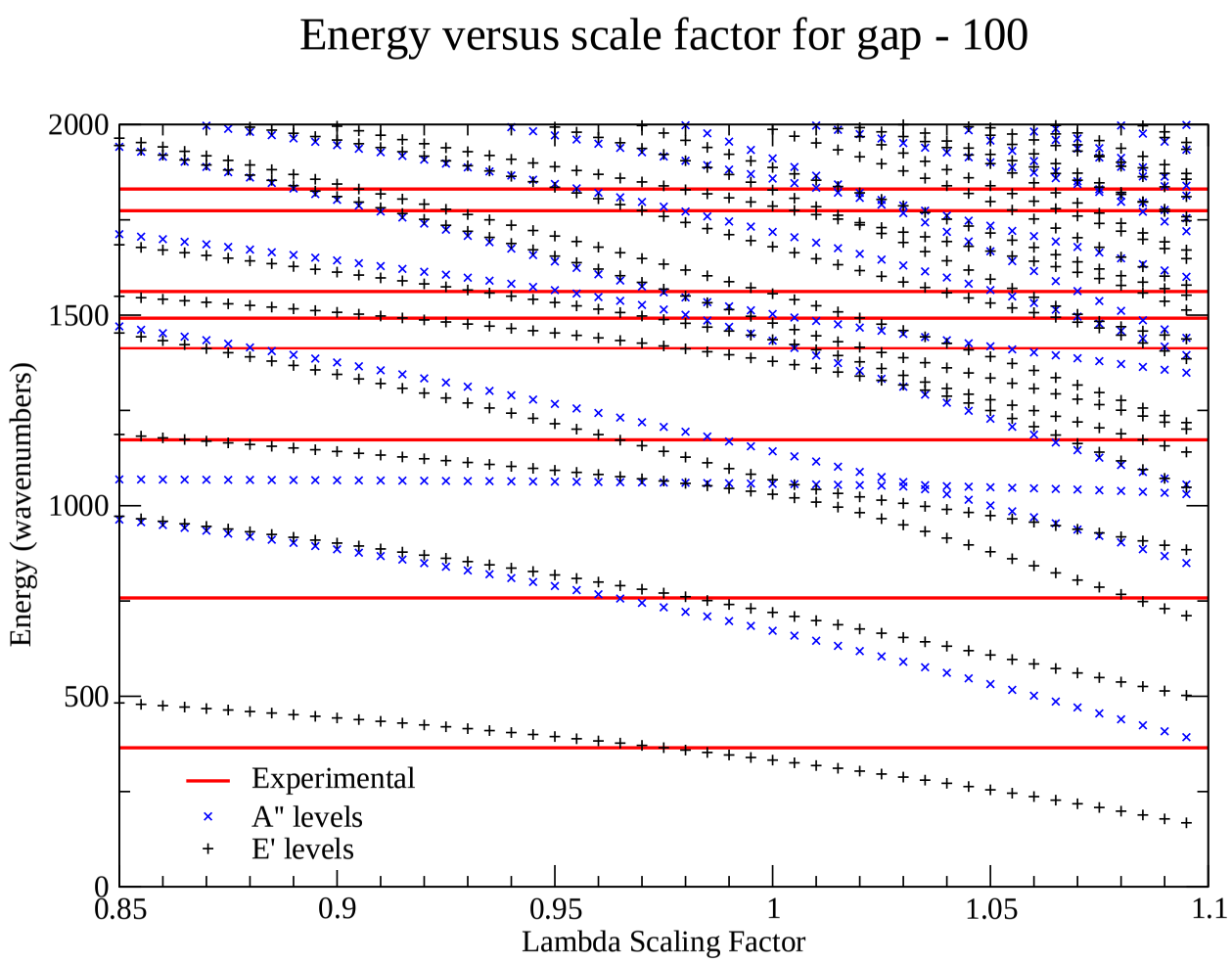

Figure 4.2: E' and A'' levels as a function of scaled λ versus Experimental data (in $cm-1$) with vertical energy gap $= \Delta - 100$

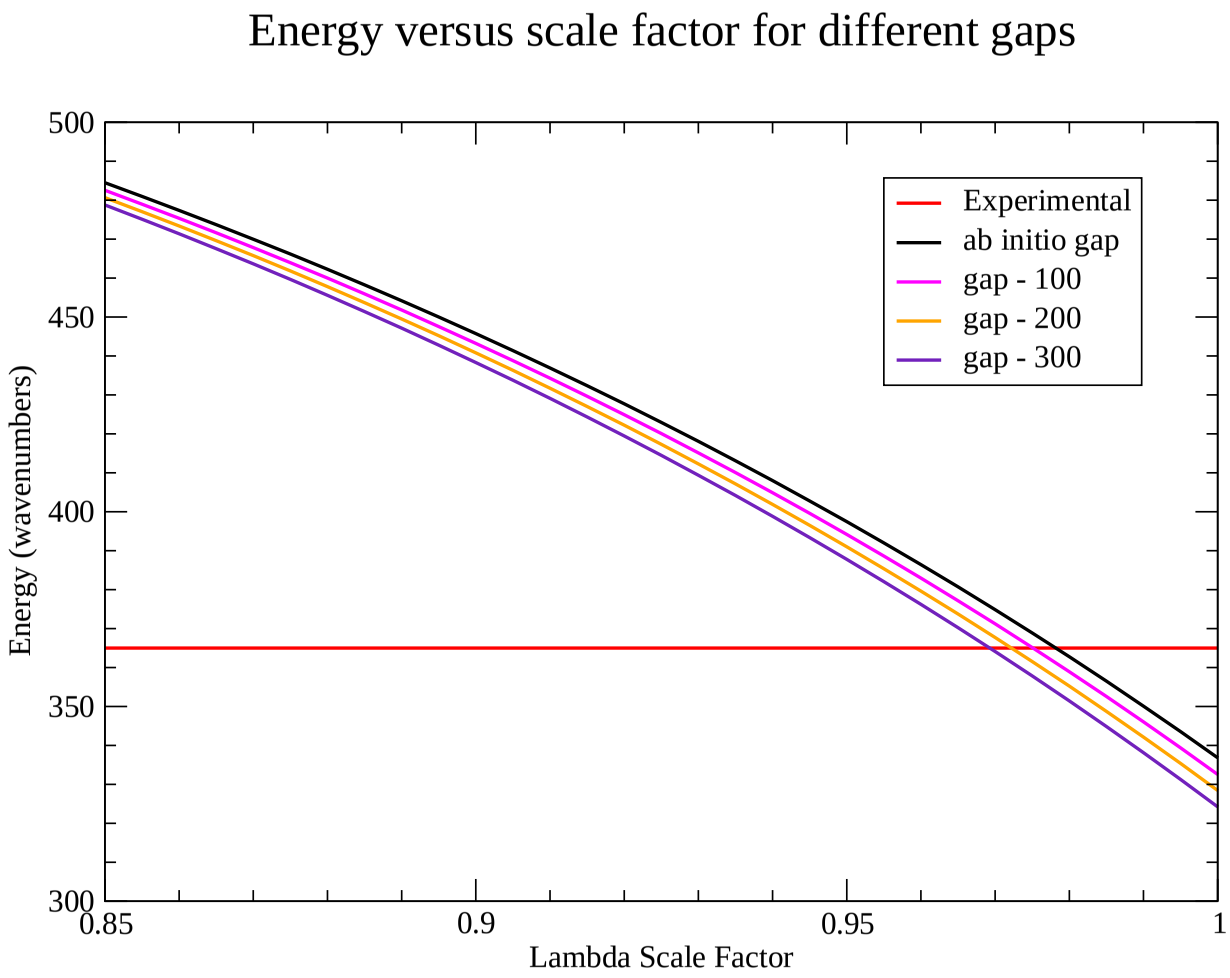

Figure 4.3: Energy versus scale factor for multiple values of the vertical gap compared to the first vibronic energy level in NO_3.

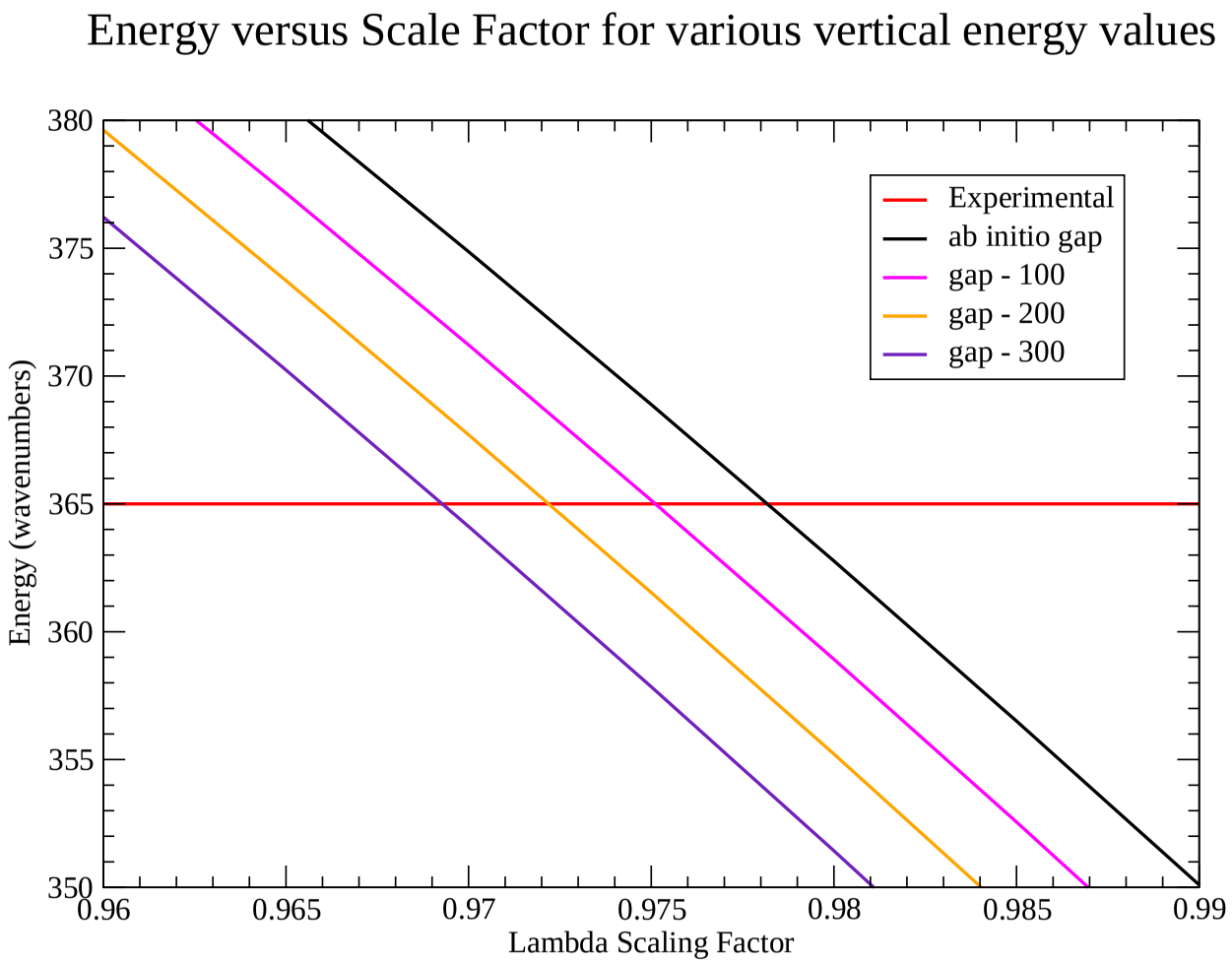

Figure 4.4: Energy versus scale factor for multiple values of the vertical gap compared to the first vibronic energy level in NO_3.

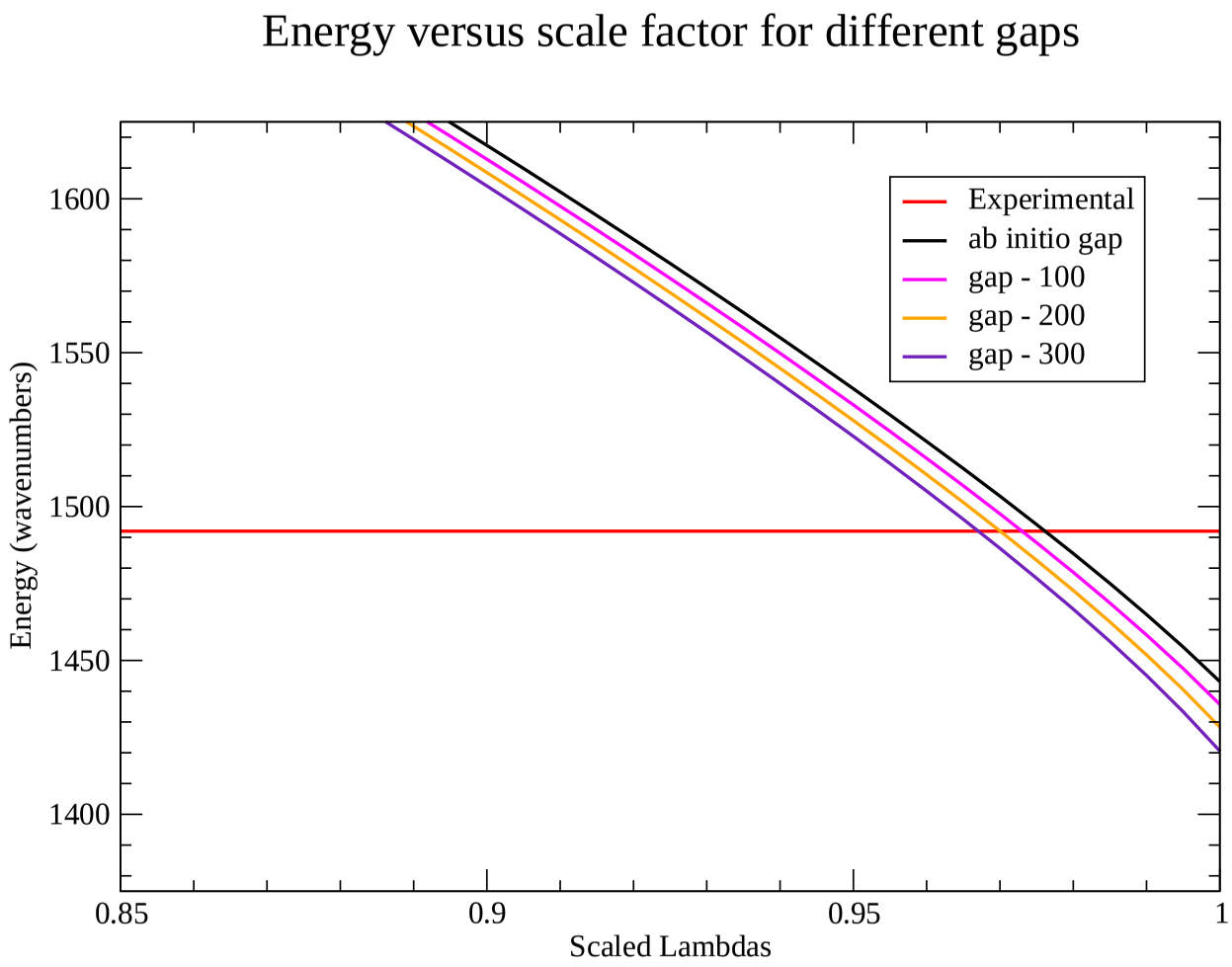

Figure 4.5: Energy versus scale factor for multiple values of the vertical gap compared to the experimental value at 1492 cm^{-1}.

value of 15106 cm^{-1} when the vertical energy is set to 325 cm^{-1} below the adiabatically calculated vertical energy at the Anion geometry. A series of calculations were then run with a λ scaling factor from 0.965 to 0.985. With a scaling factor 0.968, the energy for the diabatic vertical gap was 15108 cm^{-1} and the resulting levels are displayed in Table 4.15 along with "optimal" values for the scaling factor as a function of the change in the vertical gap. The "optimal" value has been defined as the scaling factor which reproduces the first experimentally-observed vibronic level of 365 cm^{-1}.

The results in Table 4.15 have excellent agreement with their experimental counterparts. All of the levels except the very sensitive 1173 cm^{-1} are obtained to a few wavenumbers. The difference between experiment and theory for this problematic level is 29 cm^{-1}. While this is well outside the fidelity of a typical IR spectroscopy measurement, it is within the accuracy of a photodetachment experiment. What is even more encouraging is that the procedure outlined above does not require empirical corrections to the vertical energy. If the *ab initio* gap is used and the optimal scaling factor is determined via the procedure outlined above, excellent level positions are obtained.

Table 4.15: Levels versus Experimental Values (cm^{-1}) for Δ_0, Δ_{100}, Δ_{200}, Δ_{300} and Δ_{325} where $\Delta_x = \Delta$ - x

The first 13 E' levels for "optimal" λ and the calculated gap

	Δ_0	Δ_{100}	Δ_{200}	Δ_{300}	Δ_{325}	Experimental
scale factor	0.978	0.975	0.972	0.969	0.968	
calc. gap (cm^{-1})	15438	15333	15233	15133	15108	15106
	365	365	365	365	365	365
	771	771	771	772	772	
	1065	1065	1065	1064	1065	
	1143	1143	1143	1143	1144	1173
	1420	1419	1419	1419	1419	1413
	1489	1488	1488	1488	1489	1492
	1568	1568	1569	1569	1570	1562
	1633	1634	1634	1635	1636	
	1759	1759	1759	1759	1760	
	1839	1839	1839	1840	1840	
	1922	1922	1922	1922	1923	1917
	1978	1978	1978	1979	1979	
	2073	2074	2073	2073	2074	

Chapter 5

Conclusions and Future Work

5.1 Conclusions

In this work, a methodology for parameterizing high-fidelity quasidiabatic Hamiltonians from a series of adiabatic potential energy surfaces has been established. Best practices for grid sizes, level of theory and basis sets have been determined for one of the most challenging molecules in chemical physics, NO_3. Level positions for all of the known levels of e' symmetry have been obtained to a very high accuracy and level positions for additional modes not found experimentally have been determined. This level of diabatic hamiltonian should be the gold standard for quite some time because as of now it lives right at the edge of what is computationally feasible.

A new MPI-based utility has been developed to support out-of-core (*Ocore*) methods on distributed memory systems. The method adopts a tiered approach for offloading Ocore records by first using distributed RAM based storage pools for high-speed data transfers followed by localized disk-based storage of less-frequently accessed records when the RAM-based storage pools become full. Micro-benchmark tests using the utility were performed to read/write random sequences of fixed-size records to one or more clus-

tered computed nodes interconnected via QDR InfiniBand. The tests showed that the method was able to offload large numbers of records to distributed RAM-based storage pools with a maximum aggregate rate of approximately 3 GB/sec. No significant overhead was observed when offloading to larger numbers of nodes and overall efficiencies of the micro-benchmarks ranged from 77% to 99% of peak MPI transfer rates depending on the underlying block size and offload node count.

The Ocore utility was also integrated within the CFOUR quantum chemistry application that had previously caused excessive I/O load to TACC's Lustre file systems and suffered performance degradation when having a modest number of jobs running simultaneously. As a result of using the Ocore method discussed herein on TACC's Longhorn system, the total analysis time for a parametric study of the nitrate radical NO_3 was reduced by an order of magnitude (from 300 days to 30 days) and avoided writing approximately *1 petabyte* of temporary out-of-core data to the shared file system.

5.2 Future Work

Future work with the NO_3 radical will focus on the simulation of the photodetachment and fluorescence spectra as well as a quantitative look at higher levels of the X^2A_2' state. Additionally, the spectroscopy of the intermediate "dark" A^2E'' state will be studied. While the methodology described in this work has been applied exclusively to NO_3, there are other molecules that fall into this "difficult" category. If these molecules are explored in the manner

outlined herein, it is likely that insight on open questions in spectroscopy can be obtained.

Future efforts planned for the out-of-core utility described in this work include the development of a resource stealing mechanism to leverage all available memory remaining for Ocore purposes after an application has been initialized fully. Expanding further, the approach taken herein can also serve as the basis for performing asynchronous application checkpointing, leveraging SSDs and a hierarchical storage infrastructure that is likely to exist in the exascale era.

Appendices

Appendix A

CFOUR and Ocore Integration Details

A.1 Patchfiles for CFOUR to enable Ocore

In order to integrate CFOUR with the Ocore implementation in GRVY, changes to the CFOUR source code had to be made in two places;

- libr/rddir.f – The source code for the subroutine RDDIR which gets incorporated into libr.a
- libr/wrdir.f – The source code for the subroutine WRDID which gets incorporated into libr.a

As can be seen from the patchfiles for each that are listed below, only the function calls for reading (READ) and writing (WRITE) had to be replaced with the corresponding GRVY functions grvy_ocore_read_int8 and grvy_ocore_write_int8).

Changes that were made to CFOUR's libr/rddir.f

```
2,8d1
<
< C---- ocore -------------------------------------------------
< #ifdef HAVE_MPI_OCORE
<       use grvy
<       use ocore_unit_codes
< #endif
< C---- oomie -------------------------------------------------
24,36d16
<
< C---- ocore -------------------------------------------------
< #ifdef HAVE_MPI_OCORE
<
< C     Locals for test/verification
<
<       integer            :: i
<       integer*4          :: ierr
<       logical            :: intercept_this_unit = .false.
<
< #endif
< C---- ocore -------------------------------------------------
<
41,83d20
<
< C---- ocore -------------------------------------------------
< #ifdef HAVE_MPI_OCORE
< C
< C     Unit numbers of files to intercept are ascertained from input file and
< C     made available here via the ocore_parse_unit_codes module
<
<       intercept_this_unit = .false.
<
<       do icount=1,num_files
<          if(IrealUNIT .eq. units_active(icount))then
<             intercept_this_unit = .true.
<             exit
<          endif
```

```
<       enddo
<
< !      print*,'read: unit = ',IrealUNIT,'rec = ',irec,'intercept = ',
< !     $     intercept_this_unit
<
< !!!      if(.not. use_mpi_ocore)then
<       if(grvy_ocore_enabled() .eq. 0) then
<
<          READ(IrealUNIT,REC=IrealREC,ERR=555,IOSTAT=IER)IVEC
<          IMOD=0
<
<          RETURN
<       endif
<
<       if(intercept_this_unit) then
<
< C        Read from MPI ocore ramdisk
<
<          ierr = grvy_ocore_read_int8(irec,iVEC)
<
<       else
<
< C        Non-intercepted files use normal direct i/o.
<
<          READ(IrealUNIT,REC=IrealREC,ERR=555,IOSTAT=IER)IVEC
<
<       endif
<
< #else
85,87d21
< #endif
< C---- ocore -------------------------------------------------
<
```

Changes that were made to CFOUR's libr/wrdir.f

```
2,9d1
<
< C---- ocore -------------------------------------------------
< #ifdef HAVE_MPI_OCORE
<       use grvy
<       use ocore_unit_codes
< #endif
< C---- ocore -------------------------------------------------
<
29,39d20
<
< C---- ocore -------------------------------------------------
< #ifdef HAVE_MPI_OCORE
<
<       logical   :: intercept_this_unit = .false.
<       integer*4 :: icount
<       integer*4 :: ierr
<
< #endif
< C---- ocore -------------------------------------------------
<
47,83d27
< C---- ocore -------------------------------------------------
< #ifdef HAVE_MPI_OCORE
<
< C     Unit numbers of files to intercept are ascertained from input file and
< C     made available here via the ocore_parse_unit_codes module
<
<       intercept_this_unit = .false.
<
<        do icount=1,num_files
<           if(IrealUNIT .eq. units_active(icount))then
<              intercept_this_unit = .true.
<              exit
<           endif
<        enddo
<
```

```
< !      print*,'write: unit = ',IrealUNIT,'rec = ',irec,'intercept = ',
< !     $     intercept_this_unit
<
< !      if(.not. use_mpi_ocore)then
<       if(grvy_ocore_enabled() .eq. 0) then
<
<          WRITE(IrealUNIT,REC=IrealREC,ERR=555,IOSTAT=IER)IVEC
<
<          RETURN
<       endif
<
<       if(intercept_this_unit) then
<          ierr =  grvy_ocore_write_int8(irec,iVEC)
<       else
<
< C        Non-intercepted files use normal direct i/o.
<
<          WRITE(IrealUNIT,REC=IrealREC,ERR=555,IOSTAT=IER)IVEC
<
<       endif
<
< #else
85,87d28
< #endif
< C---- ocore -------------------------------------------------
<
```

A.2 Example Ocore input file for CFOUR integration

In order to control the parameters of the out-of-core offloading, a single input file (mpi_ocore.input)

Below is an example of one such input file. The comments located within the input file example explain what each flag does. The only additional information needed is to understand which I/O out-of-core files in CFOUR map to their respective fortran unit codes.

Table A.1: The mapping of fortran unit codes in CFOUR to their respective files

Unit code →	file mapping
51	MOINTS
52	GAMLAM
53	MOABCD
54	DERINT
55	DERGAM

Example CFOUR Ocore input file:

```
# -*-getpot-*-

# input file for mpi_ocore usage with cfour

[grvy/mpi_ocore]

# use MPI out-of-core  (1=yes,0=no)
enable_ocore          = 1

# raw mpi storage pool size on each child task [MBs]
max_pool_size_in_mbs  = 11000

# lookup map size for sparse record access on master task [MBs]
max_map_size_in_mbs   = 10

# number of array elements in each ocore read/write
blocksize             = 8192

#enabled disk-based overflow for least-frequently accessed records
use_disk_overflow     = 1

# percentage of records to dump to disk when memory cache is full
```

```
watermark_ratio       = 0.2

# allow for empty records to be returned if not written previously
allow_empty_records   = 1

# dump raw read/write statistics for each record?
dump_raw_statistics   = true

[cfour/ocore]

# specify the number of files to intercept (and unit numbers
# for each file).

# the following are defined to trap files for xecc and xsdcc

num_files = 1
file_unit_numbers = '55'
```

Appendix B

Adiabatic force constants and diabatic corrections

B.1 QVC.1

As a starting point for the parameterization of the diabatic model referred to as QVC.1 (§4.3.1, the adiabatic force constants were obtained by fitting a 4th order Taylor series to the adiabatic surfaces which were generated by displacing the NO_3^1 reference geometry along the q_1, q_3a and q_3b reduced normal coordinates. In table B.1 the unique values that must be obtained in order to parameterize the full QVC.1 Hamiltonian. Where appropriate, the diabatic corrections are also given.

B.2 QVC.2

As discussed previous and in detail in Chapter 4, QVC.2 employs almost the same parametrization as QVC.1 except that it no longer systematically removes the Jahn-Teller distortions. The previous parameterization does not naturally fall out of the adiabatic fits but was constructed in order to ascertain the effects of quadratic JT effects.

Table B.1: QVC.1 adiabatic force constants(in $cm^{-}1$)

Force constants and diabatic corrections		
Parameter	Adiabatic	Diabatic Correction
$f_{1;\tilde{\mathbf{X}}}$	-868.2	
$f_{1;\tilde{\mathbf{B}}_\mathbf{a}}$	440.5	
$f_{3;\tilde{\mathbf{B}}_\mathbf{a}}$	440.7	
$f_{4;\tilde{\mathbf{B}}_\mathbf{a}}$	762.2	
$f_{11;\tilde{\mathbf{X}}}$	960.3	
$f_{11;\tilde{\mathbf{B}}_\mathbf{a}}$	1070.8	
$f_{33;\tilde{\mathbf{X}}}$	424.4	-1148.6
$f_{44;\tilde{\mathbf{X}}}$	406.6	-169.0
$f_{34;\tilde{\mathbf{X}}}$	406.0	440.6
$f_{33;\tilde{\mathbf{B}}_\mathbf{a}}$	819.1	
$f_{33;\tilde{\mathbf{B}}_\mathbf{b}}$	2027.0	1148.6
$f_{44;\tilde{\mathbf{B}}_\mathbf{a}}$	677.5	
$f_{44\tilde{\mathbf{B}}_\mathbf{b}}$	726.2	169.0
$f_{34\tilde{\mathbf{B}}_\mathbf{a}}$	83.0	
$f_{34\tilde{\mathbf{B}}_\mathbf{b}}$	-284.4	-440.6
$f_{13\tilde{\mathbf{B}}_\mathbf{a}}$	-61.3	
$f_{14\tilde{\mathbf{B}}_\mathbf{a}}$	66.4	

Table B.2: QVC.2 adiabatic force constants (in $cm^{-}1$)

Force constants and diabatic corrections		
Parameter	Adiabatic	Diabatic Correction
$f_{1;\tilde{\mathbf{X}}}$	-868.2	
$f_{1;\tilde{\mathbf{B}}_\mathbf{a}}$	440.5	
$f_{3;\tilde{\mathbf{B}}_\mathbf{a}}$	440.7	
$f_{4;\tilde{\mathbf{B}}_\mathbf{a}}$	762.2	
$f_{11;\tilde{\mathbf{X}}}$	960.3	
$f_{11;\tilde{\mathbf{B}}_\mathbf{a}}$	1070.8	
$f_{33;\tilde{\mathbf{X}}}$	424.4	-1148.6
$f_{44;\tilde{\mathbf{X}}}$	406.6	-169.0
$f_{34;\tilde{\mathbf{X}}}$	406.0	440.6
$f_{33;\tilde{\mathbf{B}}_\mathbf{a}}$	819.1	
$f_{33;\tilde{\mathbf{B}}_\mathbf{b}}$	2027.0	1148.6
$f_{44;\tilde{\mathbf{B}}_\mathbf{a}}$	677.5	
$f_{44\tilde{\mathbf{B}}_\mathbf{b}}$	726.2	169.0
$f_{34\tilde{\mathbf{B}}_\mathbf{a}}$	83.0	
$f_{34\tilde{\mathbf{B}}_\mathbf{b}}$	-284.4	-440.6
$f_{13\tilde{\mathbf{B}}_\mathbf{a}}$	-61.3	
$f_{14\tilde{\mathbf{B}}_\mathbf{a}}$	66.4	

B.3 4VC

Below are the cubic and quartic force constants as well as their corresponding diabatic corrections. The values for the linear and quadratic force constants are the same as those listed in the section on QVC.2

Table B.3: 4VC cubic adiabatic force constants (in $cm^{-}1$)

Force constants and diabatic corrections (δ)		
Parameter	Adiabatic	δ
$f_{111;\tilde{\mathbf{X}}}$	-197.3	
$f_{133;\tilde{\mathbf{X}}}$	-282.5	-7.5
$f_{144;\tilde{\mathbf{X}}}$	-28.8	-23.2
$f_{134;\tilde{\mathbf{X}}}$	-101.5	31.7
$f_{333;\tilde{\mathbf{X}}}$	-435.9	-244.2
$f_{444;\tilde{\mathbf{X}}}$	-38.8	-87.3
$f_{334;\tilde{\mathbf{X}}}$	-77.6	-43.7
$f_{344;\tilde{\mathbf{X}}}$	70.5	104.7
$f_{111;\tilde{\mathbf{B}}_\mathbf{a}}$	204.7	
$f_{113;\tilde{\mathbf{B}}_\mathbf{a}}$	-12.0	
$f_{114;\tilde{\mathbf{B}}_\mathbf{a}}$	7.5	
$f_{133;\tilde{\mathbf{B}}_\mathbf{a}}$	231.4	
$f_{144;\tilde{\mathbf{B}}_\mathbf{a}}$	63.6	
$f_{134;\tilde{\mathbf{B}}_\mathbf{a}}$	81.2	
$f_{333;\tilde{\mathbf{B}}_\mathbf{a}}$	-414.8	
$f_{444;\tilde{\mathbf{B}}_\mathbf{a}}$	45.4	
$f_{334;\tilde{\mathbf{B}}_\mathbf{a}}$	-66.8	
$f_{111;\tilde{\mathbf{B}}_\mathbf{b}}$	204.7	
$f_{133;\tilde{\mathbf{B}}_\mathbf{b}}$	250.7	7.5
$f_{144;\tilde{\mathbf{B}}_\mathbf{b}}$	67.0	23.2
$f_{134;\tilde{\mathbf{B}}_\mathbf{b}}$	51.1	-31.7
$f_{444;\tilde{\mathbf{B}}_\mathbf{b}}$	115.3	87.3
$f_{333;\tilde{\mathbf{B}}_\mathbf{b}}$	123.7	244.2
$f_{334;\tilde{\mathbf{B}}_\mathbf{b}}$	-20.5	43.7
$f_{344;\tilde{\mathbf{B}}_\mathbf{b}}$	-87.5	104.7
$f_{443;\tilde{\mathbf{B}}_\mathbf{b}}$	-87.5	-104.7
$f_{555;\tilde{\mathbf{X}}\tilde{\mathbf{B}}_\mathbf{b}}$	-90.0	

Table B.4: 4VC quartic adiabatic force constants (in $cm^{-}1$)

Force constants and diabatic corrections (δ)

Parameter	Adiabatic	δ	Parameter	Adiabatic	δ
$f_{1111;\tilde{\mathbf{X}}}$	32.9		$f_{1334;\tilde{\mathbf{B}}_\mathbf{a}}$	-5.2	
$f_{1133;\tilde{\mathbf{X}}}$	48.0	4.7	$f_{1133;\tilde{\mathbf{B}}_\mathbf{a}}$	-1.9	
$f_{1144;\tilde{\mathbf{X}}}$	1.3	1.3	$f_{3333;\tilde{\mathbf{B}}_\mathbf{a}}$	134.2	
$f_{1134;\tilde{\mathbf{X}}}$	16.9	-4.1	$f_{3444;\tilde{\mathbf{B}}_\mathbf{a}}$	3.2	
$f_{1333;\tilde{\mathbf{X}}}$	-49.3	27.0	$f_{4333;\tilde{\mathbf{B}}_\mathbf{a}}$	36.0	
$f_{1444;\tilde{\mathbf{X}}}$	-6.2	-5.2	$f_{4444;\tilde{\mathbf{B}}_\mathbf{a}}$	1.3	
$f_{1334;\tilde{\mathbf{X}}}$	-6.4	-2.6	$f_{3344;\tilde{\mathbf{B}}_\mathbf{a}}$	10.1	
$f_{1344;\tilde{\mathbf{X}}}$	1.1	1.8	$f_{3366;\tilde{\mathbf{B}}_\mathbf{a}}$	-26.0	
$f_{3333;\tilde{\mathbf{X}}}$	440.6	306.4	$f_{1111;\tilde{\mathbf{B}}_\mathbf{b}}$	32.7	
$f_{4333;\tilde{\mathbf{X}}}$	-98.2	-125.2	$f_{1133;\tilde{\mathbf{B}}_\mathbf{b}}$	40.8	-4.7
$f_{3444;\tilde{\mathbf{X}}}$	-13.1	-13.1	$f_{1144;\tilde{\mathbf{B}}_\mathbf{b}}$	6.1	-1.0
$f_{4444;\tilde{\mathbf{X}}}$	-14.5	-15.1	$f_{1134;\tilde{\mathbf{B}}_\mathbf{b}}$	14.4	4.1
$f_{3344;\tilde{\mathbf{X}}}$	72.3	48.0	$f_{1333;\tilde{\mathbf{B}}_\mathbf{b}}$	-49.8	-27.0
$f_{3366;\tilde{\mathbf{X}}}$	-4.5	4.4	$f_{1443;\tilde{\mathbf{B}}_\mathbf{b}}$	-6.0	-1.8
$f_{1111;\tilde{\mathbf{B}}_\mathbf{a}}$	32.7		$f_{1444;\tilde{\mathbf{B}}_\mathbf{b}}$	11.5	5.2
$f_{1113;\tilde{\mathbf{B}}_\mathbf{a}}$	-1.0		$f_{1334;\tilde{\mathbf{B}}_\mathbf{b}}$	-2.6	2.6
$f_{1114;\tilde{\mathbf{B}}_\mathbf{a}}$	1.0		$f_{1344;\tilde{\mathbf{B}}_\mathbf{b}}$	-8.7	-1.8
$f_{1133;\tilde{\mathbf{B}}_\mathbf{a}}$	40.4		$f_{3333;\tilde{\mathbf{B}}_\mathbf{b}}$	-272.5	-306.4
$f_{1144;\tilde{\mathbf{B}}_\mathbf{a}}$	5.6		$f_{4333;\tilde{\mathbf{B}}_\mathbf{b}}$	54.0	125.2
$f_{1134;\tilde{\mathbf{B}}_\mathbf{a}}$	15.8		$f_{3444;\tilde{\mathbf{B}}_\mathbf{b}}$	23.5	5.8
$f_{1333;\tilde{\mathbf{B}}_\mathbf{a}}$	-72.2		$f_{4444;\tilde{\mathbf{B}}_\mathbf{b}}$	12.6	15.1
$f_{1443;\tilde{\mathbf{B}}_\mathbf{a}}$	-2.0		$f_{3344;\tilde{\mathbf{B}}_\mathbf{b}}$	-75.6	-48.0
$f_{1444;\tilde{\mathbf{B}}_\mathbf{a}}$	3.3		$f_{3366;\tilde{\mathbf{B}}_\mathbf{b}}$	-26.0	

Bibliography

[1] J. Almlöf and P. R. Taylor. General contraction of gaussian basis sets. i. atomic natural orbitals for first- and second-row atoms. *J. Chem. Phys.*, 86(7):4070–4077, 1987.

[2] J. Almlöf and P. R. Taylor. General contraction of gaussian basis sets. ii. atomic natural orbitals and the calculation of atomic and molecular properties. *J. Chem. Phys.*, 92(1):551–560, 1990.

[3] Jan Almlöf and Peter R. Taylor. General contraction of gaussian basis sets. i. atomic natural orbitals for first- and second-row atoms. *The Journal of Chemical Physics*, 86(7):4070–4077, 1987.

[4] M. Baer. *Adv. Chem. Phys.*, 124:39, 2002.

[5] R. J. Bartlett, J. D. Watts, S. A. Kurchaski, and J. Noga. Noniterative fifth-order triple and quadruple excitation-energy corrections in coorrelated methods. *Chem. Phys. Lett.*, 165(6):513–522, 1990.

[6] C. W. Bauschlicher, Jr., S.R. Langhoff, and A. Kormornicki. The calculation of the dipole-moments of NiH, TiO and FeO. *Theor. Chim. Acta*, 77(4):263–279, 1990.

[7] R. C. Boehm and L. L. Lohr. *J. Phys. Chem.*, 93:3430, 1989.

[8] M. Born and K. Huang. *Dynamitcal Theory of Crystal Lattices*. Oxford University Press, 1951.

[9] M. Born and R. Oppenheimer. *Ann. Physik.*, 84, 1927.

[10] M. Born and R. Oppenheimer. Zur quantentheorie der molekeln. *Ann. d. Phys.*, 84:457–484, 1927.

[11] E. J. Bylaska, W. A. de Jong, N. Govind, K. Kowalski, T. P. Straatsma, M. Valiev, D. Wang, E. Apra, T. L. Windus, J. Hammond, P. Nichols, S. Hirata, M. T. Hackler, Y. Zhao, P.-D. Fan, R. J. Harrison, M. Dupuis, D. M. A. Smith, J. Nieplocha, V. Tipparaju, M. Krishnan, Q. Wu, T. Van Voorhis, A. A. Auer, M. Nooijen, E. Brown, G. Cisneros, G. I. Fann, H. Fruchtl, J. Garza, K. Hirao, R. Kendall, J. A. Nichols, K. Tsemekhman, K. Wolinski, J. Anchell, D. Bernholdt, P. Borowski, T. Clark, D. Clerc, H. Dachsel, M. Deegan, K. Dyall, D. Elwood, E. Glendening, M. Gutowski, A. Hess, J. Jaffe, B. Johnson, J. Ju, R. Kobayashi, R. Kutteh, Z. Lin, R. Littlefield, X. Long, B. Meng, T. Nakajima, S. Niu, L. Pollack, M. Rosing, G. Sandrone, M. Stave, H. Taylor, G. Thomas, J. van Lenthe, A. Wong, and Z. Zhang. NWChem, a computational chemistry package for parallel computers, Version 5.1. Pacific Northwest National Laboratory, Richland, Washington 99352-0999, USA, 2007.

[12] J. Chappuis. *Ann. d. l''ecole Norm. Sup.*, 159, 1882.

[13] J. Čížek. On the correlation problem in atomic and molecular systems. calculation of wavefunction components in Ursell-type expansion using

quantum-field theoretical methods. *J. Chem. Phys.*, 45(11):4256–4266, 1966.

[14] J. Čížek. *On the Use of the Cluster Expansion and the Technique of Diagrams in Calculations of Correlation Effects in Atoms and Molecules*, pages 35–89. Volume 14 of Prigogine and Rice [62], 1969.

[15] J. Čížek and J. Paldus. Correlation problems in atomic and molecular systems iii. rederivation of the coupled-pair many-electron theory using the traditional quantum chemical method. *Int. J. Quantum Chem.*, 5(4):359–379, 1971.

[16] T. D. Crawford, W. D. Allen, J. F. Stanton, and H. F. Schaefer. *J. Chem. Phys.*, 107:10626, 1997.

[17] T. D. Crawford and H. F. Schaefer III. *An Introduction to Coupled Cluster Theory for Computational Chemists*, pages 33–136. Volume 14 of Lipkowitz and Boyd [54], 2000.

[18] T. D. Crawford and H. F. Schaefer. *Reviews of Computational Chemistry*. VCH, 1999.

[19] H.F Davis, B. Kim, H.S. Johnston, and Y. T. Lee. *J. Phys. Chem*, page 2172, 1993.

[20] R. D. Davy and H. F. Schaefer. *J. Chem. Phys.*, 91, 1989.

[21] P. A. M. Dirac. Note on exchange phenomena in the thomas atom. *Proc. Camb. Phil. Soc.*, 26:376–385, 1930.

[22] M. J. Bertin et al. *Pisot and Salem Numbers*. user Verlag, Berlin, 1992.

[23] Free Software Foundation. GNU Library General Public License, Version 2.0. `http://www.gnu.org/licenses/old-licenses/lgpl-2.0-standalone.html`.

[24] J. Gauss and J. F. Stanton. Coupled-cluster calculations of nuclear magnetic resonance chemical shifts. *J. Chem. Phys.*, 103(9):3561–3577, 1995.

[25] J. Gauss, J. F. Stanton, and R. J. Bartlett. *J. Chem. Phys.*, 95, 1991.

[26] J. Gauss, J. F. Stanton, and R. J. Bartlett. Coupled-cluster open-shell analytic gradients: Implementation of the direct product decomposition approach in energy gradient calculations. *J. Chem. Phys.*, 95(4):2623–2638, 1991.

[27] M. D. Hack and D. G. Truhlar. *J. Phys. Chem.*, 104:7917, 2000.

[28] G. G. Hall. The molecular orbital theory of chemical valency. viii. a method of calculating ionization potentials. *Proc. Roy. Soc. Lond. A*, 205(1083):541–552, 1951.

[29] M. E. Harding, T. Metzroth, J. Gauss, and A. A. Auer. Parallel calculation of CCSD and CCSD(T) analytic first and second derivatives. *J. Chem. Theory Comput.*, 4(1):64–74, 2008.

[30] Michael E. Harding, Thorsten Metzroth, Jurgen Gauss, and Alexander A. Auer. Parallel calculation of ccsd and ccsd(t) analytic first and second derivatives. *Journal of Chemical Theory and Computation*, 4(1):64–74, 2008.

[31] D. R. Hartree. The wave mechanics of an atom with a non-Coulomb central field. part ii. some results and discussion. *Proc. Camb. Phil. Soc.*, 24:111–132, 1928.

[32] T Ichino, J Gauss, and J Stanton. Quasidiabatic states described by coupled-cluster theory. *The Journal of Chemical Physics*, Jan 2009.

[33] T Ichino, S Wren, and K Vogelhuber. The vibronic level structure of the cyclopentadienyl radical. *The Journal of chemical ...*, Jan 2008.

[34] Martin Isenburg and Stefan Gumhold. Out-of-core compression for gigantic polygon meshes. *ACM Trans. Graph.*, 22:935–942, July 2003.

[35] T. Ishiwata, I. Tanaka, K. Kawaguchi, and E. Hirota. *J. Phys. Chem*, page 2196, 1985.

[36] M. E. Jacox and W. E. Thompson. *J. Phys. Chem*, page 6807, 2008.

[37] A. W. Jasper, C. Y. Zhu, S. Nangia, and D. G. Truhlar. *Faraday Discuss.*, 1:127, 2004.

[38] F. Jensen. *Introduction to Computational Chemistry.* John Wiley & Sons, Inc., Chichester, England, 1999.

[39] H. S. Johnston, H. F. Davis, and Y. T. Lee. *J. Phys. Chem*, page 4713, 1996.

[40] E. J. Jones and O.R. Wulf. *J. Chem. Phys.*, 876, 1937.

[41] U. Kaldor. *Chem. Phys. Letters*, 166:599, 1990.

[42] R. A. Kendall, E. Aprá, D. E. Bernholdt, E. J. Bylaska, M. Dupuis, G. I. Fann, R. J. Harrison, J. Ju, J. A. Nichols, J. Nieplocha, T.P. Straatsma, T. L. Windus, and A. T. Wong. High performance computational chemistry: An overview of NWChem a distributed parallel application. *Comput. Phys. Comm.*, 128:260–283, 2000.

[43] B. Kim, B. L. Hammond, W. A. Lester, and H. S. Johnston. *Chem. Phys. Letters*, 131, 1990.

[44] K Klein, J Stanton, J Zhou, and T Yacovitch. Vibronic structure of the formyloxyl radical (hco2) via slow photoelectron velocity-map imaging spectroscopy and model hamiltonian calculations. *The Journal of ...*, Jan 2009.

[45] Donald K. Knuth. *The TEXbook*. Addison-Wesley, 1984.

[46] H. Koch, H. J. A. A. Jensen, T. Helgaker, P. Jørgensen, G. E. Scuseria, and H. F. Schaefer III. Coupled cluster energy derivatives. analytic hessian for the closed-shell coupled cluster singles and doubles wave function: Theory and applications. *J. Chem. Phys.*, 92(8):4924–4940, 1990.

[47] H Köppel and W Domcke.... Multimode molecular dynamics beyond the born-oppenheimer approximation. *Advances in chemical physics*, Jan 1984.

[48] Hya Krishnan, Sriram Krishnamoorthy, Gerald Baumgartner, Chi chung Lam, J. Ramanujam, and D̃avid E. Bernholdt. Data locality optimization for synthesis of efficient out-of-core algorithms. In *In Proc. of the Intl. Conf. on High Performance Computing*, pages 406–417. Springer Verlag, 2003.

[49] V. K. Kundeti, S. Rajasekaran, H. Dinh, M. Vaughn, and V. Thapar. Efficient parallel and out of core algorithms for constructing large bi-directed de Bruijn graphs. *BMC Bioinformatics*, 11:560, 2010.

[50] Leslie Lamport. *LaTeX: A document preparation system*. Addison-Wesley, 2nd edition, 1994.

[51] S. R. Langhofl, editor. *Understanding Chemical Reactivity, Volume 13: Quantum Mechanical Electronic Structure Calculations with Chemical Accuracy*. Kulwer Academic Publishers, Dordrecht, Holland, 1995.

[52] T. J. Lee and G. E. Scuseria. *Achieving Chemical Accuracy with Coupled-Cluster Theory*, pages 47–108. In Langhofl [51], 1995.

[53] libGRVY. Toolkit for HPC Application Development. `https://red.ices.utexas.edu/projects/software/wiki/GRVY`.

[54] K. B. Lipkowitz and D. B. Boyd, editors. *Reviews in Computational Chemistry*, volume 14. John Wiley & Sons, Inc., Chichester, England, 2000.

[55] Jiuxing Liu, Balasubramanian Chandrasekaran, Weikuan Yu, Jiesheng Wu, Darius Buntinas, Sushmitha Kini, Dhabaleswar K. Panda, and Pete Wyckoff. Microbenchmark performance comparison of high-speed cluster interconnects. *IEEE Micro*, 24:42–51, January 2004.

[56] A. Lund and K. Thuomas. *Chem. Phys. Letters*, 44:569, 1976.

[57] F Mittelbach M Goosens and A Samarin. *The LaTeXCompanion*. Addison-Wesley, 1994.

[58] M. Mayer, L. S. Cederbaum, and H. Köppel. *J. Chem. Phys.*, 100:899, 1994.

[59] K. Mikhaylichenko, C. Riehn, L. Valachovic, A. Sanov, and C. Wittig. *J. Phys. Chem*, 129:6807, 1996.

[60] V. R. Morris, S. C. Bhatia, and J. M. Hall. *J. Phys. Chem.*, 94:7414, 1990.

[61] U of Toronto. Methane and Carbon Monoxide in the Troposphere. `http://www.tacc.utexas.edu/user-services/user-guides/longhorn-user-guide`.

[62] I. Prigogine and S. A Rice, editors. *Advances in Chemical Physics*, volume 14. John Wiley & Sons, Inc., Chichester, England, 1969.

[63] P. Pulay. Ab initio calculation of force constants and equilibrium geometries. *Mol. Phys.*, 17(2):197, 1969.

[64] P. Pulay. Ab initio calculation of force constants and equilibrium geometries in polyatomic molecules ii. force constants of water. *Molec. Phys.*, 18(4):473–480, 1970.

[65] P. Pulay. Improved SCF convergence acceleration. *J. Comp. Chem.*, 3(4):556–560, 1982.

[66] G. D. Purvis and R. J. Bartlett. *J. Chem. Phys.*, 76, 1982.

[67] K. G. Raghavachari, G. W. Trucks, J. A. Pople, and M. Head-Gordon. A fifth-order perturbation comparison of electron correkation theories. *Chem. Phys. Lett.*, 157(6):479–483, 1989.

[68] D. A. Ramsay. *Proceedings of the Tenth Colloquium Spectroscopicum Internationale*, page 593, 1963.

[69] John Reid. The New Features of Fortran 2003. *SIGPLAN Fortran Forum*, 26:10–33, April 2007.

[70] C. C. J. Roothaan. New developments in molecular orbital theory. *Rev. Mod. Phys.*, 23(2):69–89, 1951.

[71] E. A. Salter and R. J. Bartlett. Analyltic energy derivatives in many-body methods. ii. second derivatives. *J. Chem. Phys.*, 90(3):1767–1773, 1989.

[72] E. A. Salter, G. W. Trucks, and R. J. Bartlett. Analyltic energy derivatives in many-body methods. i. first derivatives. *J. Chem. Phys.*, 90(3):1752–1766, 1989.

[73] A. C. Scheiner, G. E. Scuseria, J. E. Rice, T. J. Lee, and H. F. Schaefer III. Analytic evaluation of energy gradients for the single and double excitation coupled cluster (CCSD) wave function: Theory and application. *J. Chem. Phys.*, 87(9):5361–5373, 1987.

[74] E. Schrödinger. Quantisierung als eigenwertproblem. *Ann. d. Phys.*, 384(4):361–376, 1926.

[75] E. Schrödinger. Quantisierung als eigenwertproblem. *Ann. d. Phys.*, 384(6):489–527, 1926.

[76] E. Schrödinger. Quantisierung als eigenwertproblem. *Ann. d. Phys.*, 385(13):437–490, 1926.

[77] E. Schrödinger. Quantisierung als eigenwertproblem. *Ann. d. Phys.*, 386(18):109–139, 1926.

[78] M. Schütz and R. Lindh. An intergral direct, distributed-data, parallel mp2 algorithm. *Theor. Chem. Acta*, 95(1–2):13–34, 1997.

[79] P. E. M. Siegbahn. *J. Comput. Chem.*, 6, 1985.

[80] J. C. Slater. The theory of complex spectra. *Phys. Rev.*, 34(10):1293–1322, 1929.

[81] J. C. Slater. *Quantum Theory of Molecules and Solids, Volume 1: Electronic Structure of Molecules*. McGraw-Hill Book Co., Inc., New York, 1963.

[82] Michael Spivak. *The joy of TEX*. American Mathematical Society, Providence, R.I., 2nd edition, 1990.

[83] J Stanton. On the vibronic level structure in the no radical. i. the ground electronic state. *The Journal of Chemical Physics*, Jan 2007.

[84] J Stanton. On the vibronic level structure in the no3 radical: Ii. adiabatic calculation of the infrared .... *Molecular Physics*, Jan 2009.

[85] J. F. Stanton. *J. Chem. Phys.*, 115:10382, 2001.

[86] J. F. Stanton and J. Gauss. *J. Chem. Phys.*, 101:8938, 1994.

[87] J. F. Stanton, J. Gauss, and R. J. Bartlett. *J. Chem. Phys.*, 94:4084, 1991.

[88] J. F. Stanton, J. Gauss, and R. J. Bartlett. *J. Chem. Phys.*, 97:5554, 1992.

[89] J. F. Stanton, J. Gauss, J. D. Watts, and R. J. Bartlett. A direct product decomposition approach for symmetry exploitation in many-body methods. i. energy calculations. *J. Chem. Phys.*, 94(6):4334–4345, 1991.

[90] J. F. Stanton, J. Gauss, J. D. Watts, W. J. Lauderdale, and R. J. Bartlett. The ACESII program system. *Int. J. Quantum Chem. Symp.*, 26:879–894, 1992.

[91] P. Jørgensen T. Helgaker and J. Olsen. *Molecular Electronic-Structure Theory*. John Wiley & Sons, Ltd., Chichester, England, 2000.

[92] TACC. Longhorn User Guide. `http://www.tacc.utexas.edu/user-services/user-guides/longhorn-user-guide`.

[93] Alf J. van der Poorten. Some problems of recurrent interest. Technical Report 81-0037, School of Mathematics and Physics, Macquarie University, North Ryde, Australia 2113, August 1981.

[94] G. Varadhan and D. Manocha. Out-of-core rendering of massive geometric environments. In *Visualization, 2002. VIS 2002. IEEE*, pages 69 –76, nov. 2002.

[95] Gary V. Vaughan, Ben Elliston, Tom Tromey, and Ian L. Taylor. *GNU Autoconf, Automake, and Libtool*. Pearson Education, October 2000.

[96] E. Warburg and G. Leithäuser. *Ann. Phys.*, 209, 1907.

[97] J. D. Watts. Parallel algorithms for coupled-cluster methods. *Parallel Computing*, 26:857–867, 2000.

[98] R.P. Wayne, I. Barnes, P. Biggs, J.P. Burrows, C.E. Canosa-mas, J. Hjorth, G. LeBras, G.K. Moortgat, D. Perner, G. Poulet, G. Restelli, and H. Side-

bottom. The Nitrate Radical: Physics, Chemistry and the Atmosphere. Comission of the European Communities, Brussels, 1990.